Some treatment techniques for humid exhaust air

Pietari Lehtinen

Master of Science Thesis in Thermal and Fluid Engineering
Supervisor: Frank Pettersson
Faculty of Science and Engineering
Åbo Akademi University
June, 2019

Abstract

Work:	Master of Science Thesis
Title:	Some treatment techniques for humid exhaust air
Author:	Pietari Lehtinen, Thermal and Flow Engineering Laboratory, Faculty of Science and Engineering, Åbo Akademi University
Supervisor:	Senior Lecturer, Docent Frank Pettersson
Place and date:	Turku, 2019

This Master's thesis considers plate type of heat exchangers, with process air as both receiving and passing media for heat. The heat exchanger has a water film present due to condensation, and different two-phase flow setups are discussed. As another main topic, the air treatments related to increasing the air quality, are discussed. Additionally, the thesis briefly addresses water treatment techniques. Some results for the absorption and particle collection for spray chambers are shown.

Keywords: heat exchangers, air pollution, air treatment, water treatment

Table of Contents

Preface

This thesis did take its time, but it was worth the while. I would like to thank Senior Lecturer, Docent Frank Pettersson for finding answers to all of my thorny questions and for helping me along the way. I would also like to thank TM Systems for an inspiring and challenging opportunity to write my thesis on a live subject. From TM Systems, a special thanks goes to D.Sc. Pasi Rajala who has supported me and made this thesis go along the track from the start to the finish.

Pietari Lehtinen
Turku, June 2019

Nomenclature

Notation	Description	Unit
	Roman	
A	area	m^2
a	general coefficient	–
b	slot length	m
Bo	Bond number	–
C	constant for film thickness	–
c	concentration	varies, e.g. mg/m^3, ppm
c_p	specific heat	$\frac{J}{kg \cdot K}$
D	mass diffusion coefficient	m^2/s
d	diameter	m
E	efficiency	%
F	foam density	kg/m^3
f	friction factor	–
Fr	Froude number	–
g	standard acceleration due to gravity	m/s^2
H	height, total height	m
H_c	Henry's law constant	Pa
H^{xp}	Henry's law constant	1/atm
h_v	evaporation enthalpy	J/kg
i	specific humidity	$\frac{\text{kg } H_2O}{\text{kg dry air}}$
J	molar flow	mol/s
j	molar flux	$\frac{\text{mol}}{m^2 \cdot s}$
K	coefficient, factor in absorption	–
k	mass transfer coefficient	m/s
Ka	Kapitza number	–
Ku	Kutateladze number	–
L	length	m
M	molar mass	kg/kmol, g/mol

$\dot{m}$	mass flow	kg/s
$\dot{m}$"	mass flow per area	$\frac{\text{kg}}{\text{s}\cdot\text{m}^2}$
N	number of slots	pcs.
n	number of, count	pcs.
Nu	Nusselt number	–
Oh	Ohnesorge number	–
p	pressure	Pa
Pr	Prandtl number	–
$\dot{Q}$	heat flow	W
$\dot{q}$	heat flow per area	W/m^2
R	universal gas constant	$\frac{\text{J}}{\text{mol}\cdot\text{K}}$
r	specific volumetric resistance	$1/\text{m}^2$
Re	Reynolds number	–
s	wall thickness	m
Sc	Schmidt number	–
Sh	Sherwood number	–
Stk	Stokes number	–
T	temperature	K, unless stated otherwise
t	time	s
V	volume	m^3
$\dot{V}$	volume flow	m^3/s
v	velocity	m/s
v^*	dimensionless velocity	–
w	slot width	m
X	Lockhart-Martinelli parameter	–
x	mole fraction in liquid phase	mol/mol
y	mole fraction in gas phase	mol/mol
z	position in height	m

Greek

α	heat transfer coefficient	$\frac{\text{W}}{\text{m}^2\cdot\text{K}}$
β	angle	$^\circ$

Γ	mass flow per perimeter	$\frac{\text{kg}}{\text{s}\cdot\text{m}}$
γ	constant for film thickness in co-current film flow downwards	–
δ	film thickness	m
ε	interaction energy	J
ζ	volume fraction	–
η	particle removal efficiency	–
κ	diameter ratio	–
Λ	mean free path	m
λ	thermal conductivity	$\frac{\text{W}}{\text{m}\cdot\text{K}}$
μ	dynamic viscosity	$\frac{\text{kg}}{\text{s}\cdot\text{m}}$
ν	kinematic viscosity	m^2/s
ρ	density	kg/m^3
σ	surface tension	N/m
ς	collision diameter	Å
τ	shear stress	N/m^2
Φ	mass loading ratio parameter	–
ϕ	void fraction	–
ω	viscosity ratio	–

Subscripts

A	component A
ae	aerodynamic
air	air flow
an	annular
ave	average
B	Boltzmann
Br	Brownian
cc	counter-current
ch	channel
ck	cake
$cond$	condensation
$conv$	convection

cr	cross-current
cs	cross-section
d	droplet
da	dry air
dph	diffusiophoresis
f	film
ff	free fall
fl	flooding
g	gas
h	hydraulic
$h.e.$	heat exchanger
i	interfacial
in	incoming
l	liquid
min	minimal
mV	Murphrees'
N	Nusselts' film thickness
o	overall
or	orifice
p	particle
ppm	parts per million
pr	perimeter
r	relative
res	residence
sat	saturation
sl	superficial
sp	slip
st	slot
t	terminal
th	theoretical
tot	total
v	water vapour

w	wall

1 Introduction

Stricter regulations for air pollution are apparent in many parts of the world. To comply with the regulations, new solutions and equipment to reduce the air pollutions must be developed. This thesis tries to find solutions for the paper industry pollution problems globally. The main scope is on the pollution-laden outlet gases in the paper mill ventilation. Additionally, the thesis tackles heat recovery in air-air-type of heat exchangers with a newer model than Törnqvist (2011). The model has its basis on two-phase flow with a condensate film and condensing water vapour.

The aim together with TM Systems is to research some theories on the heat exchanger with film flow and to verify and calculate air pollution prevention with existing equipment. Also, some minor topics on general industrial ventilation and water treatments are considered. All together they can form a package for future development of the process and for future equipment configuration.

2 Background

2.1 TM Systems

TM Systems is a company founded 1974 in Turku, Finland. The company supplies various ventilation and heat recovery products and services for the pulp and paper industry. The products help the customers to achieve less energy consuming production and more effective and healthy working environments for the workers, among others. The company has its headquarters in Turku and subsidiaries in Russia and China. TM Systems has broad expertise in its field, with personnel from diverse backgrounds in the paper industry.

2.2 Purpose

In a world where more attention is continuously paid to air pollution, new solutions to reduce the pollutions have to be reached. Air pollution is a global problem, with thousands of different pollution sources, which together have negative effects on the planet and human health. The pollution types dealt with in this thesis are typical for the paper industry; particle contamination and gaseous compounds. Already now, and in the adjacent future, the restrictions for the discharge of the contaminants will continuously become stricter. For a long time in Finland, great effort has been made in different industries to reduce air pollution. Simultaneously, some other parts of the world might have struggled with making new restrictions or had trouble following them. As a result, some parts of the world are only now making stricter regulations on their pollution policies.

TM Systems steps in here. One purpose of this thesis is to research and develop processes to reduce the air pollution in the paper industry globally. Globally, the new laws and regulations regarding air pollution are made in new areas, and new solutions to meet the regulations are needed. Some of the theories discussed in this thesis might enable the development of pollution reducing equipment, specifically in the paper industry.

The considered pollutants are particles and gaseous compounds. One example of the particles are cellulose fibres, in various sizes. The fibres loosen and come off in the paper making process, and from there they can contaminate the working environment. With proper ventilation system, the fibres flow with air away from the working environment but remain in the air stream. From the ventilation system the fibres are discharged into the atmosphere, causing air pollution.

Harmful gaseous compounds are numerous. One group of these gaseous compounds are the volatile organic compounds (VOCs), which are present in the paper making process, since paper is an organic material. Coating materials and glues are also organic materials

used in the paper making process, and they can also contribute to the number of VOCs polluting the paper mill environment. Many VOCs are harmful to human health, and areas with VOC sources need to be ventilated. Without proper treatment of the ventilated air, the VOCs become air pollution from the paper mill.

The air treatments in this thesis are based on water. Water acts as a carrier, it absorbs the gaseous compounds and binds the particles from the air stream. The use of water will transfer the contaminants from the air into the water. As a side topic, the cleaning and treatment of the water is introduced.

The other main purpose of the thesis is to study more closely the heat recovery process of specific heat exchangers. The paper making process requires a paper machine, which dries the paper. For effective drying, proper ventilation of the paper machine is required. The ventilation exhaust air mainly contains recoverable energy in the form of water vapour from the paper drying. One way to recover the energy is by the use of air-air heat exchangers, where energy is transferred from one air stream into another. The heat transfer models for this type of heat exchanger are studied more closely. The thesis also addresses the condensation and the resulting condensation film inside the heat exchanger. The condensate film creates two-phase flow conditions in the heat exchanger, which can affect the total heat recovery. The knowledge and theory behind the film flows in the heat exchanger can assist in developing even more efficient equipment.

3 Heat transfer and liquid film dynamics inside an air-air heat exchanger

3.1 Heat recovery with an air-air heat exchanger in a paper mill

In the process of drying paper in a paper machine, a significant amount of energy is used. The end box in the paper machine feeds wet paper mass on the wire in the wet end. The paper mass drains in the wet end. After the wet end of the paper machine, the paper mass normally goes through a press section, where moisture from the paper mass is pressed out to a certain degree. After that, the paper dries further in the drier section of the paper machine, where the paper line is heated through heated rolls, which, are heated with steam. The dry content of the paper after the drier section is dependent on the customers' paper quality. Therefore, the amount of water evaporation in the drier section varies between paper machines. The drier section is normally covered with a hood, which will collect the evaporated water vapour. Some typical values for the hot and humid air inside the dryer section hood are $80 - 85°C$ and $120 - 180$ g_{H_2O}/kg_{da} (TM Systems, 2019).

The hot and humid air in the hood contains a significant amount of recoverable energy. The energy can be recovered with a heat exchanger, where a cold medium can absorb some of the recoverable energy from the hot and humid air. The cold medium can be air, water or a mixture of water and glycol. In this thesis, the cold medium is air, and more specifically outside air, e.g. from the paper machine hall rooftop. The temperature of the outside air varies with the geographical location of the paper machine, season and time of the day. The heated cold air is used as ventilation air to the paper mill. Typically, there is a requirement for the minimum temperature which the cold medium has to reach before leaving the heat exchanger, and to design the heat exchanger correctly one has to account for the different weather conditions to ensure the minimum temperature after the heat exchanger. The cold medium, the cold air, can be heated after the heat exchanger with e.g. steam coils, but the use of steam coils is not energy saving. The cold air is blown after the coils into the paper machine hall or inside the hood. The air-air heat exchanger can also be a part of a whole heat recovery unit, which can consist of several heat exchangers, fans and other equipment (TM Systems, 2019).

The design of the heat exchanger may vary and is determined, among others, by the cold medium, investment cost, space available, location on site and location geographically. The air-air heat exchanger design discussed in this chapter consists of smooth metal plates and the cold and the hot streams flow cross-currently. The design can be seen in Figure 1. The slots between the plates are narrow, about 15 mm, in order to maximize the heat exchanger

area without making the heat exchanger physically too large (TM Systems, 2019).

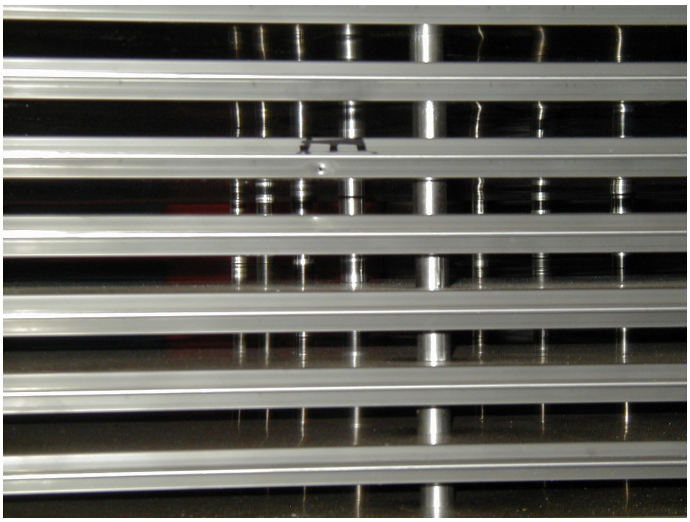

Figure 1: An air-air heat exchanger with smooth plates. A typical cross-current flow setup; The hot air runs straight down into the picture, while cold air runs from left to right inside the closed plates (TM Systems, 2019).

3.2 Air flow inside the heat exchanger

In this chapter, the basic design of the air-air heat exchanger is introduced. The hot and cold flows are cross-current, but normally in practice, the flows are modelled counter-currently, and after that, the cross-current flow setup is calculated.

When the airflow encounters the air-air heat exchanger, it can be assumed that the airflow distributes itself evenly into the different slots. That means it can be assumed there is an equally large volume flow of air in every slot. The total humid air volume flow can be determined with air mass flow and humid air density. The humid air density is calculated as follows, according to Lampinen (2015):

$$\rho_{air} = \rho_{da} + \rho_v, \tag{1}$$

where

$$\rho_{da} = \frac{p_{da} M_{da}}{RT} \tag{2}$$

and

$$\rho_v = \frac{p_v M_v}{RT}. \tag{3}$$

M_{da} and M_v is the molar mass of dry air and water vapour respectively. R is the universal gas constant and T is the air temperature in the SI-unit Kelvin. The partial pressures, p_{da} and p_v, form together the total air pressure (Lampinen, 2015):

$$p_{tot} = p_{da} + p_v. \tag{4}$$

To calculate the partial pressure of water vapour, p_v, see Lehtinen (2017). With the air volume flow, $\dot{V}$, one can calculate the average air velocity inside the heat exchanger. For N number of slots in the heat exchanger, the average velocity in one slot can be calculated:

$$v_{air,\,ave} = \frac{\dot{V}}{A_{st}N}, \tag{5}$$

where A_{st} is the slot flow area. For a rectangular slot with side lengths w and b, $A_{st} = wb$.

The heat transfer inside of a slot is highly dependent on the air flow conditions. To determine the flow conditions inside the slot, Reynolds number for the flow can be calculated. Reynolds number is a dimensionless number that tells when the flow is turbulent or laminar. Turbulent flow is preferred since a laminar flow causes the shear forces in the fluid to damp the fluid oscillations, resulting in poorly mixed fluid layers, which then leads to impoverished heat transfer (Incropera et al., 2011). For a smooth pipe, the Reynolds number can be determined according to Incropera et al. (2011):

$$Re_{air} = \frac{\rho_{air} v_{air,\,ave} d_h}{\mu_{air}}. \tag{6}$$

To calculate the humid air viscosity, μ_{air}, see Lehtinen (2017). d_h is the hydraulic diameter. For a circular tube, the hydraulic diameter is the tube diameter. But for other tube shapes, the hydraulic diameter has to be calculated. In the air-air heat exchanger, the tube has a rectangular shape, and the hydraulic diameter can be expressed according to Beek et al. (1999):

$$d_h = \frac{2wb}{w+b}. \tag{7}$$

According to Incropera et al. (2011), the fluid flow has a transition from laminar to turbulent at $Re = 2,300$, so that the flow is laminar for $Re < 2,300$. Incropera et al. (2011) state that the zone for partially turbulent flow is $2,300 < Re < 4,000$. To achieve the highest possible heat transfer, and to achieve completely turbulent flow, one should prefer $Re > 4,000$.

3.3 Heat flows inside the heat exchanger

Any two bodies, microscopic or macroscopic, that have a temperature difference between them, also have heat transfer between them. The heat transfer can be seen as one or many heat flows, and according to the first law of thermodynamics, the heat flows always have the direction from the higher temperature to the lower temperature. The three main mechanisms for heat flow are: Conduction, convection and radiation.

Conduction can be explained as molecular vibration or molecular movement. When molecules vibrate (solids and standstill liquids) or collide (gases) randomly, they give some of their momentum to the molecule with which they collided or vibrated with. That way they pass on their heat energy. Therefore, heat conduction can also be seen as heat diffusion. Conduction for fluids requires that the fluids have no bulk motion (Incropera et al., 2011).

Convection has to do with fluid bulk motion. When the fluid bulk moves over a surface, with a different temperature than the surface, it conduces to heat transfer. Adding to the bulk movement, there is also the random movement of the microscopic molecules that also contributes to the heat transfer. Both the bulk movement and the microscopic movement form the heat convection. Convection can be divided into sensible and latent heat exchange. The first, the sensible heat exchange, consists of forced and natural convection. In industry applications, the more common is the forced convection, where the fluid movement is accomplished with a fan or a pump. Natural convection is a more natural phenomenon, e.g. hot air rising in the atmosphere. In some processes natural and forced convection can be combined. The second, the latent heat exchange, has to do with phase changes. The latent heat exchange occurs always attached to sensible heat exchange (Incropera et al., 2011). Latent heat exchange can be either boiling or condensation, and the condensation is of interest in this air-air heat exchanger application.

Radiation is emitted from a material. It is usually considered for solid material, but also fluids can emit radiation. Radiation consists of moving waves, more specifically electromagnetic waves of photons. When these waves approach a material, they can be absorbed, reflected or transmitted, depending on the specific material properties (Incropera et al., 2011). Radiation is not considered in the heat transfer models in this thesis.

The setup for the heat transfer in the heat exchanger, consists of slot-wise metal plates between the cold and warm medium (air), and the flows are treated as counter-current. The heat goes from the hot and humid air to the cold air on the other side of the plate wall. The heat flow from the hot and humid air is both sensible and latent, which means that air humidity condenses on the plate wall. This forms a condensation layer on the metal plate, which then means that the condensation is assumed to occur on a water layer instead of the metal plate. Figure 2 shows the heat flows. The heat flow from the hot and humid air is

combined forced convection and condensation ($\dot{q}_{conv,1.1}$ and $\dot{q}_{conv,1.2}$), the heat flow through the water film and metal plate is conduction ($\dot{q}_{cond,2}$ and $\dot{q}_{cond,3}$) and the heat flow into the cold air is forced convection ($\dot{q}_{conv,4}$).

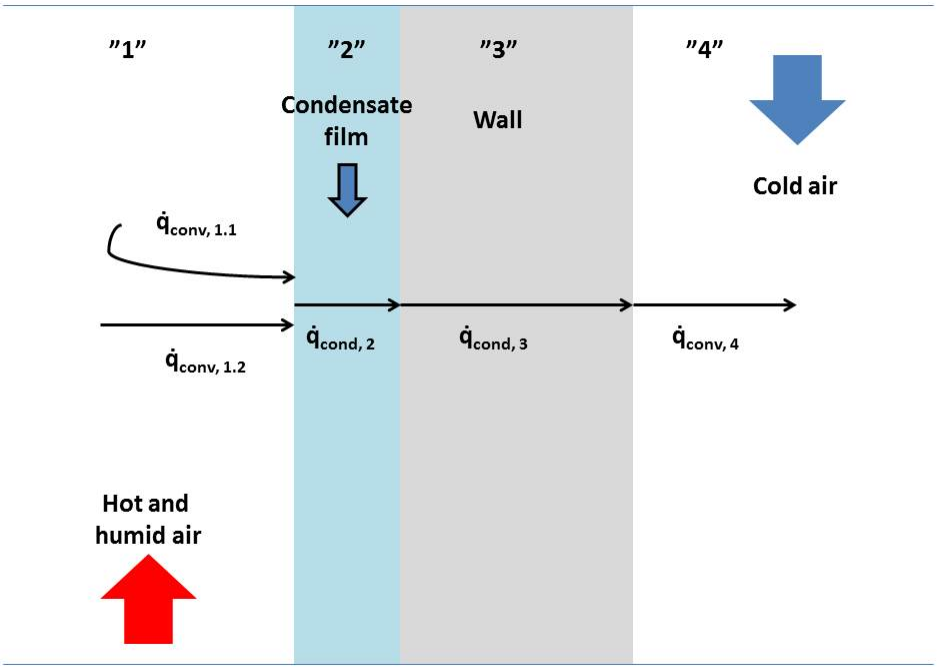

Figure 2: The heat flows in the air-air heat exchanger.

3.4 Liquid film dynamics

To be able to fully understand the fluid dynamics and to be able to calculate heat flows inside the heat exchanger, a understanding of film flow mechanics is needed. The condensate film is present on the hot air side of the heat exchanger, and that film is considered in this chapter. A falling film is a gravity driven flow, where a thin layer of liquid falls downwards over a surface (Spedding, 2010). The surface can be inclined, but in the studied heat exchanger the surface is vertical and consists of smooth metal plates. For a more complete description of the heat exchanger, see Chapter 3.1. The liquid film flow dynamics are complex, and in some cases they require complex numerical calculations done with e.g. Computational Fluid Dynamics (CFD), or experiments to accurately measure the conditions. Here is presented a less complex method to calculate film characteristics in the heat exchanger. First is presented the calculations for a free falling film, then the counter-current film flow and its flooding phenomenon and lastly the co-current film flow downwards.

3.4.1 Free falling liquid film

When a liquid falls downwards over an inclined flat surface, without any shear stress from the surrounding air or gas on top of the film, the flow is called free falling film flow. According to Bird, Stewart and Lightfoot (2007), the average falling film velocity can be calculated with Equation 8:

$$v_{ff} = \frac{\rho_l g \delta_{ff}^2 \cos\beta}{3\mu_l}, \tag{8}$$

where g is the gravity constant, δ_{ff} is the film thickness and β is the inclination angle from a vertical plane (for a vertical plate $\beta = 0°$). When the total condensate mass flow ($\dot{m}_{cond}$) and the heat exchanger geometry is known, one can derive another expression for the average film falling velocity. With a known total heat exchanger area $A_{h.e.}$, one can calculate the total volume of liquid film on the metal plates inside the heat exchanger:

$$V_{tot,l} = A_{h.e.}\delta_{ff}. \tag{9}$$

The condensate volume flow ($\dot{V}_{cond} = \dot{m}_{cond}/\rho_l$) is used to calculate the film falling time, t_{ff}:

$$t_{ff} = \frac{V_{tot,l}}{\dot{V}_{cond}} = \frac{A_{h.e.}\delta_{ff}\rho_l}{\dot{m}_{cond}}. \tag{10}$$

The average velocity for the film, v_{ff}, can be expressed with the distance the film has fallen, which is the plate height (H), under a certain time (t_{ff}):

$$v_{ff} = \frac{H}{t_{ff}} = \frac{H\dot{m}_{cond}}{A_{h.e.}\delta_{ff}\rho_l}. \tag{11}$$

Equation 8 combined with Equation 11 makes an expression for the film thickness:

$$\delta_{ff} = \sqrt[3]{\frac{3H\dot{m}_{cond}\mu_l}{A_{h.e.}\rho_l^2 g\cos\beta}}. \tag{12}$$

The liquid film thickness is not uniform on the whole plate height, but the expressions presented here can be used to approximate the free falling film thickness. The film flow can be laminar, wavy laminar or turbulent. Under certain conditions the liquid film forms waves, which are presented by Spedding (2010). The film under the wavy conditions consists of a base film at the bottom, on which the wavy layer sits on top of. In order to more accurately estimate the film flow regime, the Reynolds number for the liquid film has to be calculated. Spedding (2010) defines the liquid film Reynolds number:

$$Re_l = \frac{4\Gamma}{\mu_l}, \tag{13}$$

where Γ is the mass flow rate of liquid film per perimeter for one slot. In the case of an rectangular channel, Γ equals:

$$\Gamma = \frac{\dot{m}_{cond}}{2\,(w+b)\,N}. \tag{14}$$

To further model the wave structure for a free falling liquid film, one has to calculate the a-value introduced by Spedding (2010):

$$a = \frac{Re_l}{K_F^{0.1}}, \tag{15}$$

where

$$K_F = \frac{\rho_l \sigma_l^3}{g\mu^4}. \tag{16}$$

σ_l is the liquid surface tension. Spedding (2010) distinguishes different six top film wave types, for different a-values, according to Table 1. A picture of the major film types can be seen in Figure 3.

Table 1: Film flow regimes for a free falling liquid film (Spedding, 2010).

a-value (Eq. 15)	Top film layer	Bottom layer
$0 - 1.22$	smooth stratified	laminar
$1.22 - 2.88$	ripple sine wave	laminar
$2.88 - 140$	roll gravity wave	laminar
$140 - 1600$	capillary surge wave	laminar
$1600 - 2400$	capillary surge wave	turbulent
> 2400	overriding swell wave	turbulent

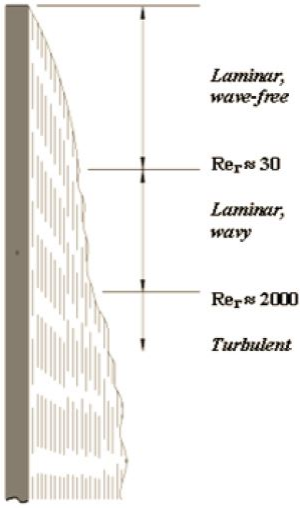

Figure 3: Simple schematic showing the major film regimes for a free falling film (Wolverine, 2007).

3.4.2 Film dynamics for counter-current flow

Inside the heat exchanger the condensate film flows downwards by gravitational force. At the same time hot air flows upwards, and has friction effects on the liquid film. Since air flows in the opposite direction than the film, the frictional forces slow down the liquid film. Assuming constant condensate mass flow, the film has to grow in thickness in order to maintain the same mass flow. The fluid dynamics for such two-phase flow condition is rather complex. A model suitable for the case of a narrow and rectangular channel, like the plates in the heat exchanger, is introduced by Drosos et al. (2006). Their method for calculating the mean film thickness requires that the counter-current flow is not under a critical condition, i.e. flooding. To estimate when flooding is present, see Section 3.4.3.

For counter-current flow inside a narrow, vertical and rectangular channel, Drosos et al. (2006) presented the following expression:

$$1 = \frac{\left(\rho_l - \rho_{air}\right) g - \frac{2}{w}\tau_{air} - \frac{2}{\phi_r b}\tau_{i,cc}}{\rho_l g}\left(\frac{\delta_{cc}}{\delta_{ff}}\right)^3 - \frac{3}{2}\frac{\tau_{i,cc}}{\rho_l g \delta_{ff}}\left(\frac{\delta_{cc}}{\delta_{ff}}\right)^2, \tag{17}$$

where:

- τ_{air} Air-wall shear stress (N/m^2)
- $\tau_{i,cc}$ Air-liquid interfacial shear stress for counter-current flow (N/m^2)
- δ_{cc} Liquid film thickness for counter-current flow (m)
- δ_{ff} Liquid film thickness for free falling film (m)
- ϕ_r Void fraction.

In Equation 17, the film thickness for counter-current flow can be solved in an iterative manner. The void fraction, ϕ_r, is the relative void of the channel and is also dependent on the film thickness (Drosos et al., 2006):

$$\phi_r = \frac{b - 2\delta_{cc}}{b}. \tag{18}$$

When air flows through the channel, it is slowed down by the wall shear stress (τ_{air}), the wall here being the slot length (b). Additionally, the condensate flows counter-currently against the air, and therefore exerts an interfacial shear stress ($\tau_{i,cc}$) on the air. The shear stresses can be calculated similarly (Drosos et al., 2006):

$$\tau_{air} = \frac{1}{2} f_{air} \rho_{air} v_{ave,\,air} \tag{19}$$

and

$$\tau_{i,cc} = \frac{1}{2} f_i \rho_{air} v_{ave,\,air}, \tag{20}$$

where

$$f_{air} = 0.079 Re_{air}^{-0.25}. \tag{21}$$

f_i is a friction factor for the interfacial shear stress. According to Sudo (1996), it can be estimated with an empirical formula:

$$f_i = 0.008 \left[1 + C_3 \left(\frac{\delta_{cc}}{d_h} \right)^{C_4} \right] \tag{22}$$

Following the same calculation scheme as Drosos et al. (2006) for Equation 22, δ_{cc} can be estimated with the Nusselt condensation formula, to make the calculations less complex. Developed by Wilhelm Nusselt, he created expressions for water vapour condensation on a falling film. Although the Nusselt formula requires that the vapour is pure, and not a mixture of air and water vapour, it can be used here. The particular expression for the Nusselt film thickness, δ_N, is given by Wolverine (2007):

$$\frac{\alpha_N(H)}{\lambda_l} \left[\frac{\mu_l^2}{\rho_l \left(\rho_l - \rho_{air} \right) g} \right]^{1/3} = 1.1 Re_l^{-1/3}, \tag{23}$$

where

$$\alpha_N(H) = \frac{\lambda_l}{\delta_N}. \tag{24}$$

$\alpha_N(H)$ is the heat transfer coefficient in the condensate film that changes with the plate height (H). $\alpha_N(H)$ cannot be used later in the Section 3.6, since the Nusselt condensation assumes pure water vapour. Rearranging Equation 23 together with Equation 24, one can obtain the same expression as Drosos et al. (2006):

$$\delta_N = \left(\frac{3\mu_l^2}{4\rho_l^2 g}\right)^{1/3} Re_l^{1/3}. \tag{25}$$

As already mentioned, the Nusselt film thickness (δ_N) can be used in Equation 22. The values for constants C_3 and C_4 are defined by Drosos et al. (2006):

$$C_3 = 41.3 Bo_h^{(C_4+0.25)} 10^{9.07/Bo_h} \tag{26}$$

and

$$C_4 = 1.63 + \frac{4.74}{Bo_h}. \tag{27}$$

The Bond number, Bo, describes the gravitational force related to the surface tension. Incropera et al. (2011) defines the Bond number:

$$Bo = \frac{g(\rho_l - \rho_{air})L^2}{\sigma_l}, \tag{28}$$

where L is a characteristic length and σ_l is the liquid surface tension. The Bond number in the formula above is usually used in the case of droplets or bubbles. For a condensate film Drosos et al. (2006) uses a modified Bond number, which is based on the hydraulic diameter, d_h:

$$Bo_h = d_h \left(\frac{g(\rho_l - \rho_{air})}{\sigma_l}\right)^{1/2}. \tag{29}$$

3.4.3 Liquid film flooding for counter-current flow

When the air velocity is large enough so that the interfacial shear force, caused by the air flow, is larger than the gravitational force acting on the condensate film, the condensate film can have a velocity profile that is positive in some parts and negative in some parts. Then it is possible that some part of the condensate film has the reversed direction, going upwards. The condensate going upwards can be in the form of film, droplets or other water "chunks". Liquid travelling in the opposite direction than supposed is called flooding (Drosos et al., 2006). For the purpose of this thesis, flooding is an unwanted phenomenon. The flooding starts to alter the liquid film characteristics, affecting the heat flow and the pressure loss.

That is why it is important to be able to predict when flooding inside the heat exchanger is present, thus to be able to avoid flooding. Figure 4 shows a principal picture of the flooding phenomena among other flow conditions. Note that under the (b) condition flooding is already present, since some portion of the condensate flow travels upwards. Conditions (c)-(e) are called post-flooding conditions, while condition (f) is co-current two-phase flow upwards.

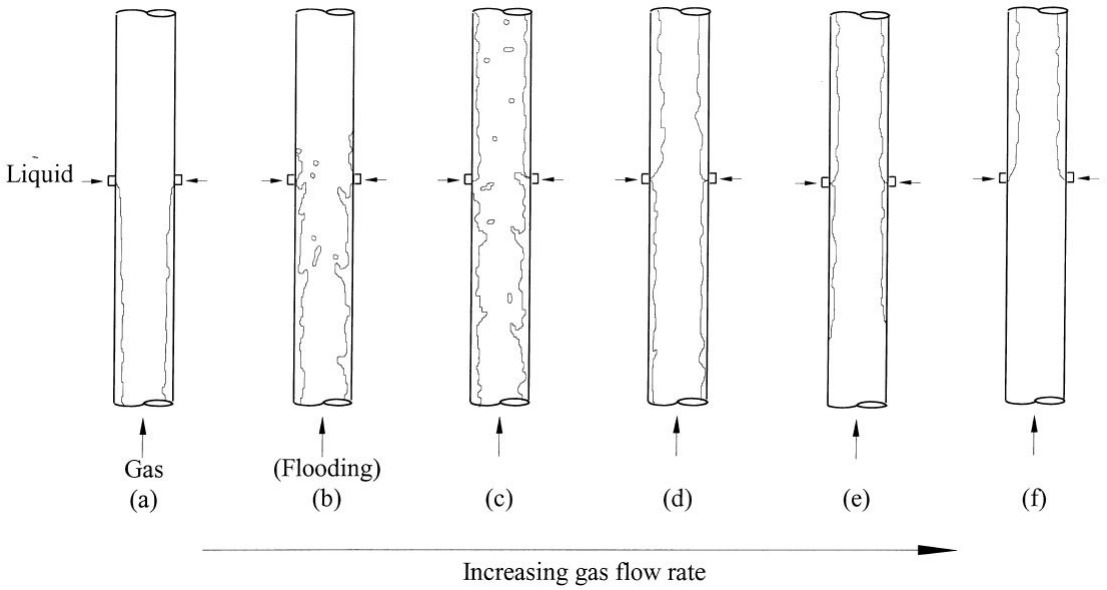

Figure 4: Different flowing schemes for counter-current vertical two-phase flow (Zapke & Kröger, 2000a).

The condensate film flooding criterion will be determined by two different methods, and the similarities and differences will be discussed. Drosos et al. (2006) covered even two other methods, but they do not fit the condensate flow rate present in the heat exchanger. The flooding criterion is given as a limit velocity for the condensate superficial velocity and gas superficial velocity. Superficial velocity is usually defined for two-phase systems, since a single phase velocity can be easily calculated, opposed to the two-phase velocity. For the liquid superficial velocity, one can calculate it by assuming the whole channel would be filled with condensate and flowing with a velocity corresponding to the mass flow:

$$v_{sl,l} = \frac{\dot{m}_{cond}}{\rho_l N w b}. \tag{30}$$

The gas velocity can, for a thin condensate film, be assumed to be the same as the superficial velocity ($v_{sl,air} \approx v_{air}$). With a known gas velocity, and the equations below, one can then determine the limit condensate superficial velocity. The real condensate superficial velocity

can also be determined when the condensate mass flow is known, and then one can compare the limit superficial velocity with the real superficial velocity and deduce about the flooding. The first flooding determining method is by Zapke and Kröger (2000a,b) and they proposed the following:

$$v^*_{sl,air} = \frac{0.0742}{v^*_{sl,l} Oh_l^{0.15}}, \tag{31}$$

where $v^*_{sl,air}$ and $v^*_{sl,l}$ are dimensionless and superficial air and liquid velocity. They are given by Wallis-type relations (Drosos et al., 2006):

$$v^*_{sl,air} = v_{sl,air} \sqrt{\frac{\rho_{air}}{gb\left(\rho_l - \rho_{air}\right)}} \tag{32}$$

and

$$v^*_{sl,l} = v_{sl,l} \sqrt{\frac{\rho_l}{gb\left(\rho_l - \rho_{air}\right)}}. \tag{33}$$

The Zapke and Kröger (2000a,b) method uses the Ohnesorge number for the condensate flow, Oh_l, and it can be calculated followingly (Drosos et al. 2006):

$$Oh_l = \sqrt{\frac{\mu_l^2}{\rho_l b \sigma_l}}. \tag{34}$$

The other method presented here is the method introduced by Drosos et al. (2006). Drosos et al. (2006) created a empirical equation combining the dimensionless and superficial Froude numbers for both air and water and the water Kapitza number:

$$Fr^*_{sl,air} = C_{fl} Ka_l^{0.4} \left(Fr^*_{sl,l}\right)^{-0.15}. \tag{35}$$

The dimensionless Froude numbers are defined by Drosos et al. (2006):

$$Fr^*_{sl,air} = \frac{\rho_{air} v^2_{sl,air}}{gb\left(\rho_l - p_{air}\right)} \tag{36}$$

and

$$Fr^*_{sl} = \frac{\rho_{air} v^2_{sl}}{gb\left(\rho_l - p_{air}\right)}. \tag{37}$$

In Equation 35, Drosos et al. (2006) uses for the constant $C_{fl} = 0.0138$ and defines the condensate Kapitza number:

$$Ka_l = \frac{\sigma_l}{\mu_l}\left(\frac{\rho_l}{\mu_l g}\right)^{1/3}. \tag{38}$$

The two methods give slightly different results. For the present heat exchanger, the Zapke & Kröger (2000a,b) method gives a higher limit velocity for the flooding than the Drosos et al. (2006) method. To not underestimate the flooding start-off, it is more safe to use the lower limit velocity, that being the velocity obtained by Drosos et al. (2006) method.

3.4.4 Co-current film flow downwards

At high air velocities, the condensate film flooding inside counter-current channel becomes dominant. The flooding is preferably avoided, since it will alter the smooth film condition and affect the heat flow calculations. The issue can be resolved by arranging the condensate film flow and air flow co-current downwards, meaning that no flooding is possible. To get the condensate film to flow in the same direction as the air, the air will have to flow downwards through the heat exchanger. This does not change the flow characteristics for the heat exchanger; hence the hot and cold flows are still cross-current.

In this thesis, downwards co-current two-phase flow, and its regimes, is studied. The flow regimes can be divided into three main regimes: Bubbly, slug and annular (Usui & Sato, 1989). The main regimes can be further divided into underclasses, but strict boundaries for the underclasses are not easily modelled, as shown by Lokanathan and Hibiki (2016). The main regime of annular flow is of particular interest in this thesis; since the gas flow rate is bigger than the liquid flow rate (the other flow regimes are present when the air flow rate is smaller than the liquid flow rate). In the litterature the different flow regimes are frequently plotted in a flow regime map. For downward two-phase flow, Usui (1989) plotted a flow regime map, shown in Figure 5. The flow regime map is restricted to a certain pipe diameter and Bond number. For other pipe diameters and Bond numbers different flow regime map must be used. Fr_L is the liquid Froude number and j_G/j_L is the volumetric velocity ratio for air to liquid. The dots are experimental results for different regimes, while the whole lines are the flow regime transition lines.

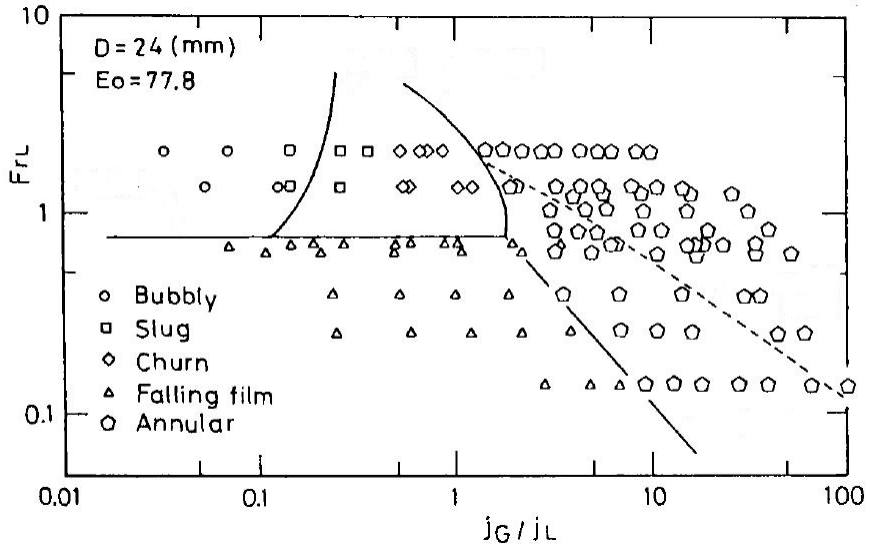

Figure 5: A flow regime map for downward vertical two-phase flow with pipe diameter of 24 mm and Eotvos number (Bond number) of 77,8 (Usui, 1989).

The liquid Froude number in the flow regime map is defined by Usui (1989):

$$Fr_l = \frac{v_l}{\sqrt{\frac{gd_h(\rho_l - \rho_{air})}{\rho_l}}}, \tag{39}$$

where v_l is the condensate film velocity downwards. The condensate film velocity can be calculated similarly for annular flow with Equation 11, when the film thickness for annular flow is known (δ_{an}). See Equation 49 and 50 for the film thickness.

Annular flow can be divided into falling film flow and annular drop flow (Usui & Sato, 1989). In the falling film flow the liquid is only present at the pipe wall as a film. In annular drop flow, there are liquid droplets in the gas phase as an addition to the liquid film at the pipe wall. The annular flow in the heat exchanger can be of falling film flow or of annular drop flow type. Since the literature does not have a clear flow transition zone for the falling-film-to-annular-drop-flow changeover, the criterion by Almabrok (2013) is used. The criterion was developed for co-current upwards flow and uses the Kutateladze number for air. The criterion, for when the two-phase flow is annular drop flow, is (Almabrok, 2013):

$$Ku_{air} > 3.1. \tag{40}$$

To determine the Kutateladze number for downwards two-phase flow, Almabrok (2013) presents three different calculation methods. In the first one Almabrok (2013) refers to Taitel, Barnea and Dukler, who calculates the Kutateladze number:

$$Ku_{air} = \frac{v_{air}\rho_{air}^{0.5}}{\left[\sigma_l g\left(\rho_l - \rho_g\right)\right]^{0.25}}. \tag{41}$$

The second method is by Richter (1981), and this method uses the hydraulic diameter in the Bond number:

$$Ku_{air}^2 = -75\frac{1 - \left(1 + \frac{Bo_h^2 f_w}{75}\right)^{0.5}}{Bo_h}, \tag{42}$$

where Bo_h is the modified Bond number defined in Equation 29. f_w is the pipe wall friction factor and Almabrok (2013) uses a value of 0.008. Almabrok (2013) points out that the Richter (1981) method does not consider the flow rate. The third method is by McQuillan and Whalley (1985), and can be written in the form:

$$Ku_{air} = C_t(Fr_l^*)^{-0.22}Bo^{0.26}, \tag{43}$$

where C_t is a constant, Fr_l^* is a modified Froude number and Bo is the Bond number, calculated using Equation 28. McQuillan and Whalley (1985) uses $C_t = 1.0$. The modified liquid Froude number is calculated as Almabrok (2013):

$$Fr_l^* = \frac{\Gamma g^{0.25}\left(\rho_l - \rho_{air}\right)^{0.75}}{\sigma^{0.75}}, \tag{44}$$

where Γ is the condensate flow per one channel perimeter (see Equation 14). Almabrok (2013) uses the McQuillan and Whalley (1985) method, since it considers both flow rates and pipe diameter. It is also used in this thesis.

The literature does not completely cover easily usable equations for the amount of droplets in the air, referred as the liquid entrainment rate, for different pipe sizes and configurations for downwards co-current vertical two-phase flow. Therefore, a simple Figure 6 by Kulov et al. (1979) for the liquid entrainment rate, can be used for a coarse estimation. The liquid entrainment rate, E, is given in volume percentage (transferred from the film into the air). Figure 6 is for a pipe diameter of 25 mm, different air velocities ($a = 50$, $b = 40$, $c = 30$, $d = 20$ m/s), liquid film Reynolds number, Re_l, and different measurement heights. The full curves corresponds to the measurement height of 300 mm, the broken curves to 500 mm and the curves with more frequent dashes corresponds to 1350 mm. As can be seen, the entrainment rate differs for different measurement heights, which means that the film thickness varies with the entrainment rate. For the heat exchanger used in the thesis, one can conclude from the film Reynolds number and air velocity that the entrainment rate will always stay under 5%. This means that the entrainment rate is assumed to not affect the

heat transfer inside the heat exchanger. Additionally Almabrok (2013) mentions that the entrainment rate is highly sensitive to the way of liquid injection into the gas flow. For two different injection types Almabrok (2013) had differences up to 60% in the liquid entrainment rate. Therefore, one should take extreme care when estimating the entrainment rate without an experimental setup.

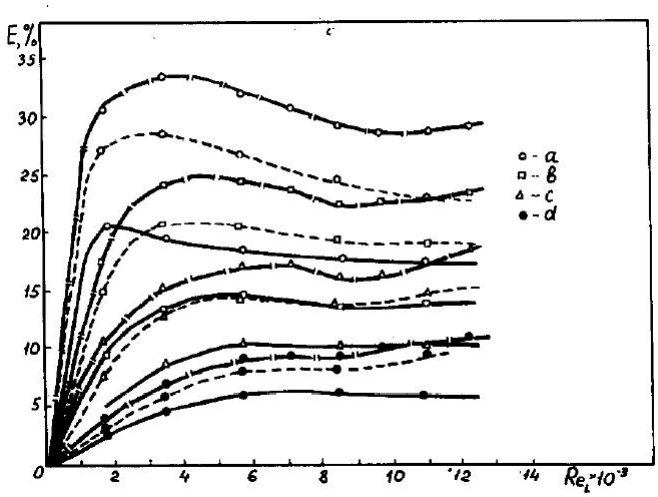

Figure 6: Liquid entrainment rate (E) for co-current film flow downwards (Kulov et al., 1979).

To calculate the film thickness for downwards co-current two-phase flow, δ_{an}, the literature offers a few different methods. Here three different methods are presented. Almabrok (2013) presents the Henstock and Hanratty (1976) method. The method uses the liquid and gas Reynolds number, which are based on the liquid and air superficial velocity. Henstock and Hanratty (1976) defines:

$$\frac{\delta_{an}}{d_h} = \frac{6.59C_1}{(1+1400C_1)^{0.5}}, \tag{45}$$

where

$$C_1 = \gamma \left(\frac{\upsilon_l}{\upsilon_{air}}\right)\left(\frac{\rho_l}{\rho_{air}}\right)^{0.5} Re_{air}^{-0.9}, \tag{46}$$

where

$$\gamma = \left[\left(0,707Re_{sl,l}^{0.5}\right)^{2.5} + \left(0,0379Re_{sl,l}^{0.9}\right)^{2.5}\right]^{0.4}. \tag{47}$$

υ is the kinematic viscosity of the fluid and Re_{sl} is the liquid Reynolds number based on the superficial liquid velocity. Kinematic viscosity is defined as dynamic viscosity divided by the

density, $\upsilon = \mu/\rho$ (Incropera et al., 2011). The Reynolds number for the superficial liquid velocity can be calculated similarly as Re_{air}:

$$Re_{sl,l} = \frac{\rho_l v_{sl,l} d_h}{\mu_l}. \tag{48}$$

The two next methods will be using the condensate film Reynolds number, since Lokanathan and Hibiki (2016) defined them accordingly. Lokanathnan and Hibiki (2016) states that the Karapantsios (1989) formula was developed for pipes with a "smaller" diameter (in the range <50 mm):

$$\delta_{an} = 0,45 \left(\frac{\upsilon_l^2}{g} \right)^{\frac{1}{3}} Re_l^{0.45}. \tag{49}$$

Almabrok (2013) modified the Karanpantsios (1989) formula for a larger pipe diameter (101.6 mm), and the modification should be applicable for smaller pipe diameters as well. Lokanathnan and Hibiki (2016) gives the modified formula, by Almabrok (2013), expressed with Re_l:

$$\delta_{an} = 1,4459 Re_l^{0.3051} \left(\frac{g}{\upsilon_l^2} \right)^{-\frac{1}{3}}. \tag{50}$$

The hydraulic diameter for the channel inside the heat exchanger lies in the range <50 mm. For the heat exchanger, the formulas 49 and 50 give slightly different results. Though, the difference in mm lies inside the standard deviation for the Almabrok (2013) formula, which is 0,1 mm. To be able to use Henstock and Hanratty (1976) formula, it needs to be updated in the way Almabrok (2013) introduces. Therefore, the author uses both the Equation 49 and 50, and chooses to use the bigger value to avoid underestimating the film thickness. Underestimating the thickness can lead to falsely improved heat transfer.

3.5 Pressure drop inside the heat exchanger

In this section the pressure drop in the air flow caused by the shear stress inside one heat exchanger flow channel is discussed. The pressure drop caused by the air entering the heat exchanger, and exiting the heat exchanger, is not considered. The flow conditions inside the heat exchanger changes when the condensation film is taken into account in the flow dynamics. The friction losses on a condensate film must be calculated differently than the friction losses on a pipe wall.

For a smooth pipe, the wall friction factor can be given by the pipe manufacturer, or it can be estimated with a formula. E.g. Aliyu et al. (2016) expresses the friction factor as a

factor of air Reynolds number:

$$f_w = 0.046 Re_{air}^{-0.2}. \tag{51}$$

When the friction factor is known, one can calculate the shear force acting on the fluid (Incropera et al., 2011):

$$\tau_w = \frac{1}{2} f_w \rho_{air} v_{air}^2. \tag{52}$$

For a smooth, horizontal and rectangular pipe with a single phase air flow the pressure drop equals (Incropera et al., 2011):

$$\Delta p = \tau_w H \frac{L_{pr}}{A_{ch}} = \tau_w H \frac{2\,(w+b)}{wb}, \tag{53}$$

where L_p is the channel perimeter and A_{ch} is the channel area. H, the height in the prior equation, is actually the pipe length, since the pipe is horizontal. For a vertical pipe the gravity effect can be considered, especially for small pressure differences, and then Equation 53 becomes:

$$\Delta p = H \left[\tau_w \frac{2\,(w+b)}{wb} \pm g \rho_{air} \right], \tag{54}$$

where the sign $\pm$ depends on the flow direction of the air (upwards/downwards).

3.5.1 Pressure drop for counter-current two-phase flow

With the two-phase flow, one cannot use the pipe smoothness as a single friction factor without considering the interfacial forces between the two phases. Drosos et al. (2006) showed that the interfacial shear stress ($\tau_{i,cc}$), for counter-current flow inside a narrow channel, can be calculated with Equation 20 and the wall shear stress (τ_w) with Equation 19 or with the Incropera et al. (2011) Equation 52. For counter-current flow, the air flow area is $w\,(b - 2\delta_{cc})$. Assuming no condensate film on the short end, the short wall shear stress is the short end length minus the film thickness on the both sides, and the interfacial shear stress length is the channel width on both sides. Therefore, Equation 54 for counter-current two-phase flow becomes:

$$\Delta p = H\left[\tau_w \frac{2\left(b-2\delta_{cc}\right)}{w\left(b-2\delta_{cc}\right)} + \tau_{i,cc}\frac{2w}{w\left(b-2\delta_{cc}\right)} + g\rho_{air}\right] = H\left[\tau_w \frac{2}{w} + \tau_{i,cc}\frac{2}{\left(b-2\delta_{cc}\right)} + g\rho_{air}\right]. \tag{55}$$

In the counter-current heat exchanger the air flows upwards, so the gravity effect is therefore increasing the pressure drop. For a clearer view of the different shear stresses, see Figure 7.

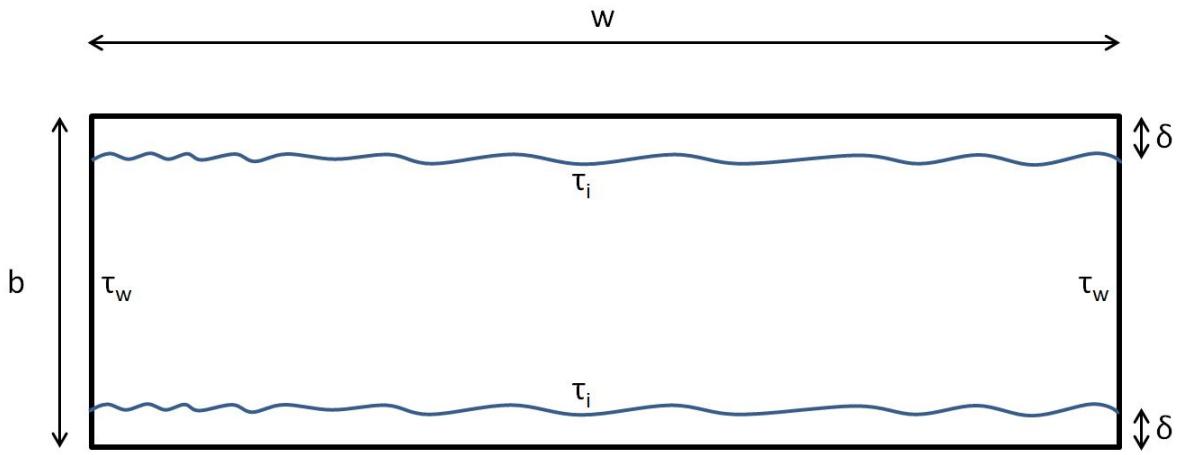

Figure 7: Dimensions and the shear stresses inside a heat exchanger slot with a condensate film present. τ_i is the interfacial shear stress between the air and the film, while τ_w is the wall shear stress between the air and the short wall. Air flows straight into or straight out of the slot.

3.5.2 Pressure drop for co-current annular flow

For the co-current two-phase vertical downwards flow, Aliyu et al. (2016) developed a new model for pressure drop in larger pipe diameters than the literature usually addresses. Aliyu et al. (2016) states that the new model may not be applicable outside of the ranges $11,300 < Re_l < 113,000$ and $3,756 < Re_{air} < 187,000$. For the a condensate flow, Re_l is usually well below 11,300. The author tried the model in a condensate film calculation, and it did not give reliable results for the governing conditions. Aliyu et al. (2016) also compared the new model with a handful of other models, and among them is the Fukano et al. model. The Fukano et al. model is valid for the governing conditions and is therefore used in this thesis. Aliyu et al. (2016) refers to Fukano et al.:

$$\frac{f_{i,an}}{f_{sl,air}} - 1 = 8.53 \cdot 10^{-4} X^{2.82} Re_{air} Re_{sl}, \tag{56}$$

where $f_{i,an}$ is the interfacial shear stress factor, $f_{sl,air}$ is the single phase air friction factor (calculated with Equation 51) and Re_{sl} is the Reynolds number for the condensate flow calculated with the condensate superficial velocity, see Equation 48. X is a Lockhart-Martinelli parameter. Lockhart-Martinelli-method is a two-phase flow calculation method, based on if only a single phase flow where present in the pipe (Lockhart & Martinelli, 1949). Aliyu et al. (2016) defines:

$$X = \sqrt{\frac{\Delta p_{sl,l}/\Delta H}{\Delta p_{sl,air}/\Delta H}}, \tag{57}$$

which for the same height for both liquid and air, can be abbreviated into the same form as Lockhart and Martinelli (1949):

$$X = \sqrt{\frac{\Delta p_{sl}}{\Delta p_{s,air}}}. \tag{58}$$

Aliyu et al. (2016) gives the expressions for the single phase pressure loss per meter:

$$\Delta p_{sl,l}/\Delta H = \frac{1}{2}\frac{f_{sl,l}\rho_l v_{sl,l}^2}{d_h} \tag{59}$$

and

$$\Delta p_{sl,air}/\Delta H = \frac{1}{2}\frac{f_{sl,air}\rho_{air} v_{air}^2}{d_h}. \tag{60}$$

The single phase air shear stress factor, $f_{sl,air}$, can be calculated with e.g. Equation 51. Similarly for the single phase liquid shear stress, Equation 51 can be modified into (Aliyu et al., 2016):

$$f_{sl,l} = 0.046 Re_{sl,l}^{-0.2}. \tag{61}$$

With the same assumptions as in counter-current flow, the total pressure drop can be expressed similarly for co-current annular flow:

$$\Delta p_{an} = H\left[\tau_w \frac{2}{w} + \tau_{i,an}\frac{2}{(b-2\delta_{cc})} - g\rho_{air}\right]. \tag{62}$$

For co-current flow the flow direction is downwards, so the gravity will decrease the total pressure drop. The interfacial shear stress for annular flow, $\tau_{i,an}$, is calculated with the interfacial shear stress factor, $f_{i,an}$:

$$\tau_{i,an} = \frac{1}{2} f_{i,an} \rho_{air} v_{air}^2. \tag{63}$$

3.6 Calculation of the heat flow

In order to determine the total heat flow, the two different heat flows from the hot air side have to be calculated. One of them is the latent heat transfer, and to calculate the mass transfer of condensation onto the water film, the literature have developed models where the gaseous phase often consist of pure water vapour. In the heat exchanger the gas phase is made of a mixture of water vapour and air. For the mixture, Lampinen and Seppälä (2017) presented a method where the total heat flow, $\dot{Q}$, consists of the latent and sensible heat transfer on the warm side, and from the warm side of the wall to the cold air, of conduction and forced convection. The method by Lampinen and Seppälä (2017) is the following:

$$\dot{Q} = \alpha_1 A_1 \left(T_1 - T_3\right) + \dot{m}^{"}_{cond} A_1 \Delta h_v = \frac{A_4}{\frac{s_3}{\lambda_3} + \frac{1}{\alpha_4}} \left(T_3 - T_4\right), \tag{64}$$

where:

$\dot{Q}$	Heat flow (W)
α	Heat transfer coefficient $\left(\frac{\mathrm{W}}{\mathrm{m^2K}}\right)$
$\dot{m}^{"}_{cond}$	Mass flow of condensation per area $\left(\frac{\mathrm{kg}}{\mathrm{m^2s}}\right)$
Δh_v	Specific evaporation enthalpy $\left(\frac{\mathrm{J}}{\mathrm{kg}}\right)$
s	Wall thickness (m)
λ_3	Wall thermal conductivity $\left(\frac{\mathrm{W}}{\mathrm{m \cdot K}}\right)$.

The different indices, in Equation 64, are: 1 – hot air, 3 – wall and 4 – cold air. They can also be seen in Figure 2. For a method on how to calculate the specific evaporation enthalpy, Δh_v, see Lehtinen (2017). To determine the heat transfer coefficients, α, for the forced convection on the hot and cold side, the Nusselt number has to be calculated. The Nusselt number, Nu, and the heat transfer coefficient are related according to Incropera et al. (2011):

$$Nu = \frac{\alpha d_h}{\lambda_{air}}. \tag{65}$$

The thermal conductivity, λ_{air}, for humid air can be calculated with the method presented in Lehtinen (2017). The Nusselt number is dependent on the flow conditions in the heat

exchanger. The method presented here is valid for any turbulent condition (also for the transition between partially and completely turbulent). Cengel (2008) presented the method with a maximum error of 10%:

$$Nu = \frac{\frac{f}{8}\left(Re - 1000\right)Pr}{1 + 12.7\left(\frac{f}{8}\right)^{0.5}\left(Pr^{1/3} - 1\right)}, \tag{66}$$

where

$$f = \frac{1}{\left[0.79ln\left(Re\right) - 1.64\right]^2}. \tag{67}$$

That being said, Incropera et al. (2011) recommends the use of Equation 66 only for $Re > 3,000$, although Incropera et al. (2011) mention that Equation 66 gives acceptable results for the rest of the partially turbulent region ($Re > 2,300$). The friction factor, f, is dependent on the pipe smoothness, but as Törnqvist (2011) notice, other expressions including the pipe smoothness still gives the friction factor similar results as Equation 67.

The thermal boundary layer and the related velocity is described by the Prandtl number, Pr, and is illustrated by Cengel (2008):

$$Pr = \frac{\mu_{air} c_{p,\,air}}{\lambda}. \tag{68}$$

Specific heat for humid air, $c_{p,\,air}$, can be calculated with the formula in Lehtinen (2017).

Although Equation 64 can be used for routine heat exchanger calculations, in this work the condensation film is of particular interest. So, the model in Equation 64 does not consider the condensation film to have any effect on the heat flow through it. Therefore, Equation 64 has to be modified in order to model the temperature effect of the condensate film. The condensate film is considered as a new layer to the wall, and is shown in Figure 2. The thickness of the water film can be calculated with the methods in Chapter 3.4. With the methods for heat conduction through composite walls by Bird et al. (2007), one can use the additivity of resistances to add the water layer to heat flow calculation. Here it is assumed that the condensation film has a low velocity downwards. With the addition of the condensation film and using the resistance theory Equation 64 becomes:

$$\dot{Q} = \alpha_1 A_1 \left(T_1 - T_2\right) + \dot{m}^{"}_{cond} A_1 \Delta h_v = \frac{A_4}{\frac{\delta}{\lambda_2} + \frac{s_3}{\lambda_3} + \frac{1}{\alpha_4}} \left(T_2 - T_4\right). \tag{69}$$

The differences to Equation 64 are that the temperature difference is now between the condensate film temperature and the respective air temperature, and that the water layer

(condensate film) thickness, δ, with the water thermal conductivity (λ_2) are added to the heat conduction part.

The mass flow of condensation per area, $\dot{m}^{"}_{cond}$, in Equation 64 and Equation 69 describes the condensation rate of water vapour on the surface in the hot side. For the calculation of the mass flow of condesation per area in the case with no condensate film, Törnqvist (2011) refers to Hogan et al.:

$$\dot{m}^{"}_{cond} = M_v \frac{p_{tot}}{RT_{air,\,sat}} k_v ln\left(\frac{p_{tot} - p_{v,\,wall,}}{p_{tot} - p_{v,\,air}}\right). \tag{70}$$

To be able to use this model in this work, it has to be modified. The condensation layer is added, and subsequently the Equation 70 becomes:

$$\dot{m}^{"}_{cond} = M_v \frac{p_{tot}}{RT_{1,\,sat}} k_v ln\left(\frac{p_{tot} - p_{v,\,2,}}{p_{tot} - p_{v,\,1}}\right), \tag{71}$$

where $p_{v,\,2}$ is the water vapour pressure at the boundary layer of the condensation film. It can be assumed that the boundary layer has the same temperature as the condensation film. The mass transfer coefficient for water vapour in dry air, k_v, can be calculated with the heat and mass transfer analogy. In mass transfer, Sherwood number, Sh, is defined analogically as Nusselt number in heat transfer (Cengel, 2008):

$$Sh = \frac{k_v d_h}{D_{v,\,d.a.}}. \tag{72}$$

Törnqvist (2011) advices that the Sherwood number can be calculated analogically to the Nusselt number with Equation 66, by substituting Prandtl number for Schmidt number (Sc):

$$Sh = \frac{\frac{f}{8}\left(Re - 1000\right) Sc}{1 + 12.7\left(\frac{f}{8}\right)^{0.5}\left(Sc^{1/3} - 1\right)}, \tag{73}$$

where f is calculated as in Equation 67. The Schmidt number is calculated according to Incropera et al. (2011):

$$Sc = \frac{\mu_{air}}{\rho_{air} D_{v,\,d.a.}}. \tag{74}$$

The mass diffusion coefficient of water vapour in dry air, $D_{v,\,d.a.}$, can be calculated with the method shown here, presented by Törnqvist (2011), who further refers to Rao et al.:

$$D_{v,\,d.a.} = \frac{1.87 \cdot 10^{-10} \cdot T_{air}^{2.072}}{\frac{p_{tot}}{10^5}}. \tag{75}$$

It is noteworthy that the temperature T_{air} is in the Kelvin unit.

4 Industrial ventilation regulations in paper mills

Industrial ventilation in paper mills can be rather complex. Air from the process, the paper drying, must be properly removed, since the drying is dependent on the air capacity to take moisture from the paper line. The paper machine hall and the operating rooms have to be ventilated so that the paper machine operators have a comfortable working environment. At the same time, air from the machine hall goes into the paper machine hood. Fresh air from outside is blown into the machine hall, and has to be planned so that there is no condensation occurring when the cool outside air enters the machine hall. There are also many more viewpoints of the ventilation, and different solutions to different paper mills. Some universal aspects regarding air quality inside the paper mill will be discussed in this chapter.

To illustrate the inside climate in a building, the different air flows in a building are classified. The different air flows in an industrial building, and their names according to the regulations from the Ministry of the Environment (2003), can be viewed in Figure 8. The airs or air flows are called: 1. Outside air, 2. Incoming air, 3. Transfer air, 4. Outlet air, 5. Return air, 6. Discarded air, 7. Circulation air and 8. Inside air. A closer examination of the transfer, return and circulating air (flows 3, 5 and 7 in Figure 8) is undertaken here, while a closer look on the incoming air is taken in the next section. Distinguishing between return and circulating air is important, as they are easily intermixed. Tähti et al. (2000) give a clear explanation of the circulating air as air that is removed from a space and returned, treated or not, into that same space. Circulating air can be treated, led through machinery and mixed with outside air and still be circulating air, if it is returned to the same space. This means that air contaminants cannot be led from one space to another when it is circulating air. Returned air is air that is removed from a space and returned into an another space. The returned air can be mixed with other airs and treated as well. Transfer air is air that goes straight from one space into another (Tähti et al., 2000). Since returned air goes between at least two different spaces, it can spread air contaminants and, therefore, returned air has stricter regulations than circulating air. Some more specific regulations on the use of return air can be found in the Ministry of the Environment (2003) regulations to 13§ in 132/1999.

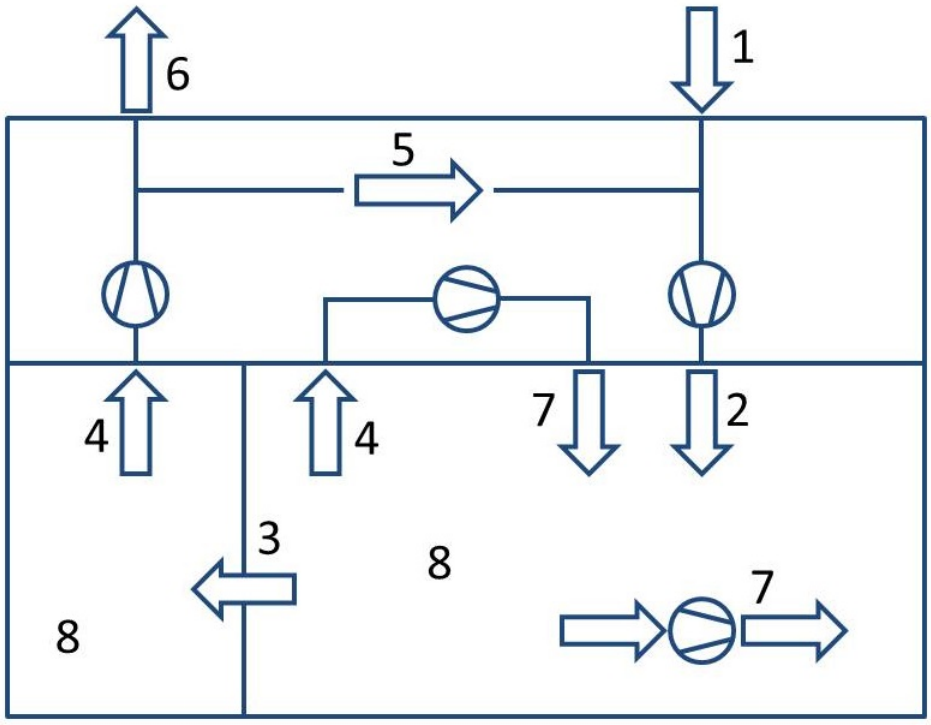

Figure 8: Air flows in a building.

Outlet air is air that is taken from a space and either used as transfer air, circulating air, returned air or discarded air. Outlet air is divided into different classes depending on the space and the contaminant sources that the air is coming from. The different classes determine if the removed air can be used as return or transfer air. Ministry of the Environment (2003) distinguishes four classes:

- Class 1. Outlet air with little contaminants and they originate from humans or building structures. The air can be used as return or transfer air. E.g. offices and business spaces are in class 1.
- Class 2. Outlet air with some contaminants. The air can be used as transfer air to some spaces, as sanitary rooms, but not as return air. E.g. dressing rooms and dining rooms are in class 2.
- Class 3. Outlet air that is contaminated by humidity, processes, chemicals and smells and therefore decreases the air quality. The air is not used as transfer or return air. E.g. sanitary rooms, kitchens and working process spaces are in class 3.
- Class 4. Outlet air that contains significantly more than acceptable concentrations of

contaminants for inside air. The air is not used as transfer or return air. E.g. fume hoods, laboratories, smoking rooms and solvent handling rooms are in class 4.

4.1 Incoming air

Regarding incoming air into the different spaces in the paper mill, the air has to be filtered. The incoming air can be outside, returned or circulation air. Different spaces have different filtering requirements and Tähti et al. (2000) categorise industry spaces into six different incoming air space types:

1. Covered process space. Typical space where working is done in short periods, and there are no fixed workstations. The air contaminants come from the process and the spaces are typical in basic chemistry, paper and metal industry. The paper machine hall is a type 1 space.

2. Industry working space. Spaces with constant working stations or with constant working; an example is workshops from the workshop industry. Typically better air distribution and channelling.

3. Space with special cleanliness. A space that has extra requirements for the process or the products, e.g. paper mills that produce food packaging. Stricter filtering than for spaces 1 and 2.

4. Special spaces. Spaces as electrical rooms and operating rooms. These spaces usually have separate instructions for the air filtering.

5. Laboratories, kitchens and smoking rooms.

6. Clean rooms. These spaces have always separate instructions made for them.

Tähti et al. (2000) mention that choosing the filter is difficult, mainly because of the EUROVENT 4/9-1997 filter classes, which are six (EU3–EU8). In Finnish practice, according to Tähti et al. (2000), three filter targets are used when choosing a filter. They are based on target values for the particle removal, and can correspond to the EUROVENT classes, when the filter penetration is max. 10%. Tähti et al. (2000) classify the filters and the corresponding EUROVENT standards when the maximal penetration is 10%, as in Table 2. In Table 2 can also be seen the corresponding EN779:13 filter classes, which have the same condition as the EUROVENT filter classes.

Table 2: Filter classes and their removal of different particle sizes.

Finnish target value (T)	Particle removal	EUROVENT 4/9-1997	EN779:13
Target value 5 (T5)	Removes particles $> 5\,\mu m$	EU4	G4
Target value 1 (T1)	Removes particles $> 1\,\mu m$	EU7	F7
Target value 0.5 (T0.5)	Removes particles $> 0.5\,\mu m$	EU8	F8

The incoming air to the space types defined above have certain filters specified for them. Tähti et al. (2000) gives different criteria for incoming air origin. Here is presented a simplified table, Table 3, of the different filters for different spaces.

Table 3: Filter classes for different industrial spaces (Tähti et al., 2000).

Space type	1.	2.	3.	4.	5.	6.
Outside air filter	T5[1,2,3)]	T1	T0.5	T0.5	T1[3)]	separate instructions
Circulation air filter	T1	T1	T0.5	T0.5	-	separate instructions

1) If the incoming air is channelled, it is recommended to use T1.

2) The incoming air can also be unfiltered, but fan and other equipment might not be able to function properly in unfiltered air.

3) Before heat recovery equipment it is recommended to use T1, and if the equipment can not be easily cleaned, it is recommended to use T0.5.

4.2 Air contaminants

When usually referring to air, one assume that air is a mixture of gases: N_2, O_2, H_2O, CO_2 and some other gases at very low concentrations. Those are the components of "pure" air, but in reality air is almost always polluted or mixed with some other compound that makes air "impure". The mixed in component may not be a problem, but when the component has harmful effects that affect human health, the air is contaminated (Seinfeld & Pandis, 2016). In almost every country there are set limits for the contaminant concentrations for a working environment. In Finland, the Finnish Secretary of State issues smallest known harmful concentrations of air contaminants regularly, and employers must follow these limit values (Tähti et al., 2000). If the values are exceeded, the employer has to immediatly take action to reduce the concentration. In Finland, the limit values are known as HTP-values (*haitalliseksi tunnettu pitoisuus)*. In the international Industrial Ventilation Design Guidebook they are referred as OEL-values (Occupational Exposure Limits, Moreno-Beltrán & Grau-Rios, 2001). OEL-values for contaminants for different countries are e.g. listed by databases such as GESTIS (GESTIS International Limit Values, Institute for Occupational Safety and Health of the German Social Accident Insurance). In this chapter, two different

contaminant classes will be discussed separately: Particulate matter and harmful gases and vapours.

4.2.1 Particulate matter; dust

Particulate matter is liquid or solid particles of any substance in normal condition air (Seinfeld & Pandis, 2016). The exception for the definition is water. To be able to identify and classify particulate matter, not only the concentration of particulates is of interest, but also the particulate sizes are important. Particulate size is typically referred as PM-size in diameter, and e.g. PM_{10} corresponds to particulates that are $< 10\,\mu$m in diameter (Seinfeld & Pandis, 2016). Similarly $PM_{2.5}$ corresponds to particulates $< 2.5\,\mu$m in diameter. Particulates can have many shapes and sizes, and therefore the diameter used is important. In aerosol technology, the diameter referred to in PM-sizes is usually the aerodynamic diameter. The aerodynamic diameter corrects for the particles not being spherical and their dynamic movement in air (Hinds, 1999). The definition for the aerodynamic diameter is that the aerodynamic diameter, d_{ae}, is the diameter of a sphere with the density of 1,000 kg/m^3 and the same settling velocity as the real particle (with the non-spherical shape) (Hinds, 1999). Particles with same settling velocities and densities have identical aerodynamic properties regardless of the particle shape. That is important, since particles are separated and measured utilising the aerodynamic properties.

The calculation of aerodynamic diameter for fibre-shaped particles can be done by methods introduced by Gonda and El Khalik (1985). To represent a fibre, they used the prolated spheroid shape. A schematic of a spheroid can be seen in Figure 9. The long diameter, d_1, divided by the shorter of the diameters d_2 or d_3, is referred to as the κ-value. For a prolated spheroid, the κ-value is $\gg 1$.

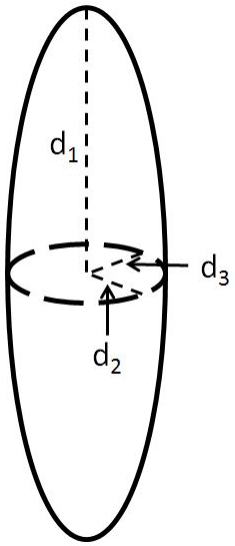

Figure 9: A schematic of a spheroid.

For a prolated spheroid, the aerodynamic diameter is (Gonda & El Khalik, 1985):

$$d_{ae} = d_{min} \sqrt{\left(\frac{1}{\frac{2}{9}\left(\frac{1}{\ln(2\kappa) - 0.5}\right) + \frac{8}{9}\left(\frac{1}{\ln(2\kappa) + 0.5}\right)} \right) \left(\frac{\rho_p}{\rho_0}\right)}, \tag{76}$$

where d_{min} is the shorter of the diameters d_2 or d_3. ρ_p is the particle density and ρ_0 is the reference density, usually 1,000 kg/m^3. From here on, in this thesis, when referring to particulates' diameter or size, it is assumed to be the aerodynamic diameter.

Particulates also have a size distribution. That means that the particulates have a range of diameters, and the range can be so large that it can stretch over two orders of magnitude (Hinds, 1999). Consider a cloud of particulates. Usually, the cloud of particulates is listed with their diameter and number of particulates with the same diameter in a long list. If the particulates are non-spherical, the aerodynamic diameter for them is calculated, and they are listed with the aerodynamic diameter. The list is usually so long, that the list is shrunk with shorter segments, so that the distribution is more easily illustrated. An example with a cloud of particulates, in this kind of list, can be seen in Table 4.

Table 4: A example of a size distribution for particulates.

Size range*, d (μm)	Count, n	Percent	Cumulative percent
0	0	0.0%	0.0%
4	94	9.4%	9.4%
6	140	14.0%	23.4%
8	161	16.1%	39.5%
9	87	8.7%	48.2%
10	67	6.7%	54.9%
14	180	18.0%	72.9%
16	61	6.1%	79.0%
20	100	10.0%	89.0%
35	90	9.0%	98.0%
50	17	1.7%	99.7%
60	3	0.3%	100.0%
Total	1000	100.0%	100.0%
*The size ranges' upper limit is given, the lower limit is in the cell above			

If one plots the size range against the cumulative percent of particulates, one will obtain a cumulative size distribution, as shown in Figure 10. From the plot, one can determine e.g. how many percent of the particles are in the PM_{10}-category; about 55% (the Table 4 happens to give the exact value, 54.9%). In the same way one can determine the $PM_{2.5}$-portion of the particulates; about 5%.

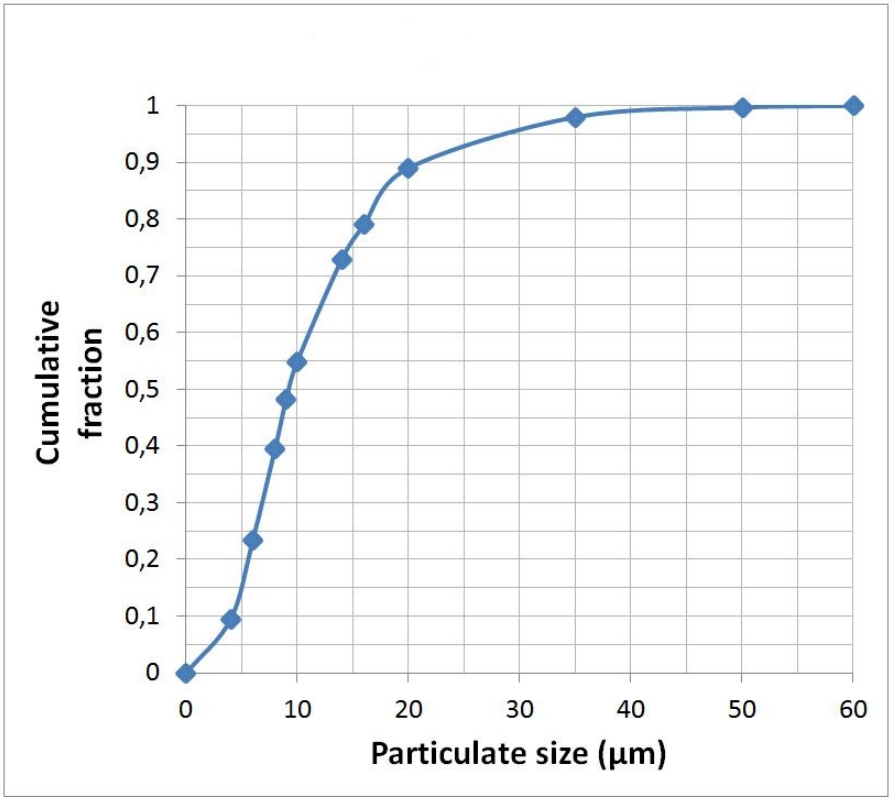

Figure 10: A cumulative particulate size distribution example according to the data for the particulates in Table 4.

Also, with the plotted cumulative size distribution the median average droplet size can be determined. The average particulate size is of importance, since the average size will be used in equipment design. Hinds (1999) defines several different average particulate sizes, and a few of them will be discussed here. The median particulate size is the particulate size on the 50% on the cumulative fraction axis in the cumulative size distribution. The median particulate size is the point when 50% of the particulates are bigger and 50% are smaller than the median (Hinds, 1999). For the data in Table 4, the median diameter is about 9.2 μm.

The rest of the discussed average particulate sizes can be calculated with the data in Table 4. The formulas for the calculation of the average particulate sizes are shown in the Table 5 below. For mass and heat transfer the Sauter mean diameter is usually used, since it gives the volume-to-area ratio, which is important for the transfers.

Table 5: A few different average diameters for the particulates distributions (Hinds, 1999).

Diameter	Formula	Value for the data in Table 4
Mean or arithmetic average	$\frac{\sum n_i d_i}{\sum n_i}$	13.63 μm
Geometric mean	$\exp\left[\frac{\sum n_i \ln d_i}{\sum n_i}\right]$	11.07 μm
Surface mean or Sauter mean	$\frac{\sum n_i d_i^3}{\sum n_i d_i^2}$	29.56 μm
Volume mean	$\frac{\sum n_i d_i^4}{\sum n_i d_i^3}$	36.70 μm

Particulate size is important when considering the harmfulness to humans. Smaller particulates penetrate deeper into our respiratory system, and usually the deeper they penetrate, the more damage they cause. According to Tähti et al. (2000), a generalised "most harmful" particle size is 2.5–3 μm. Much smaller particles as that will not get attached to our respiratory system. As two examples, Tähti et al. (2000), mention firstly, asbestos. Asbestos are small fibers with a diameter under 1 μm and length of a few μm, so they will penetrate into alveoli and are therefore very harmful. After a long time exposure to asbestos, it will e.g. cause lung cancer. The other example is coarse wood dust or saw dust. Tähti et al. (2000) says that wood dust does not penetrate into the lungs, but it will irritate mucous membranes in the nose and throat. Treated wood and board, which contain additives as glues and preservatives, can be more harmful when incorporated in the form of dust.

In a paper mill paper dust is the most known particulate matter air contaminant. As paper dries in the drying section of the paper machine, fibres will detach from the paper line and contaminate the air. Most of these fibres will be in the outlet air from the paper machine hood. Paper dust is also released from the paper rolls as it is treated after the drying process. Therefore, the paper machine hall can be dusty. Paiman et al. (2013) measured paper dust concentrations of PM_{10} size in a tissue paper mill in Malaysia. They measured both with personal sampling devices and stationary sampling devices, and received results that showed that the paper dust concentrations were above permitted levels. Paiman et al. (2013) refers to OSHA (Occupational Safety and Health Administration, USA) and ACGIH (Association Advancing Occupational and Environmental Health, USA) for the standard exposure limits for PM_{10} dust; for OSHA it is $5\,\mathrm{mg/m^3}$ and for ACGIH it is $3\,\mathrm{mg/m^3}$. Paiman et al. (2013) measured the personal dust concentrations from 14 workers working by the paper machine, and out of them ten worked by the machine and four in the control room. They

also measured dust concentrations from 14 workers who worked in the packaging area. For the 14 workers by the paper machine, the results were that the average dust concentration was about $8 - 9\,\mathrm{mg/m^3}$, with a range of $0.44 - 21.51\,\mathrm{mg/m^3}$. For the packaging area workers the results were even higher, average of $> 30\,\mathrm{mg/m^3}$ and a range of $2.29 - 63.08\,\mathrm{mg/m^3}$.

In Sweden, Westberg et al. (2016) measured inhalable dust concentrations in a pulp and paper mill in the middle of Sweden. They measured with personal sampling devices inhalable dust concentrations, PM_{10} concentrations and $PM_{2.5}$ concentrations among others. The results were: For inhalable dust the average concentration was $0.30\,\mathrm{mg/m^3}$, with a range of $0.005 - 3.3\,\mathrm{mg/m^3}$, for PM_{10} dust the average concentration was $0.17\,\mathrm{mg/m^3}$, with a range of $0.03 - 1.5\,\mathrm{mg/m^3}$ and for $PM_{2.5}$dust the average concentration was $0.08\,\mathrm{mg/m^3}$, with a range of $0.004 - 0.45\,\mathrm{mg/m^3}$. The results in Sweden are under the American exposure limits.

Separation of paper dust can be done with air filters. Companies, like EMCEL Filters Ltd., give out filter selection charts for different particulate sizes. One example can be seen in Figure 11.

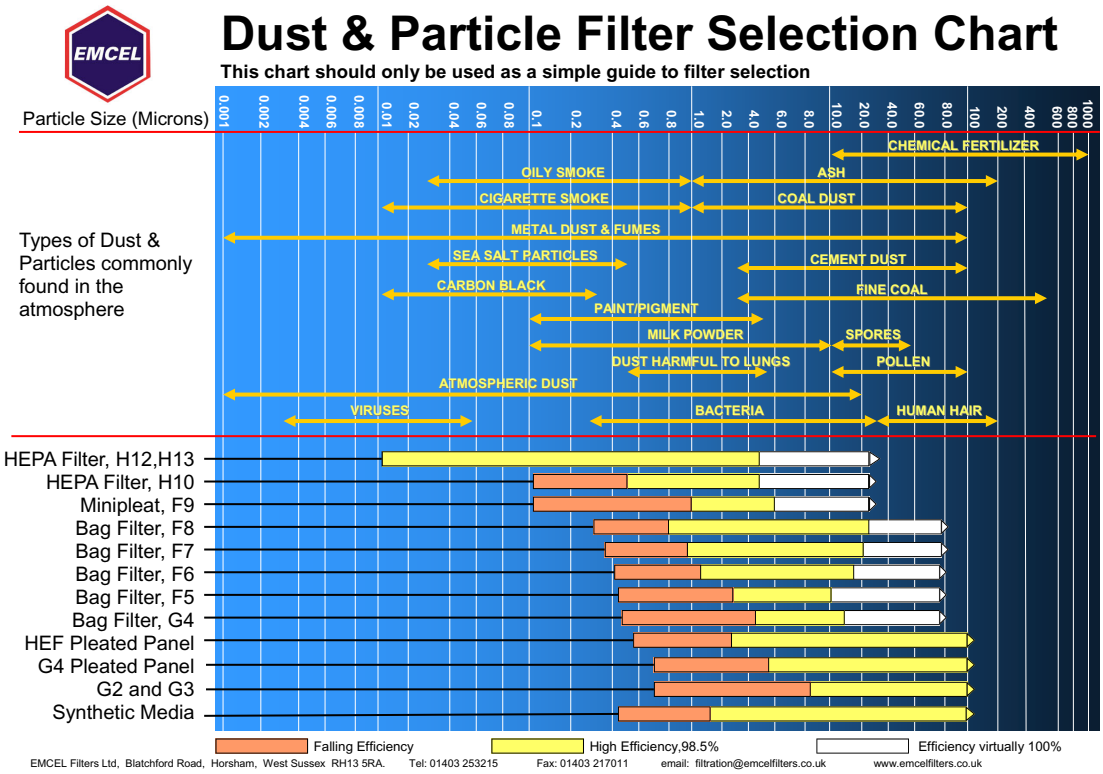

Figure 11: Filter selection chart for different particle sizes (EMCEL, 2019).

4.2.2 Harmful gases and vapours

Chemicals and chemical processes can be the source of gases and vapours that are harmful to human health. The gases and vapours can be odourless, colourless and harmful at very low concentrations. Usually they contaminate the body through breathing, but some may go through the skin (Tähti et al., 2000). There were about 60,000 known chemical contaminants in year 2000 (Tähti et al., 2000), and today there is even more. Most of those chemicals have an HTP-value, as defined above. Design values for air contaminants in a new building are defined by the Ministry of the Environment (2003). The design values are lower than the HTP-values. The design values are target values that the customer or ventilation user may require, but they have to be used for at least the building design. The measured concentrations in a new building, six months after commissioning, have to meet the design values when the ventilation has been on constantly for six months. Some of the design values are listed by the Ministry of the Environment (2003) and for some values they refer to the Finnish Secretary of State (2001). The listed values can be seen in Table 6. Tähti et al. (2000) points out that the design values are valid for a working space. That means, e.g. for an industry hall, that the hall can be seen as two different spaces; the ground space, which is a working space, and the space just under the hall roof, which is not a working space. The designed contaminant concentration values have to be valid for the ground space, where the work is done, and not necessary for the space under the roof.

Table 6: Design values for inside air contaminant concentrations (Ministry of the Environment, 2003 & Finnish Secretary of State, 2001) The average time is exposure time.

Ministry of the Environment (2003)			
Contaminant	Unit	Design value	Specification
Ammonia, NH_3	$\mu g/m^3$	≤ 20	
Asbestos	fibres$/m^3$	0	
Formaldehyde, CH_2O	$\mu g/m^3$	≤ 50	
Carbon monoxide, CO	mg/m^3	≤ 8	
Particles, PM_{10}	$\mu g/m^3$	≤ 50	
Radon	Bq/m^3	≤ 200	one year average
Styrene	$\mu g/m^3$	≤ 1	
Finnish Secretary of State (2001)			
Contaminant	Unit	Design value	Average time
Sulphur dioxide, SO_2	$\mu g/m^3$	≤ 350	1 hour
Sulphur dioxide, SO_2	$\mu g/m^3$	≤ 125	24 hours
Nitrogen dioxide, NO_2	$\mu g/m^3$	≤ 200	1 hour
Nitrogen dioxide, NO_2	$\mu g/m^3$	≤ 40	1 year
Particles, PM_{10}	$\mu g/m^3$	≤ 50	1 hour
Particles, PM_{10}	$\mu g/m^3$	≤ 40	1 year

For other contaminants, Ministry of the Environment (2003), lists the rules. For one dominant contaminant, the concentration can be a maximum of $\frac{1}{10}$ of the HTP-value (or OEL-value). For more than one contaminant, with unknown mixed effects, the maximal concentration is:

$$\sum_i \left[\frac{c_i}{(HTP)_i} \right] \leq 0.1, \tag{77}$$

where C_i is the concentration for one contaminant. In the pulp and paper industry, there are many organic compounds and processes with organic matter. Therefore, volatile organic compounds (VOC), and their limit values are important in the industry. Tähti et al. (2000), mentions two ways to account for VOC. They firstly give a design value for total VOC (TVOC), which is $< 5\,\mathrm{mg/m^3}$. Secondly, they mention that the formaldehyde concentration can be used as a relatively good index for the other VOC concentrations. They also say that a paper machine hall in Finland from 1990s typically have concentrations of formaldehyde below $0.1\,\mathrm{mg/m^3}$.

The concentration unit used previously is $\mathrm{mg/m^3}$ or $\mu\mathrm{g/m^3}$. Converting between those two is simple, it is a factor of 1000. But converting from $\mathrm{mg/m^3}$ to ppm, which is also an universally used concentration, can be more tricky. For NTP-conditions, Terrie and Boguski (2006) defined:

$$c_{i,ppm} = 24.45 \frac{c_{i,mg/m^3}}{M_i}, \tag{78}$$

where for an compound i; $c_{i,ppm}$ is the concentration in ppm, $c_{i,mg/m^3}$ is the concentration in $\mathrm{mg/m^3}$ and M_i is the molecular mass.

5 Air treatments with water

Air or gas flows containing impurities can be treated in order to reduce harmful emissions. A few different techniques using water as the main component to treat the contaminated gas are introduced. Firstly, gaseous contaminants, and specifically their removal techniques from the air, are discussed. Secondly, particle removal techniques from air are discussed. A summary of all of the treatment techniques discussed in this thesis can be seen in Table 7.

Table 7: The different air treatment techniques discussed.

Equipment	Impurity	
	Gases	Particles
Tray column	Absorption	Impaction, condensation
Spray chamber	Absorption	Impaction, condensation
Wetted-wall column	Absorption	Turbulent impaction

5.1 Tray absorption

A tray column is a high column with separation trays inside the column. A tray column can be used for both distillation and absorption. A distillation column operates near the boiling point for the liquid while an absorption column operates with the physical absorption of a gas to a liquid. The gas is a mixture of components from which some selected components are dissolved into the liquid when exposed to a large contact area (Perry & Green, 1998). A principal schematic of the absorption process can be seen in Figure 12. In an absorption process the liquid falls down through the column, while the gas moves upwards in the column. Component A is absorbed in the liquid. The liquid (L) is usually called absorbent. The incoming liquid can also have an initial concentration of component A.

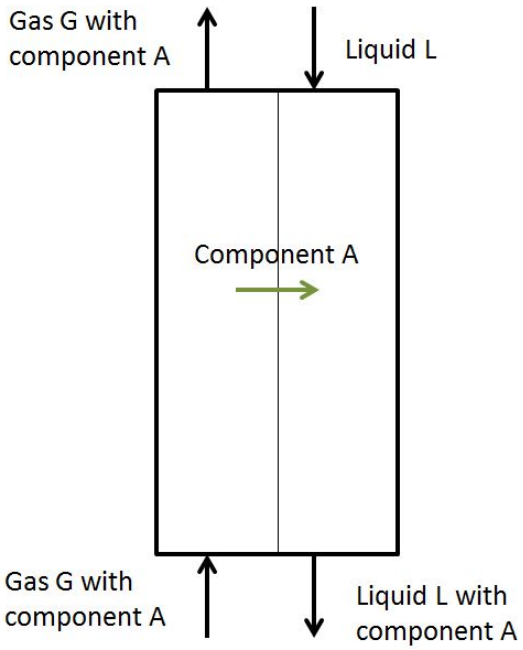

Figure 12: Schematic view of an absorption process.

According to Kriebel (2008), physical absorption is reasonable for a process when the process meets one of the following conditions:

- the gas components to be absorbed are present in relatively large amounts and the total pressure of the gas is high,
- the leaving gas from the absorber must be of high purity,
- the absorbed gas components are collected at high purity
- and the absorbent is a part of the process.

For cases when the concentration of the absorbed gas is relatively low, Kriebel (2008) points out that absorption with a chemical reaction (chemisorption) is preferred. Totally, Kriebel (2008) gives four criteria for when the chemisorption is preferred:

- low concentration of absorbed gas in the gas flow (also low partial pressure),
- not too high purity limits for the purified gas,
- the absorbed gases are acidic
- and waste heat for regeneration is available.

In this thesis the focus is on physical absorption.

Usually, literature mainly focuses on distillation type of tray columns. The absorption column type can be designed similarly to some extent, and therefore the designs illustrated here can be used for some rough calculations. In a typical distillation column the liquid flows on the trays inside the tower while the gas flows upwards; the flow setup is called cross-current flow. An overview of the cross-flow tray can be seen in Figure 13. The trays have openings in them so that the gas can flow through it, and the gas flow should aerate the liquid flow. The openings are designed so that the liquid should not flow through the holes. The tray openings can have different designs. The three main tray types are sieve trays, bubble-cap trays and valve trays (Kriebel, 2008). Illustrative pictures of the tray types are available from Sinnott et al. (2005). Also, the mechanical design of the cross-current plates can be done with methods by Sinnott et al. (2005).

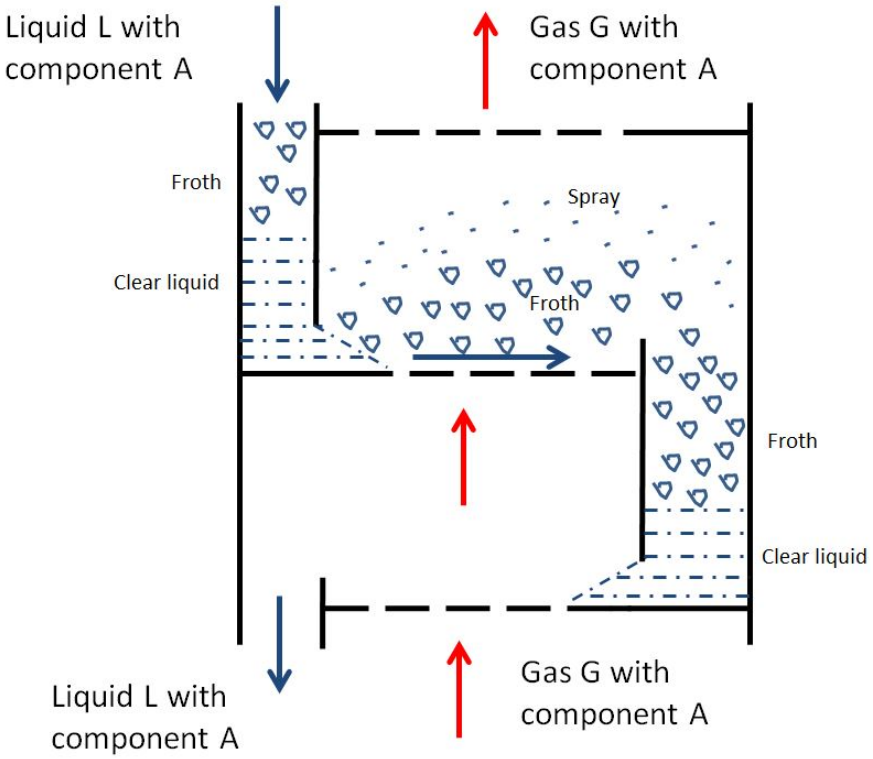

Figure 13: A typical cross-flow tray with different liquid flow zones.

The physical absorption relies on the absorbents potential to dissolve the gaseous component. The potential is dependent of the gaseous components phase equilibrium with the absorbent at the existing temperature and pressure (Perry & Green, 1998). For a small fraction of a component A in the absorbent, the phase equilibrium can be expressed with the well-known Henry's law (Perry & Green, 1998):

$$p_A = y_A p_{tot} = H_{cA} x_a, \tag{79}$$

where p_A is the partial pressure of component A, y_A is the mole fraction of A in the gas phase, H_{cA} is the Henry's law constant and x_A is the mole fraction of A in the liquid phase. H_{cA} is referred as a constant, but in reality it varies with both temperature and pressure. The literature offers accessible lists of different gaseous compounds and their Henry's law constant for different liquids. For the case when the liquid is water, Sander (2015) lists the Henry's law constants for different chemical compounds. The Henry's law constant can be expressed in many different units, and Sander (2015) also offers the conversion factors between the different units. There is also correction terms available for different temperature and pressures than the NTP-conditions. The used Henry's law constant in this thesis is the H^{xp}-form, in which the total pressure of 1 atm is cooperated. The unit for H^{xp} is $\frac{1}{\text{atm}}$.

5.1.1 Tray column design with graphical analysis

Designing a tray column, one needs to determine the number of trays in the tower. With the number of trays, one can further on determine the column height. The number of trays is typically determined graphically; the method is described by Perry and Green (1998). A form of Henry's law is drawn in a graph called the equilibrium line. The equilibrium line is given by Perry and Green (1998):

$$y = Kx, \tag{80}$$

where $K = 1/H^{xp}$. K is usually called the separation or absorption factor. The equilibrium line follows, in this form, the Henry's law. The equilibrium line is valid for conditions where the component occupies a small fraction. Zevenhoven (2015) advices that this small fraction is $<$ 2–5%. For larger fractions Zevenhoven (2015) refers to the Raoult's law.

The other line to be drawn in the graph to determine the number of trays, is the working line. Perry and Green (1998) express the working line:

$$\dot{n}_{air} \left(y - y_1\right) = \dot{n}_l \left(x - x_0\right), \tag{81}$$

where $\dot{n}_{air}$ is the total gas molar flow, $\dot{n}_l$ is the total liquid molar flow and y_1 and x_0 are points on the working line. To be able to draw the working line, the liquid and gas flows and a point from the line has to be known. The working line is a line describing the conditions inside the column. Therefore, the known point can be chosen e.g. to be the conditions at the top of the column. The assumed condition, at the top of the column for the liquid, is that

the liquid has a very low concentration of the compound A, therefore $x_0 \approx 0$. For the gas it can be assumed that the concentration of A is fixed by some requirement when leaving the column. With that information the working line can be drawn.

Numerical values for graphical analysis. A typical graph, with the equilibrium line and the working line, for determining the number of theoretical trays, can be seen in Figure 14. The condition on the top of the column is the lowest point on the working line. From there one starts to draw lines between the working and equilibrium line; first a horizontal line to the equilibrium line, then a vertical line up to the working line and so on. The last line will be drawn when one has reached the incoming compound concentration. In Figure 14, the compound A is ammonia (NH_3), the gas flow 1.4 kmol/s, the water flow 1.1 kmol/s, absorption constant K = 0.91 (NTP), outgoing ammonia concentration $2.8 \cdot 10^{-6}$ mol/mol and incoming ammonia concentration $8.0 \cdot 10^{-6}$ mol/mol. Incoming water is assumed to have no ammonia dissolved. There is one theoretical tray per one horizontal and vertical movement. That means that in Figure 14 there are two whole theoretical trays and one smaller movement in the graph. The smaller movement comes from that the incoming concentration of ammonia was $8.0 \cdot 10^{-6}$ mol/mol, so the horizontal movement can be stopped when the next vertical arrow will reach the concentration of $8.0 \cdot 10^{-6}$ mol/mol on the working line. The fraction of the last theoretical tray can be calculated as the length of the small horizontal arrow divided by a longer arrow (Perry & Green, 1998). The longer arrow is the horizontal arrow as if one would draw it the whole way to the equilibrium line. In 14 the length of the small arrow divided by the length of the longer arrow is about 0.3. That means that the total number of theoretical trays would be 2.3.

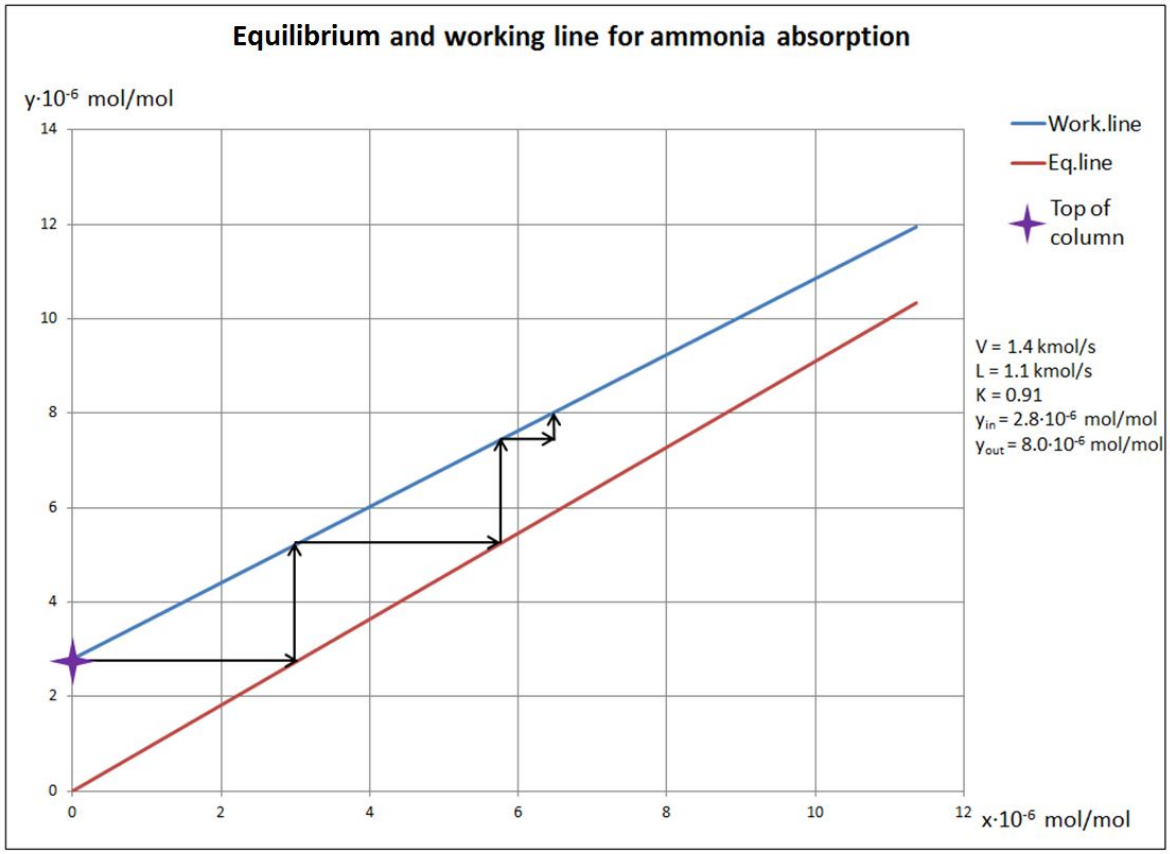

Figure 14: Determining the number of theoretical trays for an ammonia absorption process. V is the gas flow and L is the liquid flow. Number of theoretical trays is about 2.3.

For some cases the graph can look very different than in Figure 14. The equilibrium line and the working line might cross. Depending on where the lines cross, it might be that the desired absorption is physically impossible to do with the used input values. An example of this can be seen in Figure 15, with a water flow of 0.56 kmol/s. The number of trays would be infinite and the arrows will never reach the incoming gas conditions for the ammonia concentration. Also, if the liquid flow is reduced further, say to 0.05 kmol/s, and the outlet gas ammonia concentration to 0 mol/mol, the operating line will be for the most part under the equilibrium line. At those conditions the absorber will work as a stripper. A stripper function with desorption, which is the opposite of absorbing ammonia gas into the liquid. In a stripper the liquid will release ammonia into the gas. The absorption process has to be designed with enough liquid flow and relative strict outlet conditions for the gas compound concentration. Only then can the absorption be accomplished, as in Kriebel's (2008) conditions for the physical absorption.

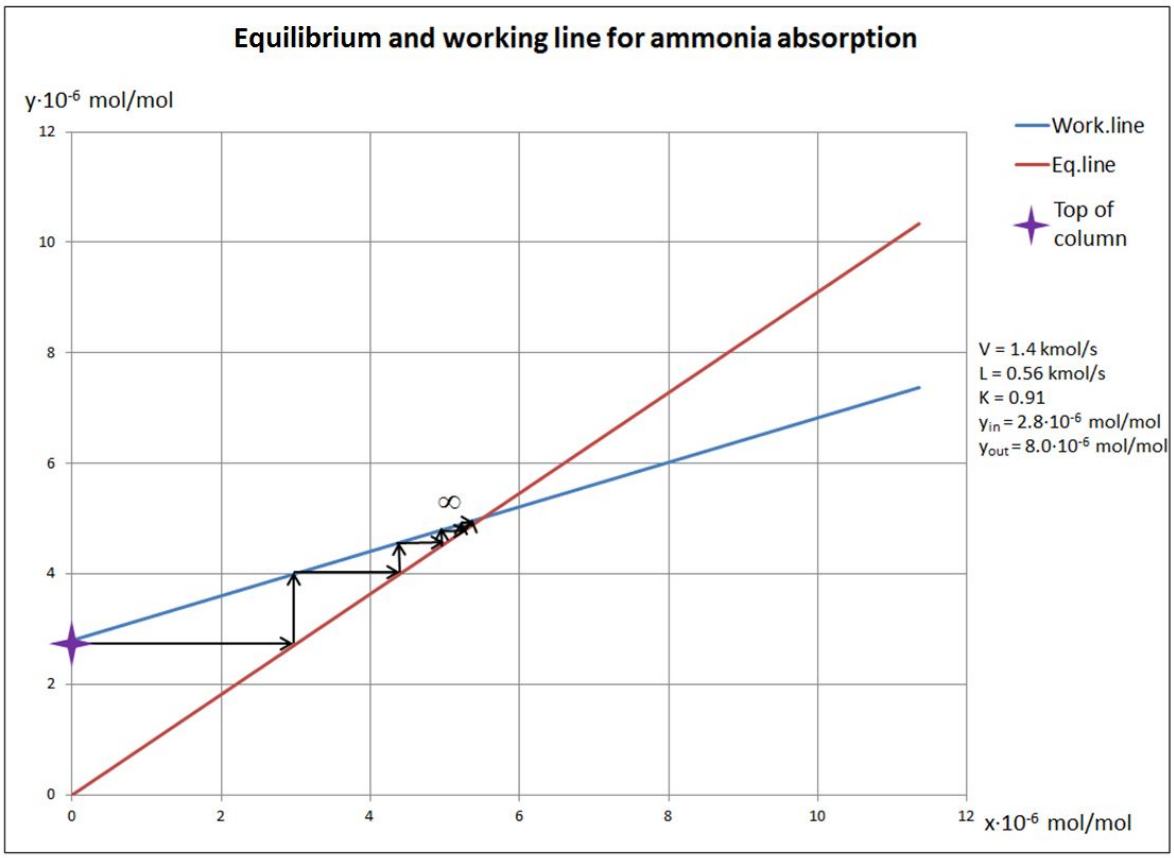

Figure 15: An example of an impossible absorption with corresponding input values. V is the gas flow and L is the liquid flow.

The method described until this point has the number of theoretical trays determined. But to design the column, the number of real trays has to be determined. Designing the number of theoretical trays, it is assumed that there is perfect mixing on the tray, so that the equilibrium between the gas phase and liquid phase is reached on every tray. That is not true in reality, so one has to correct for that the equilibrium is not reached. In the case of a distillation column the real efficiencies lies in the range 60–90%. In absorption the efficiencies are lower, for readily soluble compounds 30–40% and for hardly soluble compounds 18–25% (Kriebel, 2008). For a typical crossflow tray with bubble-caps, Sinnott et al. (2005) presented the O'Connell's absorber column efficiency, shown in Figure 16. The parameter X in Figure 16 is defined by Sinnott et al. (2005):

$$X = 0.062 \left[\frac{\rho_l}{\mu_l K M_l} \right], \tag{82}$$

where the viscosity unit is $\mathrm{mN} \cdot \mathrm{s/m^2}$.

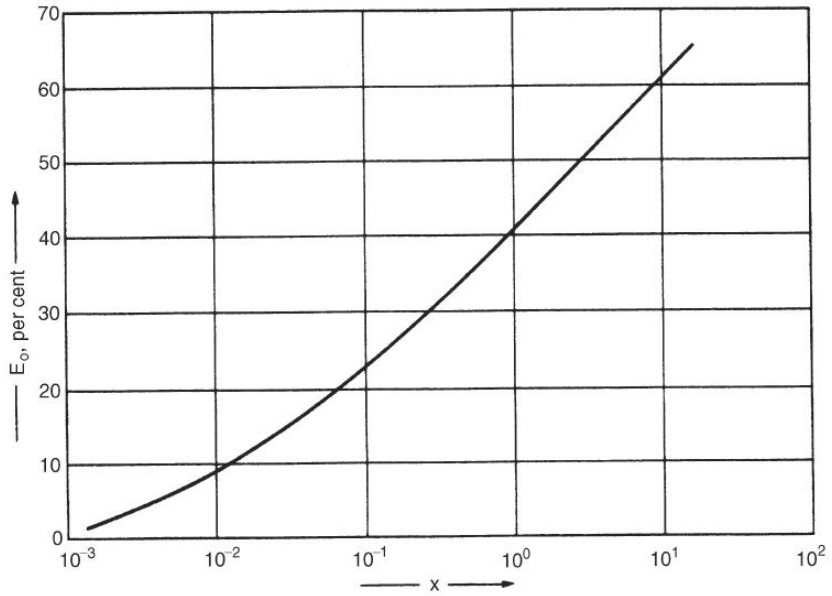

Figure 16: Overall efficiency (E_0) for an absorption column with bubble caps (Sinnott et al., 2005).

The overall efficiency of the absorption column, E_0, is defined as the number of theoretical trays divided by the number of real trays for the whole column (Sinnott et al., 2005). Another efficiency is the Murphree efficiency (E_{mV}), which is the real tray efficiency over a single tray for the gas side. They are related by Equation 83 (Sinnott et al., 2005):

$$E_0 = \frac{log_{10}\left[1 + E_{mV}\left(\frac{K\dot{n}_{air}}{\dot{n}_l} - 1\right)\right]}{log_{10}\left(\frac{K\dot{n}_{air}}{\dot{n}_l}\right)}. \tag{83}$$

When the Murphree efficiency is known, one can draw the modified equilibrium line in the graph with the working line. Perry and Green (1998) define the modified equilibrium line drawn with the Murphree efficiency as Figure 17 indicates. In Figure 17 is shown the modified equilibrium line, the old equilibrium line and the working line for the ammonia case with 2.3 theoretical trays. In Figure 17 the Murphree efficiency is 45% and the real number of trays is about 5.0. E_{mV} is defined as the length AB divided with the length AC (Zevenhoven, 2015).

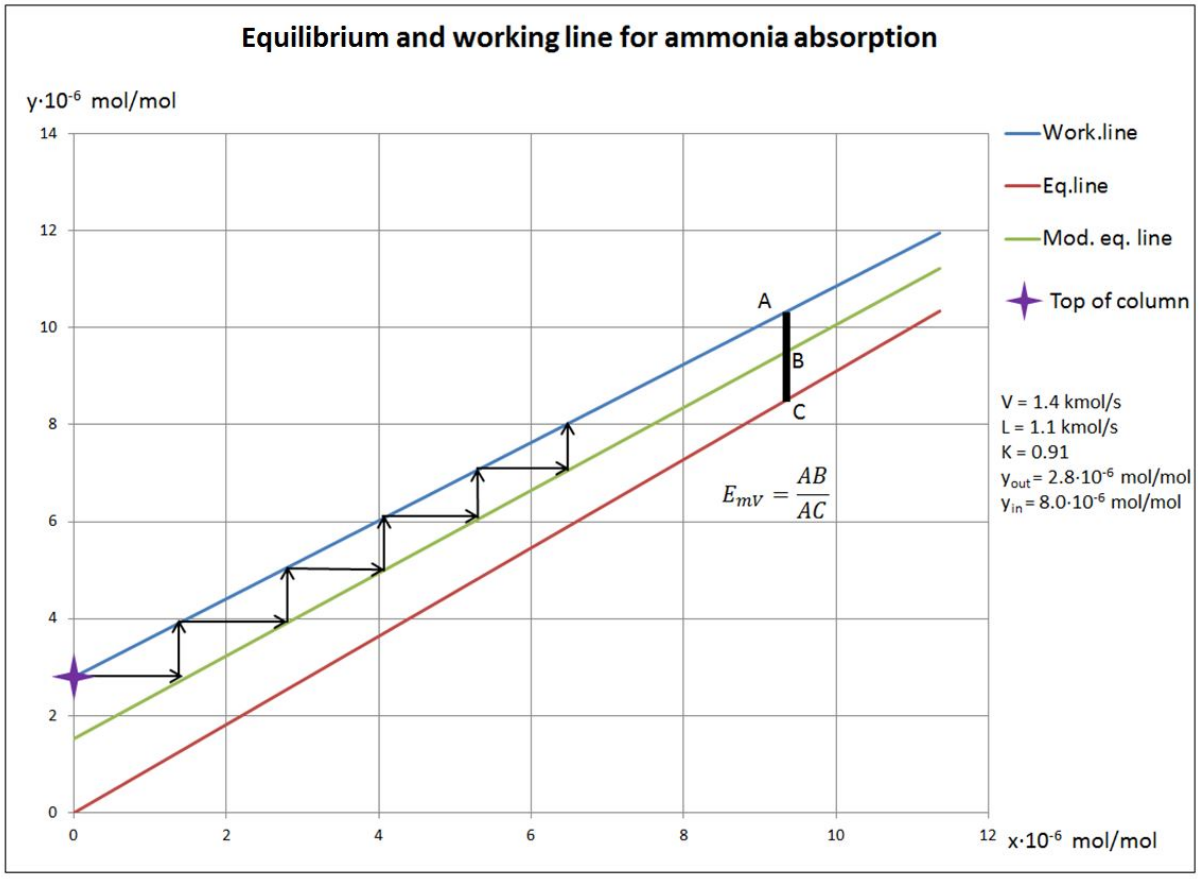

Figure 17: Real number of trays for the ammonia absorption in an absorption tray column with bubble caps (5 trays). V is the gas flow and L is the liquid flow.

A few examples of different compounds and their bubble-cap tray column graph will be shown next. The equilibrium calculations always have to be made in moles. However, the graphs can be presented in other units to make them more useful. Therefore the graphs shown next will have the gaseous side unit in ppm, and the liquid side unit in g/kg water. The graphs do not have the arrows in them, since the author gives the user the freedom to define the incoming gas concentration. Firstly, the ammonia graph with the useful units is presented in Figure 18. Secondly, a graph with formaldehyde is shown in Figure 19. Thirdly, a graph with sulphur dioxide is shown in Figure 20. Lastly, a graph with almost insoluble benzene is presented in Figure 21. In a real case, if these would be the compounds to be removed from the air stream, then the compound with the largest liquid flow would be the column design determining criteria. In this hypothetic case the compound would be benzene. After that, one would draw the working and equilibrium lines for the other compounds again, with the same water molar flow as in benzene absorbing. For the Figures below, V is the gas flow and L is the liquid flow.

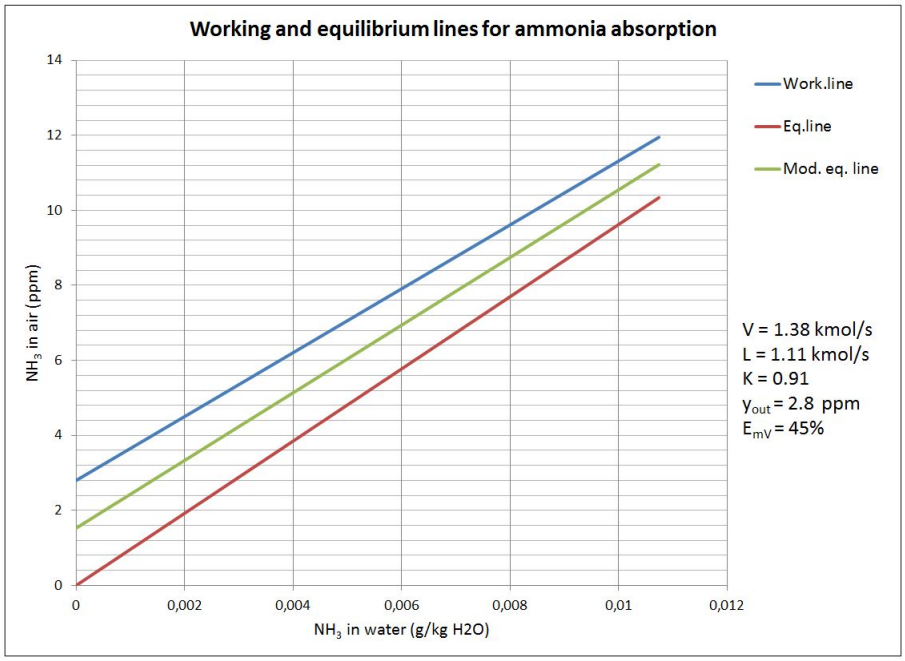

Figure 18: Typical ammonia absorption in a bubble-cap tray column. The number real trays can be determined for a Murphree efficiency of 45%.

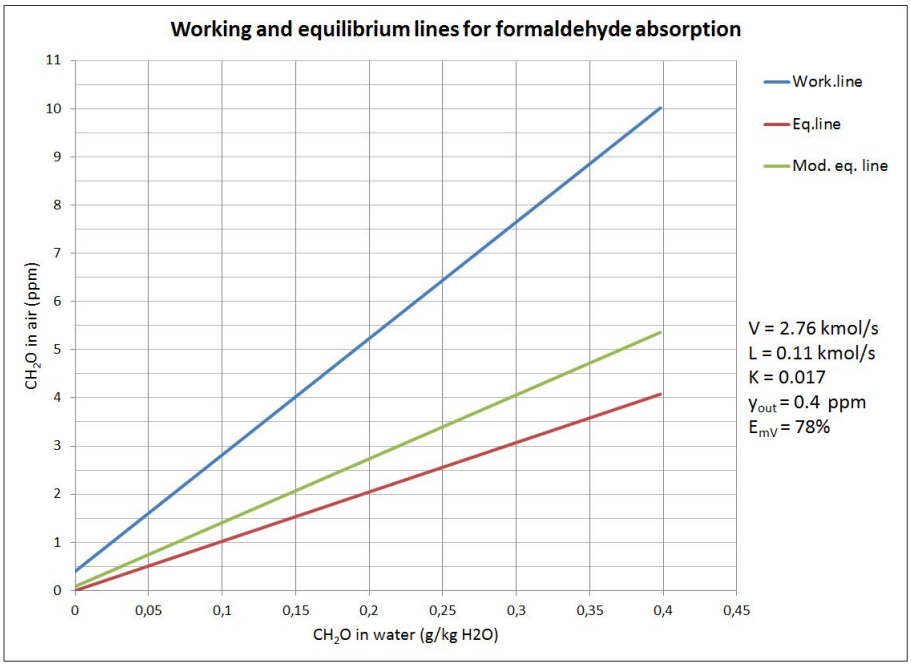

Figure 19: Typical formaldehyde absorption in a bubble-cap tray column. The number real trays can be determined for a Murphree efficiency of 78%.

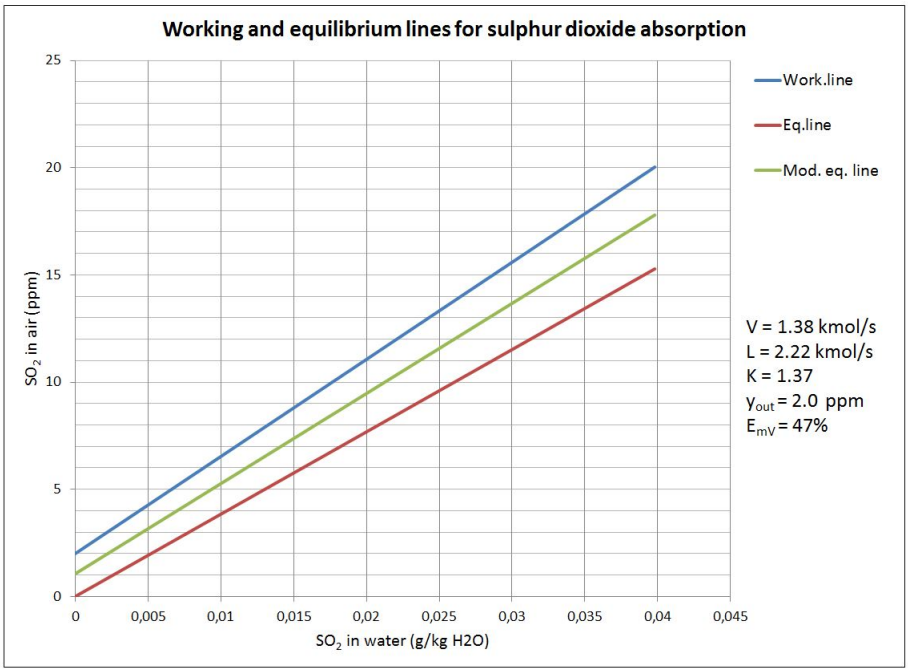

Figure 20: Typical sulphur dioxide absorption in a bubble-cap tray column. The number real trays can be determined for a Murphree efficiency of 47%.

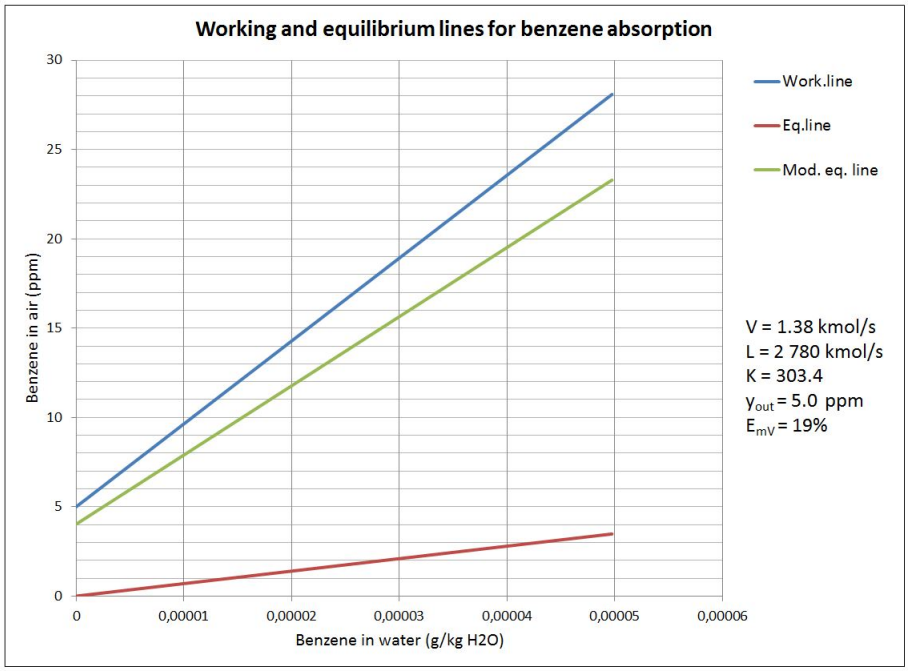

Figure 21: Typical benzene absorption in a bubble-cap tray column. The number real trays can be determined for a Murphree efficiency of 19%.

The graphs presented above are valid for bubble-caps. Bubble-cap trays have both pos-

itive and negative properties. From the negative side, the problems with the caps fouling, high maintenance rate and complex manufacturing all make the bubble caps unappealing for the purposes of this thesis. As a possible design, counter-current trays would be preferred (sometimes referred as dual-flow trays). They are less prone for fouling (Garcia & Fair, 2002). Counter-flow trays do not have any separate downcomers for the liquid, so the liquid will fall down from the same holes as the gas comes through. Unfortunately, not much research has been done on the absorption rate of the dual-flow trays. The literature cover some of the distillation dual-flow tray type, e.g. Garcia & Fair (2002) and Zhang et al. (2015) provide for the efficiency calculations. They also calculate other dual-flow tray design objects, such as the column diameter, tray opening size and maximal gas velocity. Since the absorption rate in these dual-flow trays are still widely undiscovered, the author recommends that the absorption rate for the bubble-caps can be used as a very, very rough estimate for the dual-flow trays. The author also reminds that Sinnott et al. (2005, p. 524) makes the following statement: "the plate efficiencies used in design should be based on experimental values for similar systems, obtained on full size columns". Sinnott et al. (2005, p. 524) goes on and points out that there is "no entirely satisfactory method for predicting the tray efficiencies", when they are based on the plate design parameters and the physical properties of the system.

5.2 Spray absorption

Another way to obtain an interchange of gas molecules from the air to the liquid, is by creating a spray of water droplets, through which air can flow. The studied spray chamber is a counter-current-flow-setup, where air and gas flows counter-currently; the gas flows upwards and water falls downwards as droplets. At the top of the chamber water droplets are formed by water as it flows through spray nozzles. Consider a tip of a spray nozzle as in Figure 22. Water flows from point A, inside the nozzle, to the point B, out from the nozzle outlet. From point A to B one can apply an energy balance:

$$p_A + \frac{1}{2}\rho v_A^2 + \rho g z_A = p_B + \frac{1}{2}\rho v_B^2 + \rho g z_B, \tag{84}$$

where z is height. Assuming z_B is at the outlet and z_A being right over z_B, one can say that $z_A \approx z_B$. If the water is sprayed into a chamber with the chamber pressure of 1 atm, one can further assume that $p_B \approx 0$ (gauge). The velocity at the outlet is then (from the energy balance):

$$v_B = \sqrt{\frac{2p_A}{\rho} + v_A^2}. \tag{85}$$

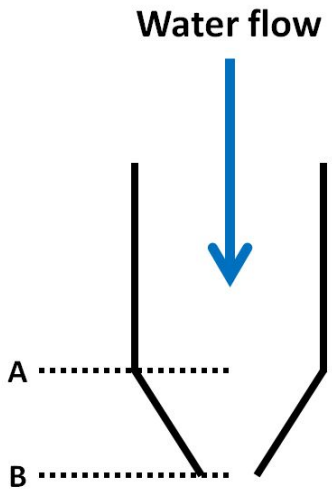

Figure 22: A simple schematic of a spray nozzle tip.

If the velocity inside the pipe or nozzle is low, it can also sometimes be assumed that $v_A \approx 0$. For simplified calculations, the droplet starting velocity can be assumed to be the velocity v_B, even if in reality the droplets are formed after about 20–30 cm after the nozzle orifice.

Spray nozzles can have different spray patterns. The spray pattern has to be considered when estimating droplet velocity out of the nozzle. The hollow-cone-spray pattern is the easiest to model, as it can be assumed that the velocity of the droplets coming out of the nozzle is the same for every direction. That is because a hollow cone nozzle sprays only in one direction in the height and width directions, see Figure 23.

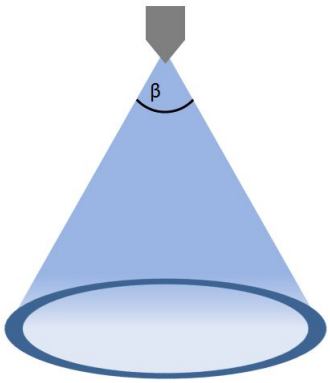

Figure 23: A schematic picture of a hollow cone spray nozzle. Water droplets are sprayed in hollow cone shape with a certain spray angle, β. The spray pattern on the ground is indicated with a blue circle.

After entering the spray chamber, the droplet velocity will be affected by drag force,

gravity and the counter-current gas flow. For the methods for calculating and accounting for the effects inside the chamber, see Lehtinen (2017).

The droplets formed by the spray nozzle are assumed to be spherical. The droplets have different diameters, and the droplets make together a size distribution of their diameters. The size distribution is treated similarly as the particulate size distribution in Section 4.2.1. Therefore, for the mass transfer treated here, the Sauter mean diameter is of importance. The mean diameters for a spray nozzle can be given by the nozzle manufacturer, or it can be determined optically or through calculation. For a simple calculated approximation of the droplet size sprayed by the nozzle, the model by Kamppinen (1997) can be used:

$$d_d = \sqrt[3]{\frac{\dot{m}_{l,th}\sigma_l}{\sqrt{\rho_{air}}\left(\Delta p\right)^{1.5}}}, \tag{86}$$

where Δp is the pressure difference between the inside and outside of the nozzle and $\dot{m}_{l,th}$ is the theoretical water mass flow through the nozzle. The theoretical water mass flow can be calculated when the nozzle orifice diameter, d_{or}, is known (Kamppinen, 1997):

$$\dot{m}_{l,th} = \frac{\pi}{4} d_{or}^2 \sqrt{2\rho_{air}\Delta p}. \tag{87}$$

A schematic of a spray chamber with one spray nozzle can be seen in Figure 24. In a real spray chamber there will be several spray nozzles, with a certain nozzle arrangement to gain a proper coverage of water droplets in the air flow.

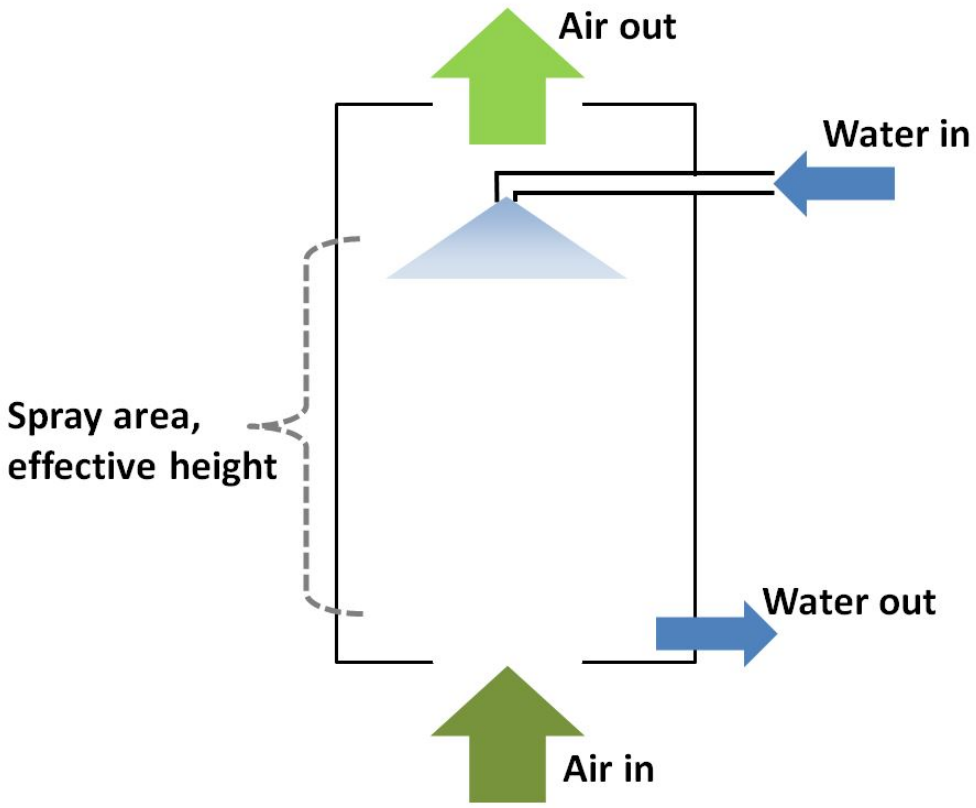

Figure 24: A simple schematic of a counter-current spray chamber.

5.2.1 Mass transfer

For the mass transfer between the droplet and the air bulk, Meyer et al. (1995) gives a model for the absorption. Their model focus on the absorption of volatile organic compounds (VOCs), but the same model can be used for other gaseous compounds, such as SO_2. The mass transfer equations presented here will be slightly modified from the model that Meyer et al. (1995) introduced. That is because their model considers that the spray chamber walls have a water film on them, and that also contributes to the heat and mass transfer. In the model discussed here, only the droplets' mass transfer is covered. The mass transfer occurring by the film on the spray chamber walls can be modelled with the equations in the wetted-wall Section (5.3).

The model by Meyer et al. (1995) uses the film theory, so the conditions at the interface between the air and droplet will be calculated. For the model in this thesis, it is further assumed that the diffusion is an one-component-diffusion, to simplify the calculations. The model by Meyer et al (1995) can be used in this thesis by the Equations (88) – (93).

Droplet mass balance	$\frac{d\,(J_d \cdot x_d)}{dz} = j_d A_{d,tot}$	(88)
Gas mass balance	$\frac{d\,(J_g \cdot y_g)}{dz} = -j_{d,g} A_{d,tot}$	(89)
Interface mass balance	$j_d + j_{d,g} = 0$	(90)
Equilibrium at the interface	$y_{i,d} = K_d x_{i,d}$	(91)
Mass flux at the droplet	$j_d = \frac{k_d\,(x_{i,d} - x_d)}{1 - x_{i,d}}$	(92)
Mass flux in the air	$j_{d,g} = \frac{k_{d,g}\,(y_{i,d} - y_g)}{1 - y_{i,d}}$	(93)

J is the molar flow, j is the molar flux, $A_{d,tot}$ is the total area of the water droplets, x is the liquid molar fraction, y is the gas molar fraction, k_d is the droplet mass transfer coefficient and $k_{d,g}$ is the droplet to gas mass transfer coefficient. The six equations in Table **??** can be solved as an equation system, when the droplet velocity is known. The method by Lehtinen (2017) gives the droplet velocity as short segments in the spray chamber height, and the same short segments can be used to calculate the molar flow through the short height dz in Equations 88 and 89. The aim is to solve the molar flows (J_d and J_g) for the one height section dz. To calculate the amount of moles transferred, the molar flow (in mol/s), has to be multiplied with the droplet residence time in the segment. The droplet residence time in one short segment dz, is calculated with the droplet velocity:

$$dt = \frac{dz}{v_d}, \tag{94}$$

where dt is the short droplet residence time. The length of the short segment can be calculated when the spray chamber height and the total number of segments are known. With the method by Lehtinen (2017), the total number of segments is given with the droplet velocity

(v_d) through the chamber.

When the droplet diameter is known, the total area of the droplets can be calculated:

$$A_{d,tot} = A_d N_d t_{res} = 4\pi \left(\frac{d_d}{2}\right)^2 \frac{\dot{V}_l t_{res}}{\frac{4}{3}\pi \left(\frac{d_d}{2}\right)^3} = \frac{6\dot{m}_l t_{res}}{\rho_l d_d}. \tag{95}$$

N_d is the number of droplets, which can be calculated from the water volume flow. t_{res} is the droplet residence time, which can be calculated with the droplet velocity profile in the chamber. If there is water vapour condensing, the droplets can grow in diameter; that effect is also discussed and calculated by Lehtinen (2017).

The equilibrium constant, K_d, can be found from or calculated from the tables given by Sander (2015), see Equation 80. The concentration of the absorbed component at the top of the spray chamber is assumed to be known (x_d and y_g). E.g. if using fresh water, $x_d = 0$, and if there is a requirement for a minimum level of pollution of the gaseous component out of the chamber, that can be used as y_g.

With the information from the model by Lehtinen (2017), the temperature profile for the air and the droplets are given in short segments through the spray chamber height. With that information, the two mass transfer coefficients, k_{dg} and k_d, can be calculated. For a turbulent flow in the droplet, Meyer et al. (1995) gives the Sherwood number for the drop:

$$Sh_d = 0.662 Re_d^{0.5} Sc_d^{0.5}. \tag{96}$$

The drop-to-gas Sherwood number is given by Cui et al. (2017):

$$Sh_{d,g} = 2 + 0.6 Re_{d,g}^{0.5} Sc_{d,g}^{0.33}. \tag{97}$$

The both Reynolds numbers, Re_d and $Re_{d,g}$ are calculated similarly, but have different viscosities and densities since the temperatures are different (Cui et al., 2017):

$$Re_d = \frac{d_d \left(v_d - v_{air}\right) \rho_{air}}{\mu_{air}}. \tag{98}$$

It is noteworthy that the velocities v_d and v_{air} have opposite directions. The Schmidt number for droplets is calculated as earlier (see Section 3.6):

$$Sc_d = \frac{\mu_{air}}{\rho_{air} D_{component,\, air}}. \tag{99}$$

The Schmidt numbers in Equations 96 and 97 differ in the temperature that they are calculated in (all variables). The interface is assumed to be at the same temperature as the drop,

therefore the Sc_d is calculated at the drop temperature. The $Sc_{d,g}$ is assumed to be in the air bulk temperature. The diffusion coefficient and its' calculation is discussed in the next subsection.

5.2.2 Diffusion calculation

For the mass transfer of a gaseous component to occur, the component has to move to the liquid and air interface from the air bulk. The driving force discussed here is the gas diffusion, which is the random movement of the gas molecules (Cussler, 2009). The gas diffusion is different for every component, thus a way to calculate the diffusion for the different components has to be used. The method used here is the Chapman-Enskog method. The formula has about 8% maximum error (Cussler, 2009):

$$D_{component,\,air} = \frac{1.86 \cdot 10^{-7} T^{3/2} \left(\frac{1}{M_{air}} + \frac{1}{M_{component}} \right)^{1/2}}{p \varsigma^2 \Omega}, \tag{100}$$

where the diffusion coefficient is given in m^2/s, and the pressure p is in atmospheres. ς is the collision diameter between the species, which are the absorbed component and air. The collision diameter is given by Cussler (2009):

$$\varsigma = \frac{1}{2} \left(\varsigma_{air} + \varsigma_{component} \right). \tag{101}$$

Cussler (2009) lists the individual $\varsigma_{component}$ for different components. For air, $\varsigma_{air} = 3.711$ Å.

To calculate Ω, more equations are needed. The interaction between the species is described by the Lennart-Johnson potential (Cussler, 2009). The interaction energy, ε, is needed for the calculation. For a single component, Perry and Green (1998), gave the formula:

$$\varepsilon_{component} = 1.15 k_B T_b, \tag{102}$$

where k_B is the Boltzmann constant and T_b is the boiling point of the species. ε_{air} can be calculated as $\varepsilon_{component}$ at $T_{b,air}$. After calculating the interaction energies separately, the geometric average of the energies is taken for the Ω calculation (Cussler, 2009):

$$\varepsilon = \sqrt{\varepsilon_{air} \varepsilon_{component}}. \tag{103}$$

Perry and Green (1998) have two options for the Ω-calculation, the one used here is:

$$\Omega = \left(44.54 T_*^{-4.909} + 1.911 T_*^{-1.575}\right)^{0.10}. \tag{104}$$

T_* is defined as (Perry & Green, 1998):

$$T_* = \frac{k_B T_{air}}{\varepsilon}, \tag{105}$$

where the temperature is in Kelvin.

The diffusion coefficient can, for most simple molecules, be estimated with Equation 100. But for bigger molecules, e.g. long hydrocarbon chains, the ς-value is not listed by Cussler (2009). For some organic molecules, Lugg (1968) listed their diffusion coefficients. The coefficients are static values, meaning they should be used carefully for temperatures outside of the NTP. NTP is the normal temperature and pressure which is 293.15 K and 1 atm. Nevertheless, Lugg (1968) gave a simple equation for correcting for a different temperature T_1:

$$D(T_1) = D\,(NTP) \cdot \left(\frac{298}{T_1}\right)^n. \tag{106}$$

n might vary for different components, Lugg (1968) used $n = 2$. The equation should be used with care.

5.3 Wetted-wall absorption

A simplified model for the wetted-wall absorption will be presented in this chapter. The model takes use of the Section 3.4, where the film thickness and velocity is calculated for both counter-current and co-current flow. The absorption model presented here can be both applied to counter-current and co-current flow. It is also valid for simple calculations for absorption in the air-air heat exchanger with a liquid film. The mathematical model is taken from the Meyer et al. (1995) article, the same as for the spray absorption. Here only, the equations describing the liquid film absorption occurring at the spray chamber walls, are used . No interchange between droplets and the film is assumed, since no droplets are present in the wetted-wall model. The modified model, for the purpose of film absorption by Meyer et al. (1995), is described by Equations (107) – (112):

Film mass balance
$$\frac{d\left(J_f \cdot x_f\right)}{dz} = j_f A_{f,tot} \tag{107}$$

Gas mass balance
$$\frac{d\left(J_g \cdot y_g\right)}{dz} = -j_{f,g} A_{f,tot} \tag{108}$$

Interface mass balance
$$j_f + j_{f,g} = 0 \tag{109}$$

Equilibrium at the interface
$$y_{i,f} = K_f x_{i,f} \tag{110}$$

Mass flux at the film
$$j_f = \frac{k_f \left(x_{i,f} - x_f\right)}{1 - x_{i,f}} \tag{111}$$

Mass flux in the air
$$j_{f,g} = \frac{k_{f,g} \left(y_{i,f} - y_g\right)}{1 - y_{i,f}} \tag{112}$$

The model is similar to the model for the droplet absorption, and the calculation of the molar flows (J_f and J_g) can be done by solving the six equations as an equation system. The interface can be assumed to be at the liquid film temperature, which can be solved with the methods discussed in chapter 3.6.

If the film covers the whole of the hot air side walls of the heat exchanger, the total area of the film ($A_{f,tot}$) can be assumed to be the heat transfer area of the heat exchanger for one height segment. To calculate the mass transfer coefficients, the equilibrium constant and the diffusion, the same methods as in the spray absorption chapter can be used, for the exception of Sherwood number. One can also assume that the film velocity is low compared to the air velocity, so the film velocity can be assumed to be 0.

The Sherwood number for the film can be calculated as in Hobler and Danckwerts (1966):

$$Sh_f = 0.023 Re_{air}^{0.83} Sc_{air}^{0.44}, \tag{113}$$

with a range $2,000 - 35,000$ in Re_{air}. A more accurate model is available from Karlsson and Svensson (2017), where they measured CO_2 absorption in a wetted-wall column:

$$Sh_f = 2.747 Re_{air}^{0.835} Sc_{air}^{0.835} \left(\frac{d_h}{H}\right)^{0.835} . \tag{114}$$

H is the height of the column and d_h is the hydraulic diameter. The Sherwood number $Sh_{f,g}$ can be calculated with same formula as Sh_f (only at the air temperature).

5.4 Particle removal with spray

Particles can be removed from an air stream with droplets. Two relevant mechanisms, for the type of air flows in paper industry and their particle removal with droplets, are presented in this thesis.

5.4.1 Collision

One effective way to remove particles from an air stream is by collision with a water droplet. The water droplets are sprayed inside a spray chamber, through which the air travels. The studied scrubber chamber is a counter-current chamber where air and gas flows counter-currently; the gas flows upwards and water falls downwards. For this type of spray chamber, Flagan and Seinfeld (1988) have developed models for the particle removal efficiencies. In order to calculate the efficiencies in the spray chamber, the droplet dynamics, thus the droplet velocity inside the chamber must be calculated (see Section 5.2). The velocity can be used to calculate the contact time between the two phases.

To remove particles from an air stream inside the spray chamber, Flagan and Seinfeld (1988) gives the expression

$$\eta_{o,cc} = 1 - e^{-\frac{3\eta_d}{2}\left(\frac{v_t}{v_d}\right)\frac{\dot{V}_l H}{v_{air} A_{cs} d_d}}, \tag{115}$$

where

$\eta_{o,cc}$ is overall particle removal efficiency for counter-current flow,
η_d is single droplet particle removal efficiency,
v_t is droplet terminal velocity,
v_d is droplet velocity,
v_{air} is gas velocity,
$\dot{V}_l$ is water volume flow,
H is spray chamber height,
A_{cs} is spray chamber cross-section area and
d_d is droplet diameter.

The overall efficiency determine how many percent of the incoming particles, of a certain size, will be removed by collision with droplets. If the particles in the incoming air stream are measured in concentration, then the overall efficiency can be multiplied with the incoming concentration to get the outgoing concentration. The efficiency can be calculated for a water droplet distribution, but an average value for the droplet diameter is then used. Here it is recommended to use the Sauter mean diameter (SMD), since the droplet area determines the collision efficiency. As mentioned before, the droplet velocity can be calculated with the methods by Lehtinen (2017). As for the droplet terminal velocity, Flagan and Seinfeld (1988) gives an estimation formula for it:

$$v_t = 958 \left[1 - e^{-\left(\frac{d_d}{0.171} \right)^{1.147}} \right]. \tag{116}$$

The Equation 116 is valid for spherical droplets with $d_d \geq 50\,\mu$m.

Some of the droplets will collide with the spray chamber walls, and they will not contribute to the collection of particles. One has to estimate how much of the water spray will go on the walls and correct the real water volume flow in Equation 115. After that, one has to determine the single droplet particle removal efficiency, η_d. For a single droplet, Flagan and Seinfeld (1988) mention that the collection of particles on a water sphere, here the water droplet, is determined by Brownian motion, impaction and interception. Also, the flow field around the water sphere is needed. With the help of dimensional analysis, Flagan and Seinfeld (1988) determines the variables describing the collection of particles on the water droplet. They also refer to the Buckingham pi theorem and define five dimensionless groups needed for the collection efficiency:

Reynolds number of a droplet $Re_d = \frac{d_d \left(v_d - v_{air}\right) \rho_{air}}{\mu_{air}}$,

Schmidt number of the particles $Sc_p = \frac{\mu_{air}}{\rho_{air} D_{Br}}$,

Stokes number of the particles $Stk_p = \frac{C_{sp} \rho_p d_p^2 \left(v_d - v_{air}\right)}{18 \mu_{air} d_d}$,

diameter ratio for particle and droplet $\kappa = \frac{d_p}{d_d}$,

and viscosity ratio for droplet and air $\omega = \frac{\mu_d}{\mu_{air}}$.

The single droplet deposition efficiency formula of particles is given by Slinn (1983), and it uses the five dimensionless groups by Flagan and Seinfeld (1988):

$$\eta_d = \frac{8}{Re_d \cdot Sc_p} \left[1 + \frac{0.4}{\sqrt{2}} Re_d^{1/2} Sc_p^{1/3} + \frac{0.16}{\sqrt{2}} Re_d^{1/2} Sc_p^{1/2}\right] + 4\kappa \left[\frac{1}{\omega} + \kappa \left(1 + \sqrt{2} Re_d^{1/2}\right)\right] + \left[\frac{2Stk_p - 2S_*}{2Stk_p - S_* + 2/3}\right], \quad (117)$$

where

$$S_* = \frac{1.2 + \frac{1}{12} ln\left(1 + Re_d/2\right)}{1 + ln\left(1 + Re_d/2\right)}. \quad (118)$$

Equation 117 considers the three collection mechanisms; Brownian motion, impaction and interception. Flagan and Seinfeld (1988) argue that the impaction is the most significant of these three, especially for somewhat larger particles. Therefore, Flagan and Seinfeld (1988) use a formula that considers only the impaction:

$$\eta_d = \left(\frac{Stk_p}{Stk_p + 0.35}\right)^2. \quad (119)$$

To calculate the Stokes number for the particle, the slip correction factor (C_{sp}) is needed. The slip correction factor is a correction factor for small particles and their movement in the fluid. Small particles do not sense the same movement-resisting forces as larger particles in the fluid (Flagan & Seinfeld, 1988). In this context smaller particles in air are particles smaller than 10 μm. The slip correction used in this thesis is the same as Flagan and Seinfeld (1988):

$$C_{sp} = \begin{cases} 1 + 1.257\frac{2\Lambda}{d_p}, & \text{when } d_p \gg \Lambda \\ 1 + 1.657\frac{2\Lambda}{d_p}, & \text{when } d_p \ll \Lambda. \end{cases} \tag{120}$$

Λ is the mean free path in the gas. The mean free path is an average distance for a molecule to travel before encountering another molecule (Flagan & Seinfeld, 1988). According to Flagan and Seinfeld (1988) the mean free path in a gas can be calculated with the following equation:

$$\Lambda_g = \frac{\mu_g}{0.499p\left(\frac{8M_g}{\pi RT}\right)^{1/2}}. \tag{121}$$

For air at NTP, $\Lambda_{air} \approx 6.51 \cdot 10^{-8}$ m, which is 0.0651 μm.

Making accurate calculations for even small particles, the Equation 117 has to be used. The Schmidt number is based on Brownian diffusion, D_B. The Brownian diffusion inside a spray chamber can be expressed as Loosmore and Cederwall (2004) does:

$$D_{Br} = \frac{k_B T C_{sp}}{3\pi\mu_{air} d_p}. \tag{122}$$

k_B is the Boltzmann constant, which is about $1,38 \cdot 10^{-23}$ J/K.

Calvert (1977) showed a method for calculating the removal efficiency for cross-current spray chambers. In a cross-current spray chamber water is sprayed from the top of the chamber and falls vertically downwards. Air flows horizontally, so that the flows are cross-current. Calvert (1977) also had the assumption that no water is sprayed on the chamber walls, so the wall-sprayed part of the water volume flow has to be removed from the presented equation:

$$\eta_{o,cr} = 1 - e^{-\frac{3\dot{V}_l H \eta_d}{2\dot{V}_{air} d_d}}. \tag{123}$$

Calvert (1977) did not present clear results for the formula, so the single droplet efficiency must be carefully chosen. Calvert (1977), mention that the calculation can be done in the same manner as for the counter-current chamber. Differences with the counter-current case appear in the droplet Reynolds and Stokes number. If the air velocity is only in the horizontal direction, the air velocity can be dropped out of the Reynolds and Stokes number-equations, since the drop is not affected in its vertical movement by the horizontal air flow.

5.4.2 Condensation effects

Condensation in a spray chamber may enhance the particle collection (Cooper, 1984). Condensation effects in the spray chamber may occur combined with the droplet impaction, and they can both be calculated simultaneously. For condensation to occur in a spray chamber, the conditions to make water vapour to condense, must be met: The incoming air has to be saturated, or near the saturation temperature. The water sprayed in the chamber has to be cold, or at least colder than the gas saturation temperature.

When a cold water droplet falls inside a spray chamber, the saturated water vapour around the droplet will start to condense on the surface of the water droplet. This movement of water molecules towards the water droplet is the basis for diffusiophoresis. The movement of condensing water molecules will help the particulates in the air to move towards the water droplet and will, therefore, be captured by the water droplet. This phenomenon is known as the diffusiophoresis "flux force", as described by Cooper (1984).

Cooper (1984) mentions that thermophoresis has an opposing effect to the diffusiophoresis. Thermophoresis is caused by the condensation. When water molecules condense on the water droplet surface, the latent heat is released and must be conducted away. The resulting heat flow or molecule movement outwards from the droplet may push or keep particles away from the droplet. Cooper (1984) refers to several sources for closer studies on the phenomenon.

Sometimes, when the air is saturated, the water vapour condensation may occur on the particle itself, rather than on the water droplet. The condensate formed on the particle enlarges the particle itself, thus increasing the particle diameter. The particle diameter is a crucial parameter when calculating the impaction efficiency, so an increase in the particle diameter will enhance the overall chamber efficiency. Cooper (1984) mentions that typically 25% of the condensing water vapour in the spray chamber will condense on the particles itself. The rest, 75%, will condense on the cold surfaces in the scrubber; the cold surfaces being the water droplets and the spray chamber walls. Cooper (1984) also mentions that, in some cases, the condensation on particles may be more important than the diffusiophoresis (the effect from condensing on the water droplets). Cooper (1984) also points out that the particle solubility in and attraction to water has a large impact on the condensation efficiency on the particle. Hydrophilic particles will already have condensation forming on them at conditions under the saturation temperature, while strongly hydrophobic particles will only have condensation form on them under supersaturated conditions.

Cooper (1984) refers to research performed by several authors showing that the condensation has a positive effect on the particle collection. One research on diffusiophoresis is by Sparks and Pilat (1970). They calculated diffusiophoresis for condensation, evaporation and

neither. Sparks and Pilat (1970) found that condensation enhances the particle collection, and evaporation diminishes the collection. Evaporation takes place in the spray chamber when the spray water is warmer than the saturation temperature of the water vapour in air. For the purposes of the thesis, we will ignore the possibility of evaporative effects. When neither condensation nor evaporation is present, Sparks and Pilats (1970) model assumes that only impaction is present and accounts for the collection efficiency.

Of all the possible condensation mechanisms – diffusiophoresis, condensation on particles and thermophoresis – Cooper (1984) states that the most important are the condensation on particles and the diffusiophoresis. They have the largest impact on the particle collection efficiency and according to Cooper (1970), the thermophoresis only has a marginal influence on the collection efficiency.

Sparks and Pilat (1970) have successfully developed a model to calculate the diffusiophoresis. The model has its basis in the vapour pressure gradient caused by the condensation in the droplet boundary layer. The vapour pressures in the boundary layer, and in the air bulk, are dependent of the respective temperatures. The temperatures and their gradients can be calculated with the models by Lehtinen (2017). The model by Sparks and Pilat (1970) can be applied to the spray chambers discussed in this thesis, but the modelling will require more work. Figure 25 shows some results that Sparks and Pilat (1970) presented for the diffusiophoresis. The data for the spray chamber are: Height is 3 m, gas/liquid flow rate is $\dot{V}_l/\dot{V}_{air} = 5 \cdot 10^{-4}$ and the droplet diameter is 0.2 mm. For the condensation diffusiophoresis curve, the pressure difference between the droplet boundary layer and the bulk is -10^5 mbar/cm, respectively for the evaporative diffusiophoresis the pressure difference is 10^5 mbar/cm.

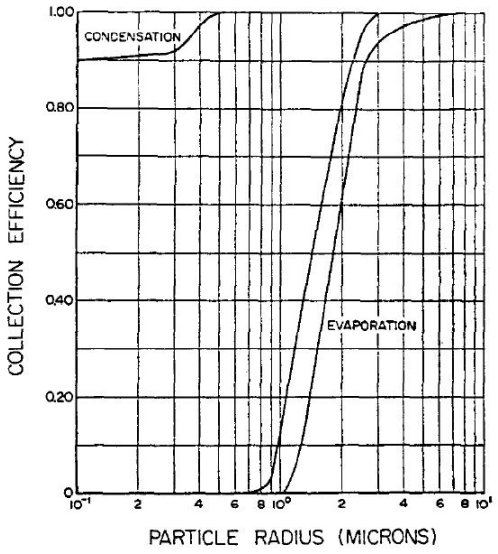

Figure 25: Particle removal efficiency for a spray chamber with condensing and evaporating diffusiophoresis simulated by Sparks and Pilat (1970).

For the condensation on the surface of the particles, Lancaster and Strauss (1971) have done some experimental work. Lancaster and Strauss (1971) claimed that the diffusiophoresis only had little effect, when compared to the condensation on the particles. They did their experiments on zinc oxide fumes, with dust in the air flow. A calculation method for the condensation on the particles was not available from them. Developing a condensation model for specific particles falls out of the scope for this thesis. To be able to fully understand and model the spray chamber for the condensation effects, more research is needed.

5.5 Particle removal with tray column

Particles from the air flow can also be removed with a tray column. The particle collection mechanisms are the same as for a spray chamber. The particles collide with the water flow on the trays and with the foam on top of the tray. The flow conditions and a schematic picture of the foam or froth formed above the tray can be seen in Figure 13. Additionally, the particles are collected with diffusiophoresis, although the conditions for the condensation have to be met (see Section 5.4.2).

Noll et al. (1986) present a model for calculating the particle collection efficiency for a tray column. The model is for sieve trays, which are simple round holes in the tray. Therefore, for different tray designs, the method might need correction. The calculation method by Noll et al. (1986) has several steps in it. Here are presented the basic equations for one tray removal, so for a more detailed and whole-tray-column calculation, see Noll et

al. (1986), and their reference Calvert and Gandi. Noll et al. (1986) present the first tray particle collection based on the impaction:

$$\eta_{impaction} = 1 - e^{-\frac{40F^2 d_p^2 \rho_p C_{sp} v_{holes}}{9\mu_{air} d_{holes}}}, \tag{124}$$

where F is the foam density, C_{sp} is the slip correction (see Equation 120), v_{holes} is the air velocity through the holes in the tray and d_{holes} is the diameter of the holes. According to Noll et al. (1986) the foam density can be estimated to be 0.4.

The second particle collection is with diffusiophoresis (Noll et al., 1986):

$$\eta_{dph} = 0.85\zeta, \tag{125}$$

where the volume fraction of condensing gas, ζ, is:

$$\zeta = \frac{\frac{\dot{m}_{cond}}{\dot{m}_{da}}}{i_{in} + \frac{M_v}{M_{da}}}. \tag{126}$$

i_{in} is the air specific humidity for air under the tray. $\dot{m}_{cond}$ is the mass flow of condensate under the normal operation of the tray column. Once both particle collection efficiencies are calculated, the single tray overall collection efficiency can be calculated:

$$\eta_o = 1 - \left[\left(1 - \eta_{impaction}\right)\left(1 - \eta_{dph}\right)\right]. \tag{127}$$

Calvert and Jhaveri (1974) made some calculations and experimental work with sieve plates for the particle collection. In their model, they considered particle collection by impaction, diffusiophoresis, thermophoresis and centrifugation in the air bubbles on the tray. The prediction for the particle collection, or as in the graph, the particle penetration, is shown in Figure 26. In the Figure, the penetration fraction is $1-\eta$. The particle collection varies with the condensation rate per dry air rate. There are particle penetration rates for up to four sieve trays. The particle aerodynamic diameter is assumed to be 0.75 μm, and the particles are assumed not to grow, when going up from one tray to another. In reality, the particles are wetted when they go through a tray. When the particles are wetted, their diameters grow, so the collection rate of the wetted particles is increased when going from a tray to the next tray and so on.

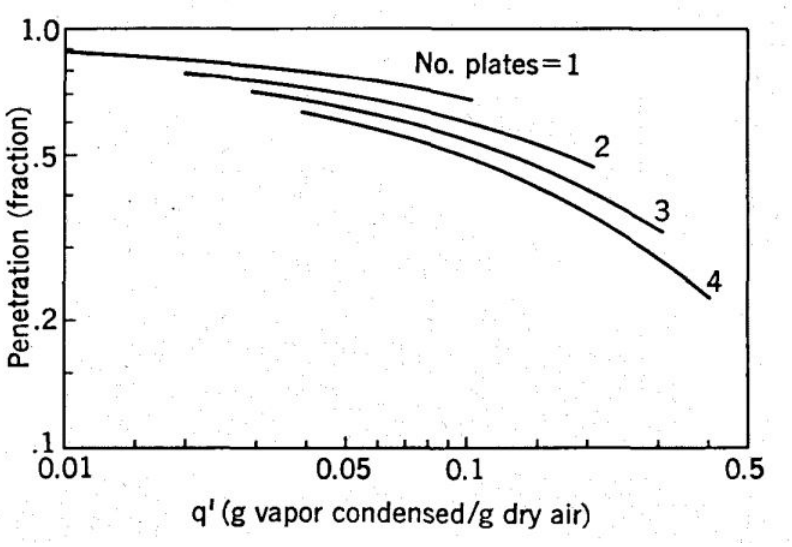

Figure 26: The penetration rate for 0.75 μm particles versus the condensation rate (Calvert & Jhaveri, 1974) for a sieve tray column.

In Figure 27, by Calvert and Jhaveri (1974), is shown some experimental results acquired from their pilot column and the dependency of the particle concentration. In Figure 27 the dots are the experimental values and the solid lines are the mathematical calculation models. The air conditions for the experimental work was: air volume flow 2.8–5.2 m^3_{da}/min (at 1 atm and 0°C), moisture 1.2–33.4%-vol. and temperature 20–71°C. The pipe for the pilot column was 10.2 cm in diameter, and the holes in the tray were 3.2 mm in diameter; on one tray there were 60 holes. The water flow was 0.64 l/min and the particle diameter 0.75 μm. The particles were iron dioxide particles, with a density of 2.5 g/cm^3.

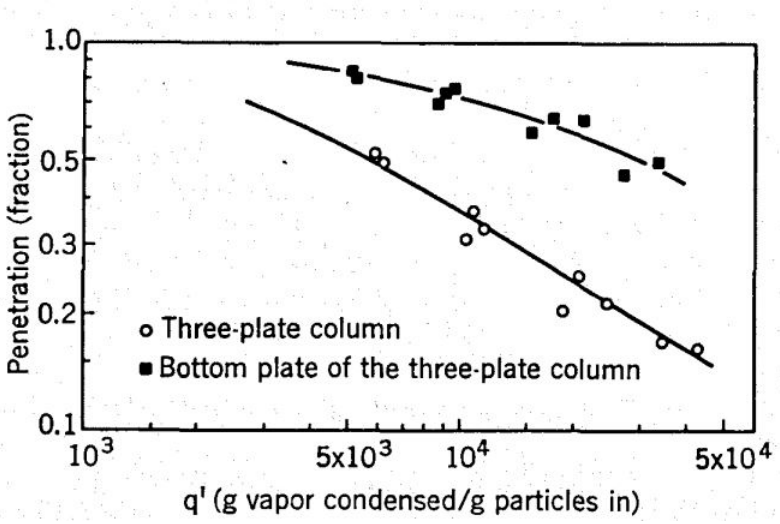

Figure 27: Particle penetration for varying condensation and particle concentration in a pilot tray column (Calvert & Jhaveri, 1974).

Finally, Figure 28 predicts the particle collection for different particle sizes for the Calvert and Jhaveri (1974) pilot column. n_i is the particle concentration in no. of particle per cm^3.

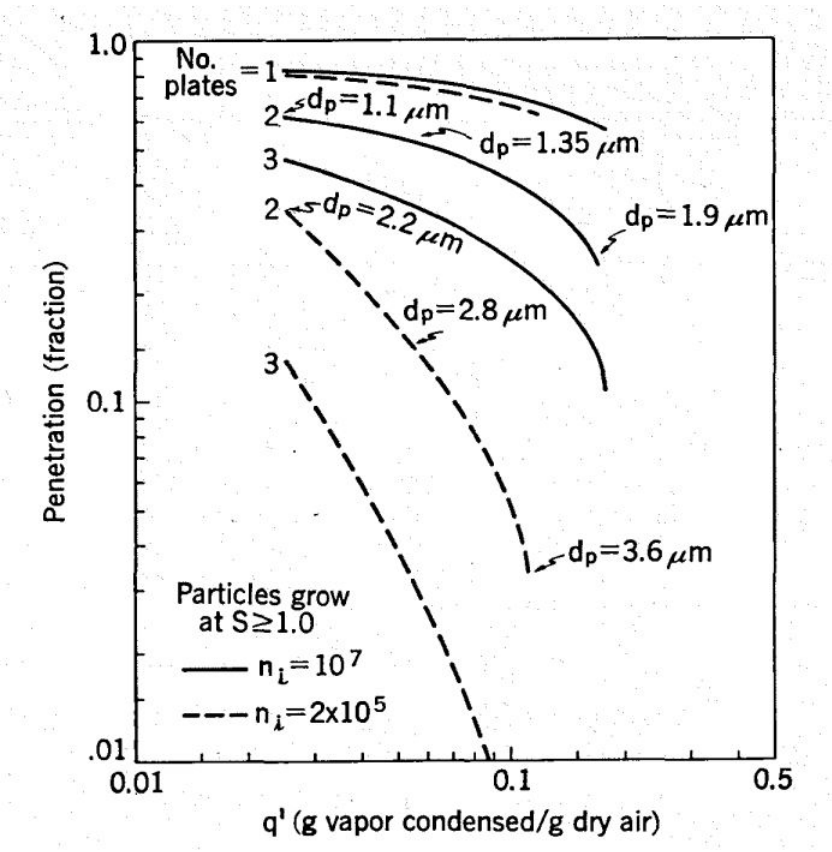

Figure 28: Prediction of particle collection for different particle sizes and vapour condensation in a tray column (Calvert & Jhaveri, 1974).

5.6 Particle removal with wetted-walls

As the last method for removing particles from an air stream, a wetted-wall setup is considered. The simplified model presented will concentrate on a co-current flow direction, where the flows are downwards. The model can, with some caution, be applied to the air-air heat exchanger with the liquid film on the hot air side walls. When the air enters the heat exchanger, some particles will flow with the air through the heat exchanger, while other particles will collide with the liquid film at the walls. The particles move in the air streams main direction, but also partly in the other directions because of the turbulent flow conditions in the air. That movement will cause particles to collide with the liquid film. A simple schematic of the wetted-wall particle collection can be seen in Figure 29.

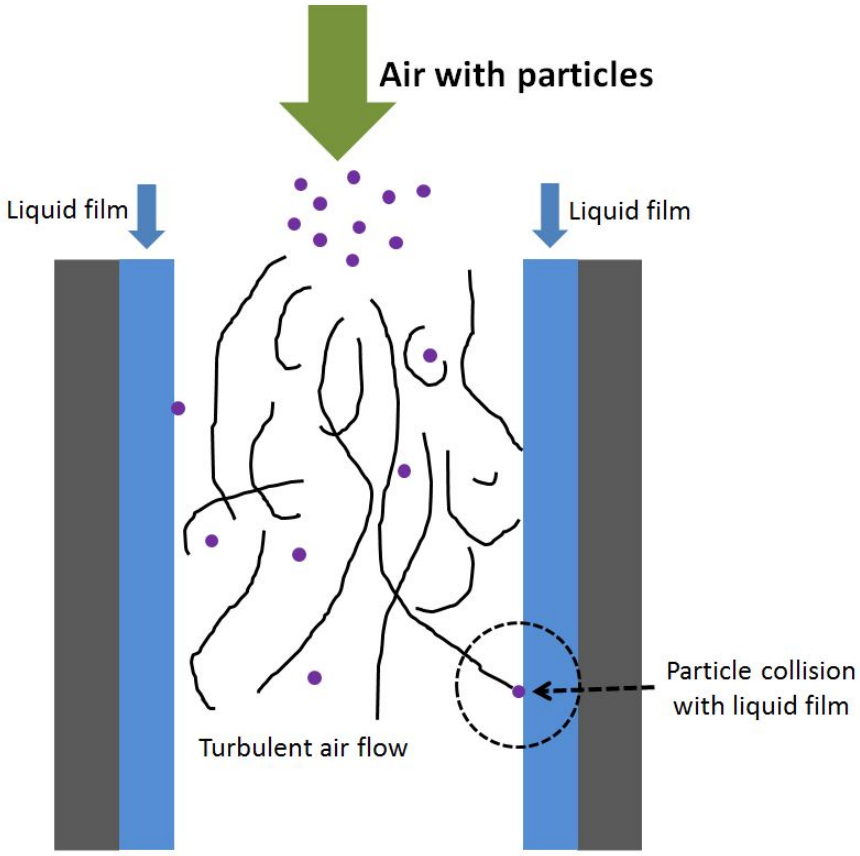

Figure 29: A simple schematic showing the principle for particle collection in a wetted-wall.

For the model considered in this thesis, the simplifications for the particle collection include:

- The liquid film is seen as a smooth surface,
- when a particle collide with the liquid film, it sticks onto it and does not re-enter the air stream,
- the air stream is turbulent and
- only particles, which motion is controlled by the air turbulence and the air motion, are assumed to be present.

The last criterion is important, since in the model presented here, only particle collision caused by the air turbulence will be present. The last criterion is estimated by Sommerfeld (1992). Sommerfeld mention that only small enough particles' motion will be controlled by the turbulence. Larger particles will, e.g. hit a wall in a tube bend when the air flow will curve around the bend. Small enough particles will follow the air current and does not

touch the wall. To approximate the particle sizes, whose movement will be dominated by the turbulence, Sommerfeld (1992) presented:

$$d_p < \sqrt{\frac{18\mu_{air}d_h}{0.7K\overline{v_p}\rho_p}}, \tag{128}$$

where d_h is the tube hydraulic diameter and $\overline{v_p}$ is the streamwise velocity for the particle in the air stream and ρ_p is the particle density in kg/m^3. K is a constant, and $K\overline{v_p}$ tells the fraction of transverse particle fluctuations in the velocity. Sommerfeld (1992) uses a K-values of 0.05 and 0.1. A few calculated values for the maximal particle sizes that are affected by the turbulence can be seen in Table 8 below. The particle density is 1,000 kg/m^3, particle velocity is 15 m/s and air viscosity is $18 \cdot 10^{-6}$ kg/(m $\cdot$ s).

Table 8: An example of largest particle diameters, which motion will be dominated by the turbulence.

	d_p (μm)	
d_h (mm)	K=0.05	K=0.1
20	111	79
30	136	96
40	157	111
50	175	124

To estimate how often particles collide with the pipe wall, the results by Vreman (2015) were used. Using the assumption of a particle always sticking to the wall when a collision occurs, makes it possible to estimate the total particle removal efficiency when the number of collisions is known. Vreman (2015) simulated downwards air-particle flow, with copper particles of 70 μm in diameter and 8800 kg/m^3 in density. The channel was 40 mm in diameter and the mean air velocity downwards about 9.2 m/s. The concentration of copper particles was given as a mass loading ratio parameter Φ, with the value of 0.8. Vreman (2015) defined Φ as:

$$\Phi = \frac{\zeta\rho_p}{\rho_{air}}, \tag{129}$$

where ζ is the particle volume fraction in air. The volume fraction can be converted into concentration; $c_{g/m^3} = \zeta\rho_p \cdot 10^3$. That gives the concentration of copper particles: About 960 g/m^3. The results from Vreman (2015) for the particle-wall collisions were the following: For smooth walls, the collision rate was 335,000 collisions per second. For rough walls, with roughness 10 μm, the collision rate was 2,000,000 collision per second. For rough walls, with wall roughness of 20 μm, the collision rate was 3,166,000 collision per second.

To calculate a similar rate of collisions for fibre particles, closely similar data was used. The fibre concentration in the wetted-wall setup was kept the same as for copper particles, 960 g/m^3 (giving same Φ, 0.8). The wall was assumed to have the roughness of 10 μm, even though the walls are wet. The wetted-wall height was 2 m, the channel diameter was 40 mm and the air and particle velocity was 10 m/s. From this data, the number of particle-wall collisions were estimated to be 2,000,000 per second. The fibre particles were assumed to have the aerodynamic diameter of 70 μm and a density of 1,000 kg/m^3. The height was segmented into 2,000 segments, in order to calculate the collisions occurring segment-wise. The particles residence time in one segment were 0.0001 s, and in that time, 200 particle-wall collisions occurred. Those 200 particles were removed from the air stream, so that the concentration of fibres into the next segment was lower. After all the segments, the number of collected particles were about 400,000, which is about 0.025% of the total number of particles.

If one was to calculate, with the Sommerfeld (1992) method in Equation 128, the largest particles that will be majorly affected by the turbulence for the copper particles, the particle size would be 66 μm and 47 μm for $K = 0.05$ and $K = 0.1$ respectively. That means that the copper particles are not affected by the turbulence, in the simulation, as much as they should be to estimate reliable results for lighter particles. For 70 μm fibre particles with the density of 1,000 kg/m^3, Table 8 shows that 70 μm fibre particles are majorly affected by the turbulence. To correct for this, the number of collision could be increased. With a ten times larger collision rate, the number of collected particles is ten times higher, 0.25%.

One can say that the collection efficiency of 0.025% is low. The collision rate has to be over 1000 times higher, in order to reach appropriate collection efficiencies for a 2 ms high wall. With a higher wall more particles can be collected; A 4 m high wall has a collection efficiency of 0.05%. The results are still very simplified and have to be verified with experiments before real collection efficiencies can be calculated. An experimental setup would also give indication of how well particles are sticking onto the wetted-wall and about the wetted-wall real smoothness. The experiments fall out of the thesis scope.

6 Water treatments

When the air is treated with some of the air treatment techniques discussed in Chapter 5, water catches the pollutant, whether it is particles or an absorbed compound. Therefore, in order to reuse the water in the air cleaning equipment, the water needs to be cleaned from the absorbed components or particles. Disregarding the removal of particles or absorbed components, can make the equipment to clog and the water to lose its air cleaning properties, among others. In this chapter, a few different techniques regarding particle removal are discussed, from which liquid filtration is discussed more profoundly.

6.1 Liquid filtration

Consider a liquid flow with suspended solids, in this case solid particles. This water suspension is pumped through a membrane, which will make the particles stop by the membrane and not pass through, while allowing the water to pass. This operation of removing the particles from the liquid stream is called filtration (Cheremisinoff, 1998). The cleaned water, which passes through the membrane, is in filtration usually referred to as filtrate. The membrane, which separates the particles and the liquid, is called the filter medium. The particles separated by the filter medium, can either be deposited inside the filter medium on the porous membranes, or on top of the filter, as in Figure 30. If the particles are deposited on top of the filter medium, the particles stacked up there, will be referred to as the filter cake. The type of filtering is known as cake filtration (Cheremisinoff, 1998). The other filtration type, the filter-medium filtration, is based on the particles being deposited inside the filter, in the porous structure. In practice, the cake filtration is the more common in industry (Cheremisinoff, 1998).

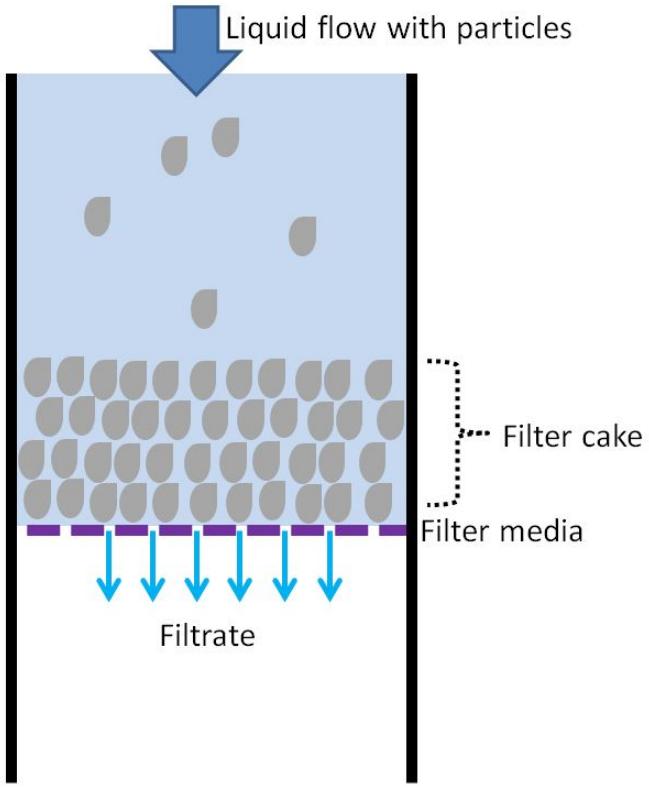

Figure 30: A simple schematic of cake filtration.

Purchas (1984) distinguishes also the surface straining filtration type, where the filter medium has pores, which allow the penetration of a portion of particles. Small enough particles will penetrate the filter medium, while large enough particles will be deposited on top of the filter medium, just as in cake filtration. These surface straining filters can be applied before the main filter with the smallest pores, to strain out larger particles.

The most important parameter for filtration is the type of filter medium used. The pores in the filter medium should be such, that the particles do not penetrate the filter medium. That is in order to obtain pure filtrate or to efficiently collect the filter cake (unless the filter is a surface straining filter). Therefore, the particle composition and size is of importance. When the particle size is known, the pore size in the filter medium can be selected. The pore size is different for different filter types (Cheremisinoff, 1998). Examples of the filter medium is cotton or wool fabric, metal wire, sand, coal, metal powder and porous stones such as quartz. More about the filter medium is discussed in Section 6.1.1.

The filtration is usually done in two different modes; constant pressure filtration or constant throughput filtration. In the first, the pump power pushing the suspension towards the filter is constant. As the filtration goes on, more particles are stacked up by the filter, which increases the pressure drop over the filter, although the filtration of particles is more

efficient with a thicker cake. A thicker cake decreases the throughput of the filtrate, as the filtration goes on. The filter needs to be cleaned when the throughput of filtrate is too low. In the second one, the constant throughput filtration, the pump operates at various rotation rates. As the pressure drop over the filter increases, the pump raises its rotation rate, so that the throughput of filtrate through the filter is constant. The filter needs to be cleaned when the pump cannot raise its rotation rate anymore or the pump power consumption becomes too high (Cheremisinoff, 1998).

When considering the filter medium and the filter cake, they both have certain porosity. Porosity is the voidage fraction of the filter medium or the cake. The filter cake can be either compressible or incompressible, which means that for a compressible filter cake, the porosity of the cake will change during the filtration. The cake filtration is discussed in detail in Section 6.1.2.

Designing the filtration process can be complex, mainly because of the different variations in the properties of the liquid suspension, the delicacy of the variations in the filter cake and the liquid suspension for the process conditions and the massive lists of different equipment available for the filtration. Some of the filtration equipment used for the type of suspension available from the air treatments discussed in this thesis, will be discussed in Section 6.1.5.

There are two main parameters in the filtration operation. They are the temperature of the liquid suspension and the pressure drop over the filtration process. The temperature of the liquid suspension affects the viscosity of the suspension, which affects the filtration. For the liquid suspension with a small amount of paper fibre particles in it, the viscosity of the suspension is very little affected by the fibres. The viscosity of the suspension is largely decided by the liquid and its change in temperature. The high pressure before the filter may alter the properties of the fibres, causing them e.g. to break up. The break up may cause the small fibres to penetrate through the filter cake and into the filter medium, which is undesirable. The entrainment of the pressure-broken particles into the filter medium is known as pore clogging (Cheremisinoff, 1998).

6.1.1 Filter medium

As already discussed, the two main types of filtering are the cake filtering and the filter-medium filtering; they require different types of filter medium. The volumetric rate of filtrate through the filter medium and cake is proportionally dependent on the pressure gradient over the process and inversely proportionally dependent on the filter mediums' porosity, pore connectivity, tortuosity and the filter cake.

The filter medium can be classified with the rigidity of the material. Here flexible filter medium is first discussed. The most common type of flexible filter medium is the woven

material, which can be of organic or non-organic origin (Cheremisinoff, 1998). There are many different woven materials, and a summary of the different woven materials and their suitability for different process conditions can be seen in Table 9. Other flexible filter medium is also woven metal, rubber medium, paper fibre cloths and metallic salts, such as copper sulphate (Cheremisinoff, 1998).

Table 9: Examples of woven filter media and some process conditions for them (Cheremisinoff, 1998).

Woven fibre	Durability in		Fibre tensile strength	Temperature limit (°C)
	acids	alkalis		
Acrilan	Good	Good	High	135
Asbestos	Poor	Poor	Low	400
Cotton	Poor	Fair	High	150
Dacron	Fair	Fair	High	175
Dynel	Good	Good	Fair	95
Glass	High	Fair	High	315
Nylon	Fair	Good	High	150
Orlon	Good	Fair	High	135
Saran	Good	Good	High	115
Teflon	High	High	Fair	82
Wool	Fair	Poor	Low	150

Examples of rigid filter media is metallic medium, ceramic medium, coal medium, ebonite medium, charcoal, salts, sand, gravel and brick. All of the different materials have their own properties, which must be accounted for when choosing the filter medium. The metallic filter medium can be perforated plates, slotted plates or powdered metal made out of steel, bronze or copper. Ceramic filter medium is made of quartz or chamotte, together with e.g. silicate glass. Ceramic medium operates well in acidic suspensions, but alkali suspensions make them erode. Sand is used e.g. when filtering drinking water. A bed of sand can be from 10 cm to 1 m high (Cheremisinoff, 1998).

When the filtration objective is to clarify the liquid, a simple table with different filter media and the appurtenant particle size limit for the penetration of the filter medium can be used for filter medium selection. This kind of data can be seen in Table 10.

Table 10: Purification boundaries in particle sizes for different filter media (Purchas, 1984). The values are directional.

Filter medium	Smallest particle size collected (μm)
Solid fabrics (wedge wire)	50
Porous plastics (flexible)	50
Bonded medium	50
Porous carbon	40
Porous plastics (rigid)	40
Sintered woven metal	30
Depth cartridges	12
Cellulose paper	12
Nonwoven fabrics	12
Woven fabrics	12
Woven monofilament plastics	12
Woven wire	8
Perforated metal	5
Sintered metal powder and fibres	5
Porous ceramics	2.5
Glass paper	0.8
Precoat powder	0.075
Membranes	0.01

If the particles are so small that the filter medium on its own cannot separate the particles, an addition of precoat powders might be needed. Precoating adds a layer of "filter medium" on top of the existing filter medium. The added filter medium will enhance the filtration and capture smaller particles (Purchas, 1984). According to the Table 10, one can with the addition of precoating, collect as small as 0.075 μm particles. More of the additives can be found in Section 6.1.4.

Generally, the objective for the filtration can be of four different types: Clarification of the liquid, separation of solids for recovery, separation of both the liquid and solids for recovery or separation of the liquid stream to accomplish other factory operations (Cheremisinoff, 1998). The aim for the filtration here is to purify the water, so that it can be used again in the air treatment, so the first of the four objectives is present.

6.1.2 Cake filtration

The cake filtration operation relies on the cake formation of particles on top of the filter medium. According to Cheremisinoff (1998), the cake formation is practically possible when the particle concentration, in volume of the suspension, is over 1%. In lower concentrations than this, pore clogging of the filter medium can become a problem. When the concentration

of the particles is about 0.1-1% in volume, the concentration of the particles has to be increased with thickeners, so that the cake filtration can be accomplished (Cheremisinoff, 1998).

In practice the cake filtration is seldom operated upwards in the vertical direction. That is mainly because of the formation of the cake. In the direction against the gravity, the particles will not form easily a cake on the filter medium surface, because gravity is pulling the particles downwards. Therefore, the filtration is usually done in the vertical downwards or horizontal direction.

As discussed, the filter cake can be of two types; compressible or incompressible. Cheremisinoff (1998) defines that if the particles can easily or readily be deformed under high pressure, the cake consisting of these particles will be compressible. During filtration the compressible cake will be compressed together, decreasing its porosity and therefore the liquid flow area. This means that the pressure drop over the cake increases as the filtration goes on. Paper fibres can be seen as compressible. Incompressible filter cakes can be, according to Cheremisinoff (1998), inorganic particles over 100 μm, e.g. sand and calcium carbonate.

The cake filtration process can be seen as a cycle, with the following steps:

- Start of the process,
- cake formation,
- cake drying,
- cake washing,
- cake drying,
- cake discharge and
- reassembly and continuing of the filtration.

Washing of the filtration cake with is done in many cake filtration processes, mainly for two different reasons. Either the filter cake is the end product, so it must be cleaned from all of the suspension liquid, or, then the filtrate is the end product, in which case the cake has to be washed, so that all of the suspension liquid can be collected. Neither of those is of interest here, because the suspension liquid only has to be cleaned from the particles in order to be used again in the air treatment equipment. Therefore, washing can be neglected in this case.

The cake discharge must be done at some point, since the pressure drop over the cake becomes too large eventually. In batch filtration the discharge of the cake must be done manually. In a continuous filtration process, like in the drum filtration, the cake discharge is

done automatically (Cheremisinoff, 1998). More about the specific filtration processes can be found in Section 6.1.5.

Cheremisinoff (1998), presented the basic equation for cake filtration:

$$v_{filtrate} = \frac{1}{A}\frac{dV}{dt} = \frac{\Delta p}{\mu_l \left[r_{ck}\zeta_0 \left(V/A\right) + R_{fm}\right]}, \tag{130}$$

where $v_{filtrate}$ is the filtrate volumetric velocity, A is the filter area, Δp is the pressure drop over the filter, μ_l is the suspension dynamic viscosity, r_{ck} is the specific volumetric cake resistance (m^2), ζ_0 is the volume ratio of cake to filtrate and R_{fm} is the filter medium resistance (1/m). The equation can be modified for the constant pressure filtration and the constant throughput filtration. For constant pressure filtration Equation 130 becomes (Purchas, 1984):

$$\frac{1}{\dot{V}_{filtrate}} = \frac{dt}{dV} = a_1 V + a_2, \tag{131}$$

where

$$a_1 = \frac{\mu_l r_{ck} \zeta_0}{2\Delta p A^2} \tag{132}$$

and

$$a_2 = \frac{\mu_l R_{fm}}{\Delta p A}. \tag{133}$$

a_1 and a_2 is used to lump together all the parameters. That is usually necessary, since the parameters are experimentally determined.

6.1.3 Filter-medium filtration

When the concentration of particles in the liquid stream is low enough, filter-medium filtration is preferred over cake filtration. In this type of filtration the particles will penetrate into the filter medium, where they are captured by the thin passages and walls in the filter medium pores. This capture will, when the filtration is ongoing, increase the liquid flow resistance of the filter medium. At some point the filter medium pores are so fully occupied by the particles, that the filter medium has to be replaced (Cheremisinoff, 1998).

The filter-medium blockage can be caused by three mechanisms (Cheremisinoff, 1998):

- Pores in the filter medium can be blocked by single particles that block the pore passage.

- Pores can become blocked gradually; the particles will concentrate in a single passage until the passage becomes blocked.
- Intermediate-type of filtration can block the filter medium.

According to Cheremisinoff (1998), the gradual blocking is the most common in industry, so the modelling will concentrate on that phenomenon.

A calculation model for the filter-medium filtration is presented by Cheremisinoff (1998). The equations can be solved, but they require information of the filter medium and experimental data. The formulas for the filter-medium filtration are presented below in Equations (134) – (138) (Cheremisinoff, 1998).

$$\frac{a_3}{2}t = \frac{t}{a_6} = \frac{1}{v_l} \tag{134}$$

$$\mathrm{a_3} = \frac{2a_4}{v_l^{0.5}} \tag{135}$$

$$\mathrm{a_4} = \frac{\zeta_0}{\pi L_{pores}} \left(\frac{a_5}{N_{pores}} \right)^{0.5} \tag{136}$$

$$\mathrm{a_5} = \frac{\pi \Delta p}{8 \mu_l L_{pores}} \tag{137}$$

$$\mathrm{a_6} = \frac{N_{pores} \pi L_{pores}}{\zeta_0} \left(r_{pores}^2 - r_{pores,new}^2 \right) \tag{138}$$

The formulas are valid for a filter medium with the area of 1 $\mathrm{m^2}$. The parameters are: v_l is the filtration rate per unit area of filtration (1 $\mathrm{m^2}$), t is the time passed from the filtration start, ζ_0 is the volume fraction of accumulated cake inside the filter medium per filtrate recovered, L_{pores} is the average length of the pores in the filter medium, N_{pores} is the number of pores in the filter medium (for 1 $\mathrm{m^2}$), Δp is the pressure difference over the filter medium, r_{pores} is the average radius for the pores in the filter medium and $r_{pores,new}$ is the average radius of the pores in the filter medium when the particles have blocked some of the pores. Once experimental data for a system is obtained, one can with the equations design a similar system.

6.1.4 Filter aids

Choosing the right material for the filter medium can be challenging. Sometimes the particles to be filtered can be so small that the filter medium has to be made of special material. The special material can be rather expensive, so in some cases it may be more competitive to use filter aids. Filter aids are chemicals that are added into the liquid suspension. There are

two types of filter aids. Precoat-type of filter aids will add an extra layer of filter medium on top of the existing filter medium, hence collecting more and smaller particles. Precoat do not interfere with the filter cake; the cake will form on top of the precoat-layer. Precoating will block pore clogging of a filter medium. Admix-type of filter aids interacts with the filter cake. They blend in with the filter cake and decrease the cake compressibility and increase the cake permeability (Chen, 2016).

Common filter aids are perilite and diatomaceous earth (DE). They are both silica based minerals. Perilite can be mined from volcanic rock and DE from ancient seabed. The minerals can be grinded to small particles, and the smaller particles they are grinded into, the smaller particles they can collect, when acting as the filter aid. On the other hand, the filtration rate will drop when smaller particles are used. Therefore, a balance between the filter aid particle size and the filtration rate is to be considered (Chen, 2016).

6.1.5 Filtration equipment

Filtration apparatuses are numerous and choosing between the equipment can be complicated. The picking of the right equipment depends on the liquid suspension properties, cake properties, process conditions and flow capacity. Only after that can the selection between continuous or batch equipment be made (Cheremisinoff, 1998). Cake filtration can be either batch filtration or continuous filtration, while filter-medium filtration usually is done as batch filtration. Four different filtration equipment, which can be seen as suitable for the suspension present, is discussed next.

A rotary drum filter is a submerged and hollow drum, on which the outer surface area is covered with the filter medium. A simple sketch can be seen in Figure 31. Inside the drum there is underpressure, produced by a fan, that sucks air and liquid through the filter medium inside the hollow drum. The drum filter is submerged to a certain depth (Cheremisinoff, 1998). The drum rotates while being submerged in the liquid suspension. The side of the drum that rises from the liquid when the drum rotates will draw up the filter cake formed on the filter medium. The filter cake dries after it has risen from the liquid. After that the cake is usually washed, and after that the cake is allowed to dry again. Before the same segment of the filter medium will be submerged again, the cake is scraped off the filter medium by knifes or specific scrapers.

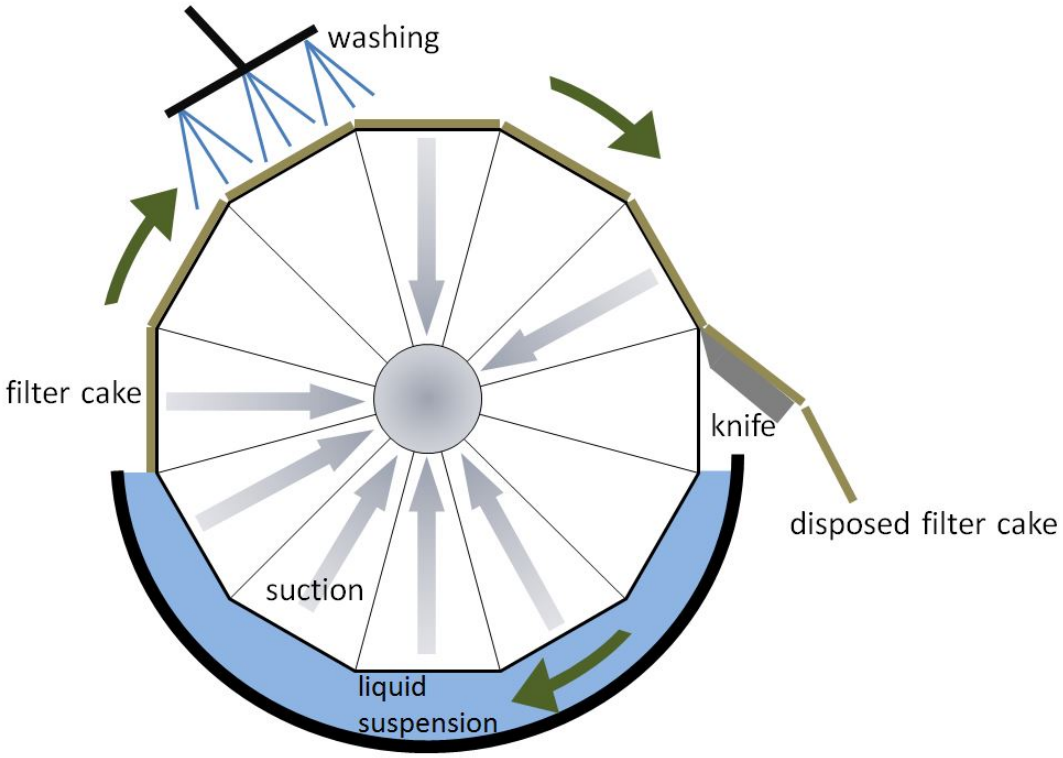

Figure 31: Side view of a rotary drum filter.

Rotary drum filters are suitable for a wide range of liquid suspension, but they are usually used for low-concentration suspension, with a narrow particle size distribution. A wide size distribution may result in filter medium clogging (Cheremisinoff, 1998).

A belt filter is a horizontal belt, on which the liquid suspension is deposited. The belt has the filter medium on top, and a support structure underneath, usually made of rubber. Gravity and sometimes suction from a vacuum pump will make the liquid go through the filter medium, while the belt moves. As the belt moves, the cake dries, and finally at the end of the line, the filter cake is disposed (Sparks, 2012). An example of the belt filter can be seen in Figure 32.

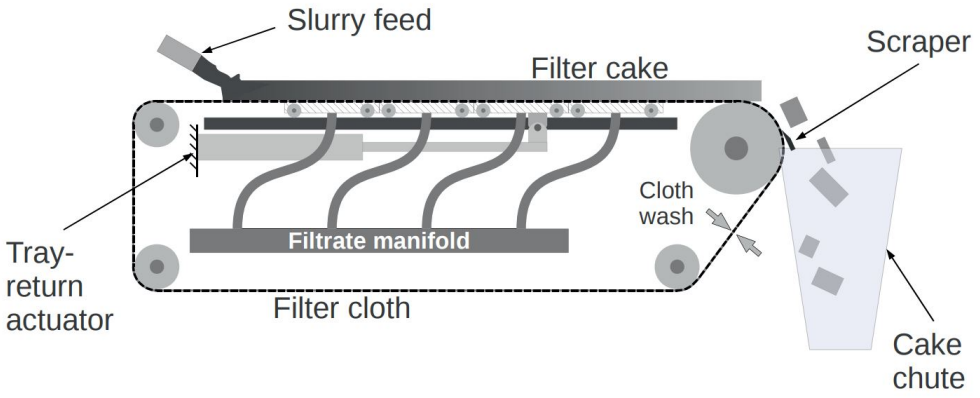

Figure 32: One type of a belt filter configuration (Sparks, 2012).

The belt filter requires a large space, since the belt is horizontal. The design of the filters is relatively simple and the cake thickness can also be relatively thin. Also, the filter medium has to come back around to the suspension liquid input upside down, unused. That means that there is unused filter medium area, which is unwanted (Cheremisinoff, 1998).

A disc filter has the same working principle as the rotary drum filter. The filter cake is formed on the both sides of a disc that rotates in the liquid suspension. The cake dries when the disc rotates out of the suspension, and a knife will cut off the dried cake. There can be several discs in one filter machine, so a large filtering area can be acquired (Tarleton & Wakeman, 2007). A simple schematic of the filter can be seen in Figure 33.

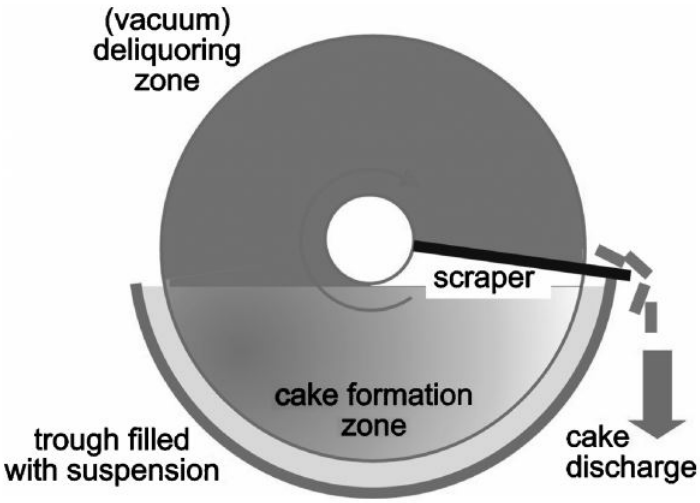

Figure 33: A schematic of the disc filter (Tarleton & Wakeman, 2007).

A disc filter can have a relatively small floor space, since the disc can be placed closely

to each other. The washing of the cake and the filter is hard to accomplish properly since the discs are closely together (Tarleton & Wakeman, 2007).

Cartridge filters are widely used in the industry. There are many different designs available. A typical cartridge filter is made of one or more layers of a sheet wound around a perforated middle structure (Purchas, 1984). A cartridge filter made of woven yarn can be seen in Figure 34.

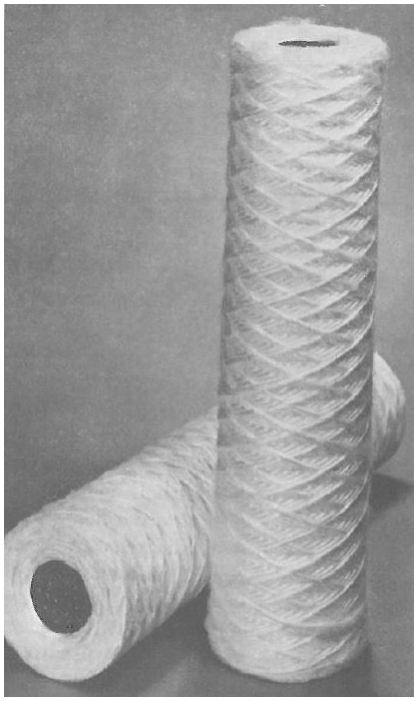

Figure 34: A woven cartridge filter made out of yarn (Purchas, 1984).

The filter works so that the suspension is fed on the outer layer of the filter, wherefrom the liquid is filtered as it flows towards the middle of the filter (the hollow centre). Then the shells or sheets are layered so that the most outer layer has the biggest mesh size, so that the bigger particles will stick to the uppermost layers, and the smaller particles will stick in the inner layers. The layering of the mesh sizes can also be the opposite, if the suspension is fed into the middle of the filter (Cheremisinoff, 1998).

According to (Cheremisinoff, 1998), the cartridge filters' applications include keeping spray nozzles unclogged, filter recirculating water, filter cooling tower water, filter condensate and filter water used in scrubbers among others. Cheremisinoff (1998) also lists what the paper industry use cartridge filter for, and among the applications, is filtering white water, fresh water and mill water.

The materials of the sheets are different and some typical sizes of the mesh for the material are (Cheremisinoff, 1998):

- Wire mesh, mesh size normally 10–700 mesh,
- fabric, 30 mesh – 1 μm,
- slotted screen, 10 mesh – 25 μm and
- stainless steel screens, 10–30 mesh.

Cheremisinoff (1998) gives some recommendations for the mesh size for different liquids in the paper industry:

- White water, clarified, 30–100 mesh,
- freshwater, 30–200 mesh and
- mill water, 60–100 mesh.

The mesh size can be converted into smallest collected particle size. The chart for different materials can be seen in Table 11. The data is from equipment suppliers (Cheremisinoff, 1998). For the finest fabric filters the mesh size is not listed.

Table 11: Normal filter mesh size and their particle collection.

Material	Mesh size	Smallest particle collected (μm)
Wire mesh	10	1650
	20	890
	30	585
	40	380
	60	230
	80	180
	100	140
	150	115
	200	84
	250	60
	400	45
	700	30
Perforated plate	10	1575
	20	1125
	30	600
Slotted screen	10	1600
	30	610
	60	230
	100	150
	200	75
	325	50
Fabric	60	230
	80	180
	100	140
	150	115
	250	60
	500	40
	-	15–20
	-	5–10
	-	1–3

The materials are also dependent on the process conditions. Stainless steel can be used in pH 4–14, polypropylene at pH 1–14, cotton at pH 3–11 and so on (Cheremisinoff, 1998). Temperature also gives its own limits for the materials. A list with process conditions, chemicals and recommendations for the filter material is given in the Appendix.

The cartridge filters can be operated as single filter or as multiple filters. A single filter requires service when the filter pores are full. The filters are interchangeable, so that if a single filter needs service, it can be changed for another one during the service. Cartridge filters can be operated with backwashing. That is useful for multiple filters, as the pressure

drop can be monitored for the filters, and when the pressure drop rises to a certain level, the backwash of the filters can be employed. This can be done separately for every filter, so that the filtration can be done continuously (Cheremisinoff, 1998).

6.2 Sedimentation

The liquid used in the air treatment equipment contains particles. If the water is left in a tank, the particles will eventually separate from the liquid. They can fall to the bottom of the tank, or if lighter than the liquid, settle on top of the water. The process is called sedimentation, and is caused by gravity. The particles that settle out is often referred to as sludge. The sludge can also settle, and that process is known as consolidation. If the consolidation needs mechanical support, that is referred to as thickening (The International Water Association, 2019).

The particles may interfere with each other during the sedimentation. According to The International Water Association (2019), the interference begins when the concentration of the particles is larger than 1% in volume of particles per volume of liquid. The different interference regimes can be seen in Table 12 below. The volume of the particles per volume of liquid can be measured by filling a tank with the suspension. After a relatively long time, the liquid and particles have separated, and a rough estimate of the volume of particles per volume of liquid can be determined (The International Water Association, 2019).

Table 12: Interference of particles in sedimentation (The International Water Association, 2019).

Concentration in volume/volume	Particle interference
<1%	Low.
1–8%	Some.
8–18%	Fully hindered, the suspension properties are also determined by the particles.
18–26%	Fully hindered, appearance changes.
>26%	Fully hindered, sedimentation needs thickening.

Two different equipment for sedimentation is briefly presented and then some improvements to the process is introduced. The most iconic sedimentation equipment is the horizontal flow tank. It consist of a large tank, where the flow of suspension is horizontal. During the low-speed flow through the long tank, the particles have time to settle at the bottom of the tank. At the end of the tank, clarified liquid is drawn out of the tank at the top, while sludge is drawn out from the bottom. The tanks are large, so their required floor space is also large (The International Water Association, 2019).

One way of reducing the floor space for the sedimentation, is by using an inclined settler. The flow of suspension can be forced into inclined pipes or on inclined plates, thus reducing the floor area. The setup can be counter-current, co-current of cross-current. That means that the particles moves in the other direction, e.g. in the counter-current inclined settler against the liquid current (The International Water Association, 2019). An example of an inclined settler can be seen in Figure 35.

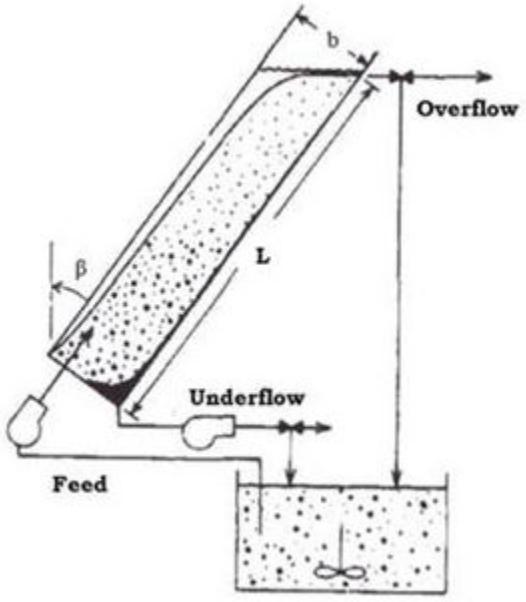

Figure 35: A schematic of a counter-current inclined settler (Grigorova & Nishkov, 2015).

When the particles and the liquid have densities that are close to each other, the normal settling, in a tank, is slow, and it might be preferable to use additives in the suspension. Coagulation agents can be added into the suspension which will stick onto the particle surface. The coagulation agent will stick to particles and in a process called flocculation, the particles are made to collide with each other making the particles form lumps. The larger lumps of particles settle faster. Therefore, the coagulation process and the flocculation is done before the sedimentation (The International Water Association, 2019).

The settling can be made even faster with the addition of ballast. Ballast will stick to the particle lump formed by the coagulation agent and increase the particle density. An increase in the density will dramatically shorten the settling time. Typical ballasting agents are fine sand and bentonite (The International Water Association, 2019).

6.3 Hydrocyclones

Hydrocyclones are conical liquid-solid separators. Their separation depends strongly on the densities of the liquid and solids, so an adequate difference in the densities of the liquid and the solid particles is needed. For paper dust, the density lies relatively close to waters. In order to use hydrocyclones for the separation, ballasting, described in Section 6.2, is needed to increase the particle density (Bradley, 2011).

The suspension is tangentially fed into the top part of the upside-down conical cyclone. The suspension travels in a vortex, firstly downwards, against the inner walls of the cyclone, then secondly in a vortex in the middle upwards. The liquid turns at the bottom of the cyclone, where also the underflow is disposed from the cyclone. From the middle part on the top of the cyclone, overflow is taken out. Particles, with relative high density, will exit in the underflow (Bradley, 2011). A figure of the hydrocyclone can be seen in Figure 36.

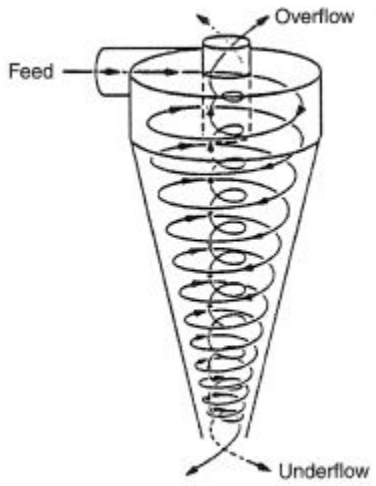

Figure 36: A simple schematic of a hydrocyclone (Bradley, 2011).

Particles are separated into the underflow by centrifugal force. The smallest particles that the cyclone is able to separate is about 5 to 10 μm. Decreasing the cyclone diameter will result in separation of smaller particles. The cone length will also affect the separation, and according to Bradley (2011), even smaller particles than 5 μm can be separated with a long cone structure. The small diameter will affect the fluid flow capacity; so many cyclones might be required to be installed in parallel, in order to handle the whole suspension flow.

7 Modelling and results

The thesis have several topics, e.g. heat exchangers and air quality. The result section will mainly focus on the practical models, where model verification with measured data is possible.

Of the theoretical topics, the heat exchanger studies gave an understanding of the flows characteristics in the air-air heat exchanger. Additionally the author made an simplified calculation tool for the film heat exchangers. Though, the model will need some refining after measurements are available from film heat exchangers. The discussed topic on air quality, ventilation and air contaminants will deepen the knowledge on ventilation and possibly help in the understanding of pollution regulations. The water treatments section will serve as an additional part to help develop future process equipment.

Air treatments are a central part of the thesis and the models discussed cover several methods. The wetted-wall and tray column methods are left on a theoretical basis, but the understanding of them will give some rough estimation and comparison between different models. The spray chamber method is the one with some measured data, so it will be majorly covered in the results. The absorption method with the spray chamber will be used in the results to compare the absorption model discussed with real measurements. Also, calculations with particle removal efficiencies for a theoretical spray chamber will be shown.

7.1 Spray chamber absorption modelling

A modelling of the absorption of gaseous contaminants were done with methods in Chapter 5.2. The calculation model is implemented into the programming and calculation tool Matlab. The model will be firstly compared with results from a spray chamber used to remove sulphur dioxide from engine exhaust gas. Secondly, the model will be compared with hydrogen sulphide and sulphur dioxide absorption in a spray chamber from a paper mill exhaust.

The counter-current spray chamber experiments for engine exhaust gas in the marine industry were conducted by Caiazzo et al. (2013). The test spray chamber consisted of a round pipe, 160 mm in diameter and 1880 mm in height. The gas flow rate used for the comparison was 40 m^3/h. The absorbed component was SO_2 and the liquids used were distilled water and seawater. The results for the distilled water will be used since the water used in a possible future spray chamber will not be seawater. The water flow was varied into the spray chamber, with flows of 0.1, 0.2, 0.3 and 0.4 m^3/h with corresponding droplet diameters of 0.9, 0.66, 0.72 and 0.4 mm. Water is sprayed into the chamber with a spray nozzle with a spray angle of 60°. Inlet gas concentration of SO_2 was 500 ppm and the

temperature 250°C. With that information, a simple comparison between the experimental values from Caiazzo et al. (2013) for the SO_2 absorption and the model presented in this thesis could be performed.

The results are presented in the graph below, in Figure 37. The spray pressure is given for the model (2 bars), since the spray pressure was not given for the data points. The absorption is given as percentage of 500 ppm left in gas after absorption. 0 % means that there is 0 ppm left after the spray chamber. Both the data and the model show that when more liquid is used, and when keeping the same gas flow, more SO_2 can be absorbed. The model and the data have som deviations. Also, the spray pressure nor the spray nozzle types were given for the data points. Four different mechanisms causing the deviations will be discussed.

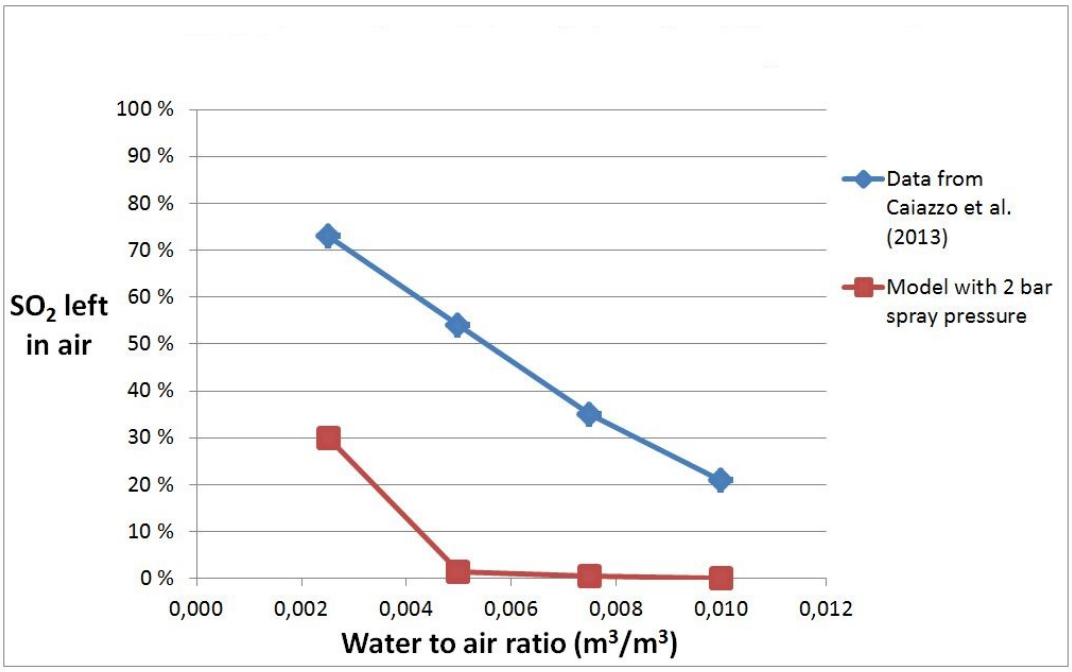

Figure 37: Model and data comparison of SO_2 absorption in the experimental spray chamber with an inlet concentration of 500 ppm SO_2.

The spray pressure gives the starting velocity for the droplets in the gas stream. A higher spray pressure gives higher velocity, which will give shorter contact time between the gas and liquid. The shorter contact time means that the absorption is decreased.

The water is sprayed in at an angle of 60° inside a pipe with a diameter of 160 mm. The water droplets will inevitably hit the spray chamber, or pipe, inside walls. Therefore, the droplets are continuously removed from the air stream and lands on the pipe wall. The water on the wall will also contribute to the absorption, but with a lower rate than the droplets.

The amount of water sprayed on the pipe inner walls was not mentioned in the data from Caiazzo et al. (2013), but a significant amount can be expected to hit the walls, mainly because of the relatively narrow pipe diameter.

When the SO_2 is absorbed, it will react with water, or more specifically with the OH^--ions in the water. This reaction will cause the concentration of SO_2 in the water to decrease, which will allow more SO_2 to be absorbed, because of the disrupted equilibrium between the liquid and gas phase. In the model in this thesis it is assumed that the absorbed SO_2 is almost instantaneously consumed by the OH^--ions. In a real spray chamber this can be achieved with the addition of an alkali solution to the spraying water. With very low concentration of SO_2 in the gas, it might even be unnecessary to add any alkali, since the OH^--ions will consume all of the present SO_2 without needing more. The chemical reactions between the components will not be modelled further.

In the experiments by Caiazzo et al. (2013) it can be assumed that the SO_2 is not consumed instantaneously by the OH^--ions. That is because of the high concentration of the SO_2 in the gas flow and the use of distilled water. In the experiments by Caiazzo et al. (2013), they concluded that seawater were better for the absorption than the distilled water. That was because of the salts that were present in the seawater. The salts will also react with the SO_2 absorbed, and reduce the concentration, causing more efficient absorption. Also in the model developed by Caiazzo (2012) for the same experimental spray chamber, they modelled the reactions of SO_2 in the spray droplet. That would be the most correct way to model the absorption, but the modelling of the reactions for the absorption in this thesis goes beyond the thesis scope.

To compare the model in this thesis with the corrections for the model, few different scenarios for the corrections were calculated. The simple examples can be seen in Figure 38. The first modification to the calculation is to use 8 bar spraying pressure instead of 2 bars. The change to the drop velocity will somewhat change the removal of SO_2, in a negative direction. The next modification was to change the amount of water available as droplets (changing the spraying pressure back to 2 bars). The rest of the water is assumed to be present at the chamber wall – inert to the absorption. The change of the water present to the absorption is shown in Figure 38. The change has a larger effect for the smaller water flows than larger. That could depend on several things; among others that if using the same nozzle for a larger flow, a bigger part of the water would in reality end up on the walls. Therefore, the percentage of water on the walls should probably increase when increasing the water flow up to 0.01. As the last modification to the model, the reaction of SO_2 is not assumed to occur at all in the droplet. It can be clearly seen that the absorption is significantly slower if no reaction would be present.

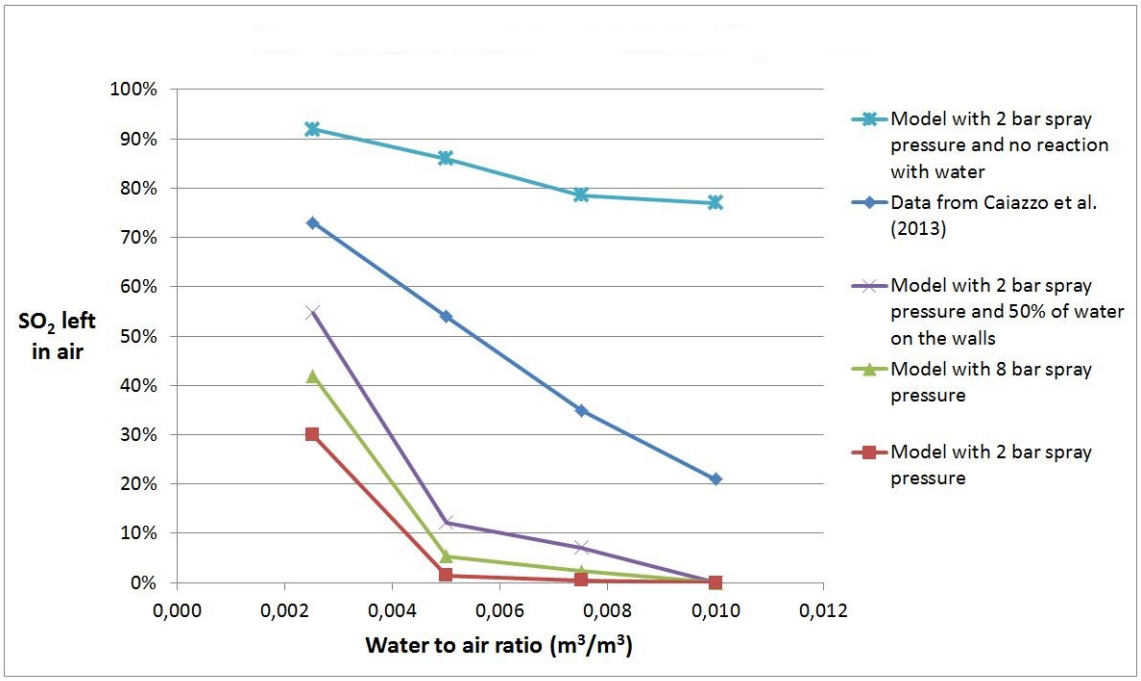

Figure 38: The data and different models for 500 ppm absorption in the conditions from the spray chamber in Caiazzo et al. (2013).

In the model by Caiazzo et al. (2012), the evaporation effect affecting the droplet surface temperature is considered. The exhaust gas in Caiazzo et al. (2013) is dry, and therefore the droplets will evaporate in the spray chamber. The evaporation will affect the droplet temperature, and since evaporation requires energy, then some of that energy is taken from the droplet, decreasing its temperature. The different temperature will affect the diffusion, since the diffusion is temperature dependent. The other evaporation effect, diffusiophoresis, as in Section 5.4.2, is not considered. The diffusiophoresis for the case of evaporation can create a slight overpressure on the surface of the drop, and hinder the diffusion of SO_2. That can also affect the model.

An accurate absorption model would also require that internal circulation of the droplet is modeled. That was done by Caiazzo et al. (2012). The model from Caiazzo et al. (2013) is more accurate for the case in Caiazzo et al. (2013) than the model in this thesis. But with the right modifications to the model in this thesis, it could also provide for a relatively proper model for the Caiazzo et al. (2013) data.

Another case for the spray chamber was measured by the author and D.Sc. Pasi Rajala from TM Systems. The spray chamber is located in China, on the roof of a paper mill. The data for the spray chamber is presented in the Table 13. There are two levels in the spray chamber, and the flow setup was a mix between cross-current and counter-current. The

equivalent chamber height is 4.5 m per level. The droplet velocity was calculated with the methods by Lehtinen (2017).

Table 13: The process conditions for a spray chamber with own measurements.

Equivalent chamber height	4.5 m
Air flow	18 m^3/s
Air temperature, in	62 °C
Air humidity, in	78 g/kg
Water flow	8.55 kg/s
Spray pressure	3 bars
Spray angle	80°
Water temperature	47 °C

Concentrations of H_2S and SO_2 were measured from the air inlet and outlet of the spray chamber. The gas concentrations were low. The droplet absorption model in this thesis was used to calculate the absorption, with the assumptions that the absorbed gas is rapidly consumed by OH^--ions. The simulated results can be viewed in Table 14 below.

Table 14: Measured and calculated removal of H_2S and SO_2 for the spray chamber with own measurements.

H_2S				
Measured			Simulated	
Relative amount in	1		Relative amount in	1
Relative amount out	0.1		Relative amount out	0.32
Absorption efficiency	90%		Absorption efficiency	68%
SO_2				
Measured			Simulated	
Relative amount in	1		Relative amount in	1
Relative amount out	0.2		Relative amount out	0
Absorption efficiency	80%		Absorption efficiency	100%

The simulated results differ somewhat from the measured concentrations. The deviations can depend on the same reasons as in the case by Caiazzo (2013). Additionally, the effect of condensing water vapour can enhance the absorption through diffusiophoresis, and that could affect the hydrogen sulphide absorption. Condensation is present in the spray chamber since the air is humid, as opposed to the air in Caiazzo (2013).

Under the measurements the inlet concentration was constant. For other inlet concentrations there are no measurements available. Retaining the same assumption that the absorbed gases immediately react, the simulations retain the same absorption efficiency for different inlet concentrations.

7.2 Spray chamber particle impaction modelling

Some calculation examples of the particle collection efficiency with the collision mechanism is presented. The collision principles are presented in section 5.4. The fluid flows are counter-current and the collection of particles is only based on the impaction and thus, Equation 119 is used for the single droplet collection efficiency. The conditions in the spray chamber are presented below in Table 15.

Table 15: The conditions inside the spray chamber for particle impaction model testing.

Air mass flow	25 kg/s
Air volume flow	37 m^3/s
Chamber cross-sectional area	16 m^2
Chamber height	4 m
Pressure inside spray nozzle	2 bar

The droplet velocity inside the chamber is calculated with methods by Lehtinen (2017). The resulting average droplet velocity inside the chamber is about 7.21 m/s. The water mass flow is varied in Figure 39. One can clearly see that a larger water mass flow, hence larger $\dot{V}_l/\dot{V}_{air}$, makes the overall removal efficiency more efficient. The water flow is assumed to not hit the chamber inside walls.

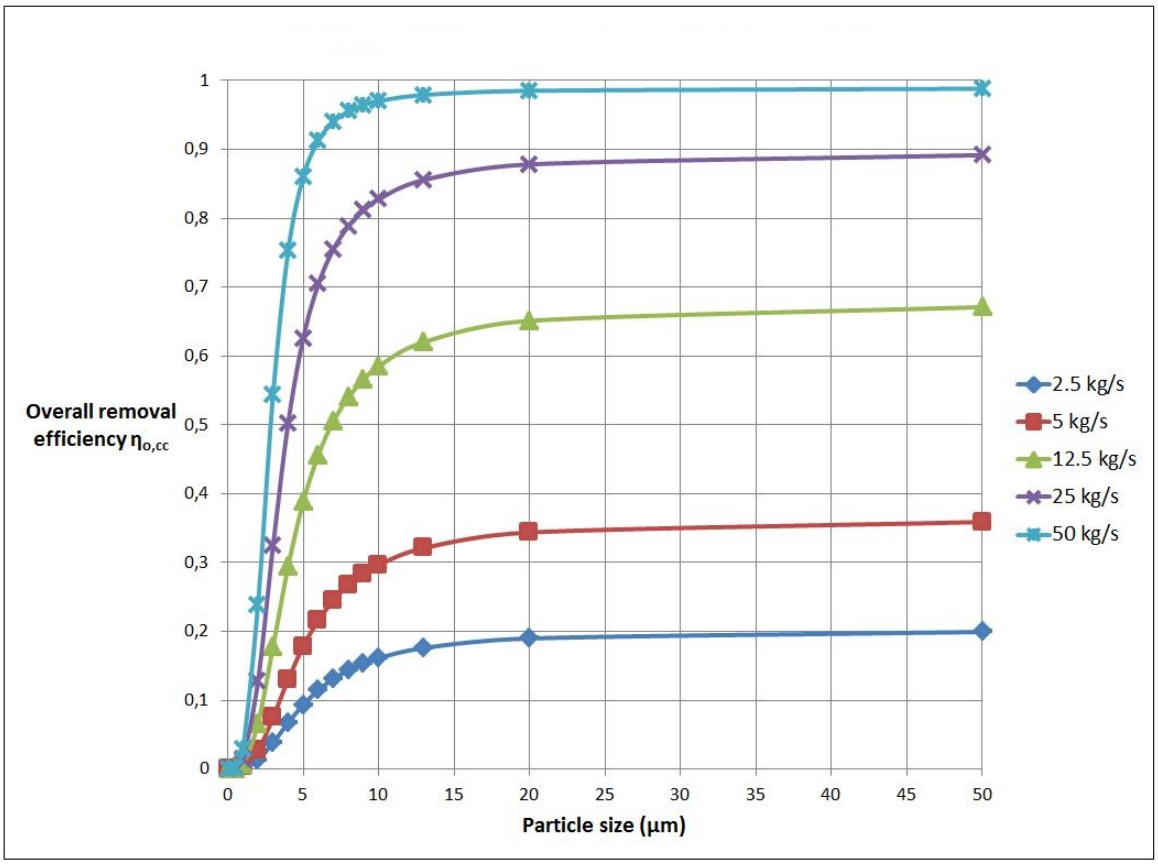

Figure 39: Particle removal efficiencies calculated with a model for a spray chamber with different water flows.

A simple graph displaying the droplet velocity inside the chamber as a function of the chamber height can be seen in Figure 40. It shows the droplet velocity profile obtained with the Lehtinen (2017) droplet motion method. At the same time is plotted the overall particle removal efficiency inside the chamber as a function of the chamber height. The droplet velocity inside the whole chamber for the overall efficiency is the constant value at the specific height taken from the Lehtinen (2017) calculation. The particle removal efficiency is calculated for different particle sizes. 0 m is at the bottom of the chamber, while 4 m is at the top of the chamber. The water mass flow is 30 kg/s.

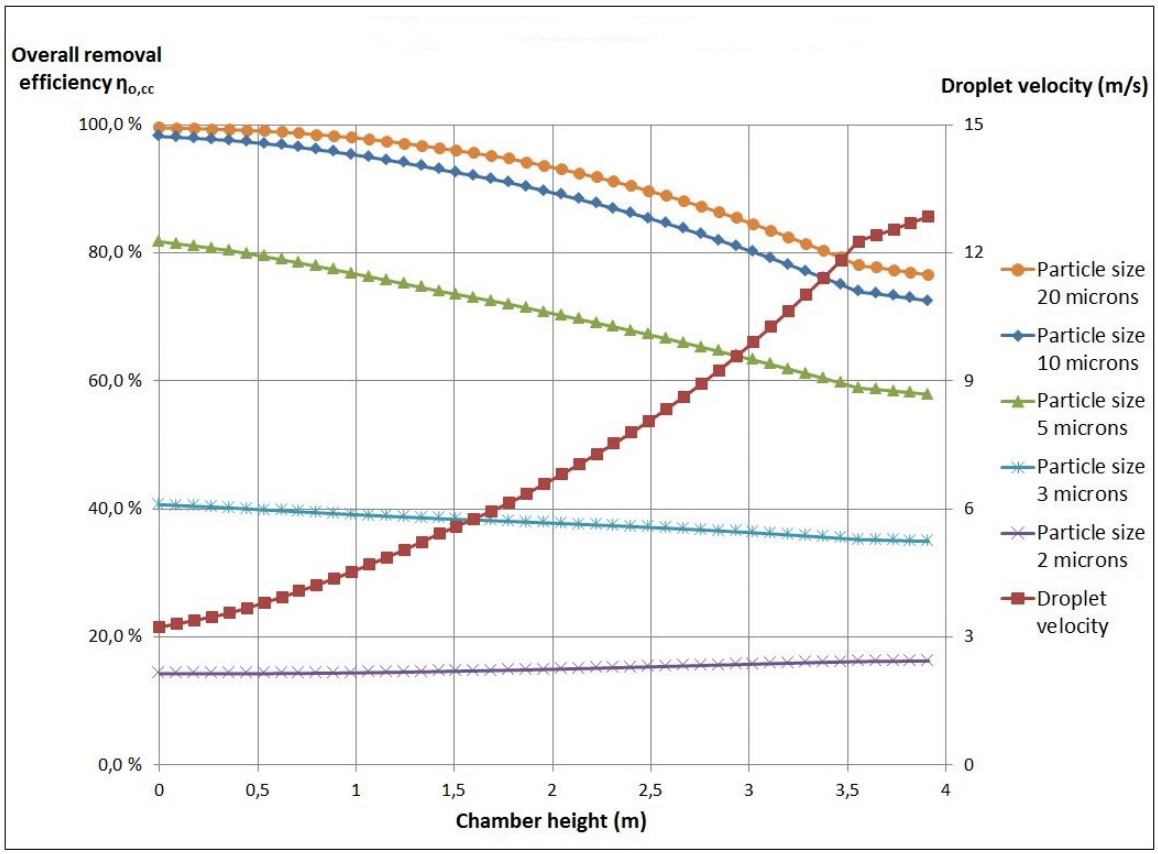

Figure 40: Overall efficiency of particle removal as a function of the chamber height (4 m).

What is clear in Figure 40, is that a lower droplet velocity makes the particle removal more efficient – at least for larger particles. Collection of 2 μm particles in diameter is not affected by the change in droplet velocity inside the spray chamber. It has probably to do with the particles being so small, so they follow the air flow closely, resulting in that they do not collide with the droplets that much.

In Figure 41 spray chambers with different number of spray levels are shown. The spray water is collected between the levels, and after that it is sprayed into the next level. One can also see the configuration as several different spray chambers connected in series. The water flow is also 30 kg/s.

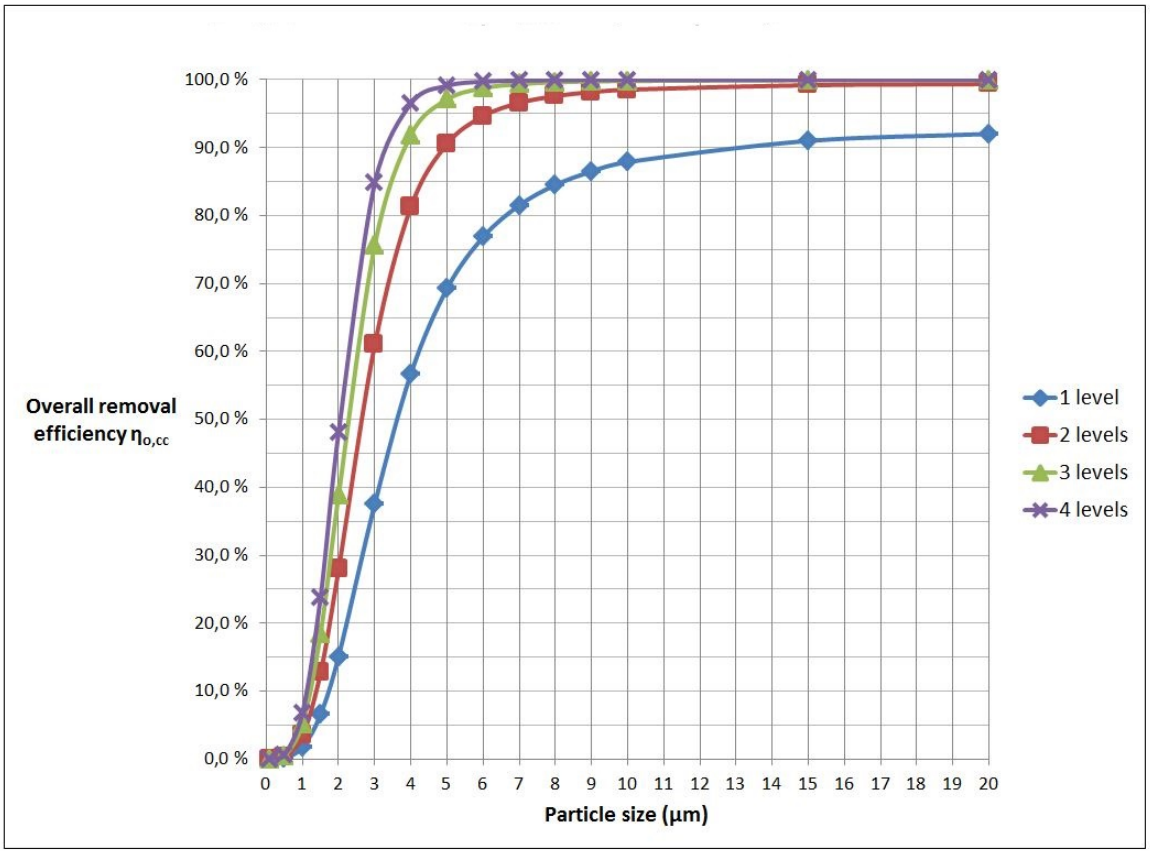

Figure 41: Particle removal in a spray chamber with different number of spray levels.

Overall, the particle impaction results seem realistic. For a future spray chamber the particle collection efficiency can be calculated beforehand, and after that tested for by measurements of the particle concentrations.

8 Conclusions

The aim of the thesis was, firstly, to research air treatment with three different equipment: Spray chambers, tray columns and wetted-wall techniques. Secondly, regulations on the air treatments and general industrial ventilation were to be studied. Thirdly, treatment methods of the water used in the exhaust air treatments were to be studied and developed. Lastly, the condensation effects in the air-air heat exchanger were to be studied and some calculation formulas for it were to be introduced. The first and the last aim were the most important and most detailed in this thesis. Therefore, the second and third aim were briefly introduced and treated.

For the air-air plate heat exchanger, the necessary flow cases were studied. The arrangement of the condensate film and the air flow was counter-current and co-current two-phase flow on the hot air side. For both cases, methods for calculating the film thickness and pressure drop were developed. For the counter-current flow, some criteria on the flow stability and flooding was studied. Former methods (Törnqvist, 2011) for the heat transfer calculations were modified and expanded in order to perform heat transfer calculations with the condensate film. The heat transfer model can be implemented and used to perform calculations on air-air heat exchangers. The author developed a simplified calculation tool for the film heat exchanger. More future work is required to arrange measurements and modelling to verify the heat transfer model and the calcualtion tool.

Air treatment techniques with water to remove particles and gases from the exhaust air were discussed and introduced. The use of tray columns and wetted-wall columns were left on the theoretical stage, though some had a few easy example calculations performed on them. The spray chamber case was implemented in Matlab and a model by the author was verified against measurements of the absorption of gaseous compounds. Some example calculations by the author on the particle collection efficiency were performed on the spray chamber. The air treatments discussed are dependent on several parameters. To ensure correct equipment dimensioning and design, more measurements on the air treatment techniques is needed. The three different techniques can be compared amongst each other in order to make rough estimates to find the most suitable equipment.

Different and typical concentrations of particles and gaseous compounds in paper mills and required ventilation terminology and configuration were discussed briefly. They provide an understanding and a basis for the equipment required to treat the air and to comply with the pollution regulations. Also, water treatment after the air treatment was discussed briefly. A few different techniques for the water treatment were introduced, including filtration, sedimentation and hydrocyclones. For the mixture in this thesis, the filter techniques,

especially cartridge filters, can be seen as a future treatment technique for the water.

The different parts in this thesis form a package that can be utilized in the future for equipment dimensioning. Although the principles discussed are left on a theoretical base, they still offer a valid starting point for real process design. Therefore, the future equipment will require measurements to further modify and develop the models for better accuracy.

Summary in Swedish – Svensk sammanfattning

Detta diplomarbete har som avsikt att behandla några olika teman som berör luftrening av utsläpp från pappersbruk. Utsläppen som här behandlas är partikelutsläpp och gasutsläpp. Partikelutsläppen är närmast fibrer, såsom cellulosafibrer och pappersfibrer som lossnar under papprets torkningsprocess. Gasutsläppen kan vara mångfaldiga och kan bestå av bl.a. volatila organiska ämnen (VOC). Dessa ämnen kan ha sitt ursprung i olika lim och ytbeläggningsämnen som tillsätts på pappret under torkningsprocessen. Torkningsprocessen ventileras, och därmed åker utsläppen ut i atmosfären. Med kontinuerligt striktare utsläppskrav, måste utsläppen reduceras. Som ett mål för detta diplomarbete har varit att hitta och forska i några olika sätt att minska på utsläppen.

Ett annat huvudtema har varit att teoretiskt undersöka huruvida en kondenseringsfilm påverkar en luft-luftvärmeväxlares prestanda. Värmeväxlaren används för att förvärma ingående luft till pappersmaskinen eller hallen där pappersmaskinen står eller båda. Luft-luftvärmeväxlaren som använts i arbetet är en plattvärmeväxlare med släta plattor där de två olika luftströmmarna flödar i kors mellan varannan platta. Den varma luften, ofta från kåpan på pappersmaskinen, innehåller vattenånga från torkningsprocessen. Den varma luften avger värme mestadels genom kondensering av vattenångan. Kondensatet bildar en film på värmeväxlarytan, och kan därmed bidra till eller förhindra värmeöverföringen i värmeväxlaren. Samtidigt blir flödesdynamiken på varma luftens sida ett tvåfasflöde, med kondensat och luft. Arbetet behandlar både tvåfasflödet och filmens påverkan till värmeöverföringen.

Två sidoteman har varit industriventilation och vattenrening. Industriventilation har fokuserat på allmänna förordningar och terminologi. Vattenrening har behandlats p.g.a. att luftreningsmetoderna alla baserar sig på metoder som använder sig av vatten. När vattnet tar emot föroreningar från luften, blir vattnet förorenat, och måste renas. Vattenreningsmetoderna som behandlas är främst filtrering, men även sedimentation och hydrocykloner.

Matematiska modeller och formler presenteras för flera behandlade ämnen. Men det som varit speciellt viktigt för detta arbete har varit modellen för absorption av gaser och borttagning av partiklar från luftströmmen i ett sprejtorn. För absorptionen har en modell implementerats i kodnings- och beräkningsprogrammet Matlab. Absorptionsmodellen har också verifierats med självuppmättna och i litteraturen givna värden.

Arbetet har gjorts tillsammans med TM Systems Finland Oy. TM Systems är ett företag som specialiserat sig på industriell ventilation. Deras produkter betjänar främst pappers-

bruk, där stort luftutbyte behövs i processen.

Värmeväxlaren

Luft-luft plattvärmeväxlaren har varm och fuktig luft som värmeavgivande medium och kall luft som värmeupptagande medium. Den varma och fuktiga luften kondenserar på de kala ytorna och ger då upphov till en kondenseringsfilm, som bildar ett tvåfasflöde med luften. Värmeväxlaren kan arrangeras så att flödesriktningarna för filmen och luften kan vara olika. Arbetet behandlar först en flödessituation där vatten- och luftströmmen har olika riktning. Luftströmmen är då riktad uppåt och vattenströmmen är riktad nedåt. Kondensatfilmens tjocklek kan bestämmas med några olika sätt enligt litteraturen och dessa diskuteras närmare. Drosos et al. (2006) beskriver flödesdynamiken för en smal kanal med motströmflöden, där vatten rör sig nedåt och luft uppåt, och hur kondensatfilmens tjocklek kan bestämmas. Filmtjockleken används i värmeöverföringsberäkningarna. Utöver filmtjockleken för de två huvudsakliga flödesarrangemangen presenteras även beräkningssätt för tryckfallet i luften när den passerar genom kanalen med tvåfasflöde.

För motström där vatten rör sig nedåt finns ett gränsfall. Litteraturen känner till fenomenet som ett slags översvämningsläge, där tvåfasflödet övergår till ett instabilt läge. Det finns olika typer av översvämningslägen, men ett bestämmande kriterium är när hastighetsprofilen för filmen är sådan att de yttersta lagren av filmen har motsatt riktning än filmens "bulk"-riktning. Det betyder att de yttersta lagren av filmen rör sig uppåt i kanalen, medan resten av filmen rör sig nedåt. Översvämningsläget kan också bidra till överbryggning, där kanalen stundvis kan täppas till av filmen. Filmtjockleken kan inte längre bestämmas under översvämningsläget eftersom filmen befinner sig i en oförutsägbar flödessituation. Översvämningsläget är en oönskad flödessituation, och därför är det viktigt att kunna förutspå när flödet övergår till översvämningsläget. Arbetet presenterar en beräkningsmetod för detta.

Därtill finns det ännu ett sätt att arrangera flödesriktningarna. Flödesriktningarna kan riktas i medström, så att både luften och filmen rör sig nedåt i värmeväxlaren. Arbetet presenterar sätt att beräkna filmtjockleken även för medström. I medström nedåt finns det ingen risk för översvämning. Däremot kan de förekomma s.k. "filminblandning", vilket innebär att luftströmmen kan riva loss vatten från filmen, så att det blandar sig i luftfasen. Vatten kan då vara närvarande i luftströmmen som droppar, som har samma riktning som luften. Ingen beräkningsmetod för filminblandning presenteras, men en grafisk bestämning visas.

Informationen om filmtjockleken i de två olika flödesarrangemangen är viktig vid värmeöverföringsberäkningen. I arbetet ses kondenseringsfilmen som en extra yta på plåten som sepa-

rerar den kalla och varma luften. Därmed modifieras tidigare beräkningssätt (bl.a. Törnqvist, 2011), så att filmen läggs till som en vägg mellan den varma och kalla strömmen. Den varma luftens vattenånga antas kondensera på vätskefilmen vid vätskefilmens temperatur. Därmed måste filmens temperatur bestämmas. Det nya beräkningssättet för värmeöverföringen presenteras.

De olika beräkningssätten om filmtjocklek och värmeöverföring lämnas i arbetet på teorinivå. För att få pålitliga resultat från en kalkyleringsmodell behövs verkliga mätningar så att beräkningssätten kan verifieras. Trots detta, bildar teorierna en bas för framtida design och planering av värmeväxlare.

Luftbehandling

Luftbehandlingen är indelad i två delar: Absorption av gaser och borttagning av partiklar från luften. För båda delarna behandlas tre olika apparater: Ett sprejtorn, bottenkolonn och kolonn med en vätskefilm.

För en bottenkolonn flödar gasen uppåt igenom bottnar i kolonnen. Bottnarna kan ha olika design, en typ av design är en rund plåt där det har borrats små hål i – luften flödar igenom hålen. Vätskan flödar i kolonnen över botten. Vid ena ändan av botten finns en fallzon för vätskan, där den faller ner till nästa botten. Vätskan rör sig nedåt i kolonnen, men är i kontakt med luften i korsflöde ovanpå botten. Absorptionen på bottenkolonnen bestäms oftast grafiskt. Grafiskt kan man då t.ex. bestämma hur många bottnar en dylik kolonn behöver. Bestämningen grundar sig på potentialen för vätskan att absorbera gasen från luften. Potentialen beror på ämnets fysikaliska egenskaper. Efter att antalet botten har bestämts, kan kolonnens storlek bestämmas. För bottenkolonnen ges beräkningsmetoder för borttagning av partiklar ur ett luftflöde.

Ett sprejtorn är en kammare, inuti vilken vatten sprejas genom munstycken. I arbetet är sprejtornen sådana att vattnet sprejas nedåt som droppar medan luften flödar uppåt – flödena är då i motström. Absorptionen baserar sig på att gasmolekylerna har en potential att absorberas i vattendropparna. Absorptionseffektiviteten beror på flera olika parametrar, bl.a. luftens och vattendropparnas dröjtid i tornet. Avlägsnandet av partiklar baserar sig på att partiklar träffar vattendroppen och blir då fast i vattnet. Träffen kan ske på olika sett; direkt kollision mellan partikeln och droppen används i det presenterade beräkningssättet. Kondenseringseffekten på träffarna diskuteras även.

Vätskefilmskolonn är en kolonn med en vätskefilm på den inre väggen av kolonnen. I arbetet rinner filmen nedåt medan luften flödar uppåt. För absorptionen finns det i litteraturen metoder för att bestämma dess effektivitet i en vätskefilmskolonn. För avlägsnandet av partiklar är beräkningen besvärligare. Avlägsnandet baserar sig på antalet kollisioner av partiklar med vätskefilmen. Antalet kollisionen bestäms av luftens turbulenta egenskaper

som kan vara svåra att bestämma utan en noggrannare flödesanalys. En grov estimering görs på beräkningen av antalet kollisioner.

Andra teman

Arbetet behandlar också vattenrening. Luftreningen baserar sig på att använda vatten som det renande ämnet. Efter reningsprocessen blir vattnet förorenat, och måste renas. Det aktuella kapitlet har som mål att presentera olika reningssätt för att i framtiden kunna välja en passlig process. Reningssätt som behandlas är filtrering, sedimentation och hydrocykloner. Filtrering behandlas noggrannast, eftersom vattensuspensionen med fiberpartiklar är en lämplig suspension för filtreringen. Basprinciper för filtrering, såsom kakfiltrering och filtrering med filtermedium, behandlas i arbetet. Därtill presenteras några olika filtreringsapparater och deras funktionsprinciper. Sedimentation och hydrocykloner behandlas kort.

Ett allmänt tema som behandlas är industriventilation. Ventilationen innehåller luftströmmar och egen terminologi, som introduceras i arbetet. Dessa luftströmmar har olika förordningar och krav på renhet och andra bestämmelser om bl.a. toxicitet och hygien. Förordningarna ställer också krav på ventilationsapparater, och syns direkt i sådana applikationer som luftfilter på inkommande luft. Gränser för skadliga gaser i luften diskuteras. En diskussion förs också om skadliga koncentrationer av pappersfibrer i inandningsluften.

Resultat och diskussion

Resultaten koncentrerar sig på sprejtorn. Gasabsorptionsmodellen verifieras med självuppmätt data och data från litteraturen. Absorberade gaser är divätesulfid och svaveldioxid. Diskussion kring modellens och datas lämplighet förs, och det visar sig att modellen beskriver datat till en tillförlitlig grad. Utöver absorptionen i sprejtornet presenteras några modellbaserade resultat för borttagningen av partiklar i ett sprejtorn. Resultaten är rimliga, men de är dock overifierade.

Som en helhet behandlar arbetet mest teori om olika beräkningsmodeller. Beräkningsmodellerna fungerar som en bas för design och planering av apparater. För sprejtornet finns det verfieringsdata som använts i arbetet, men för de andra metoderna som behandlats är nästa steg i processen är att få mera uppmätt data och anpassa modellerna till det.

References

Aliyu, M. A., Lao, L., Almabrok, A. A. & Yeung, H. (2016). Interfacial shear stress in adiabatic downward gas/liquid co-current annular flow in pipes. *Experimental Thermal and Fluid Science, 72*, pp. 75–87.

Almabrok, A. A. (2013). *Gas-liquid two-phase flow in up and down vertical pipes.* Ph. D. thesis. Cranfield University, UK.

Beek, W. J., Muttzall, K. M. K. & van Heuven, J. W. (1999). *Transport Phenomena.* Wiley, USA, 2nd edition.

Bird, R. B., Stewart, W. E. & Lightfoot, E. N. (2007). *Transport Phenomena.* Wiley, USA, 2nd edition.

Bradley, D. (2011). *Hydrocyclones.* Article on Thermopedia. Source: http://www.thermopedia.com/content/862/. Visited 18.3.2019.

Caiazzo, G., Langella, G., Miccio, F. & Scala, F. (2013). An experimental investigation on seawater SO_2 scrubbing for marine aplication. *Environmental Progress & Sustainable Energy, 32*, pp. 1179–1186.

Caiazzo, G., Di Nardo, A., Langella, G. & Scala, F. (2012). Seawater scrubbing desulfurization: A model for SO_2 absorption in fall-down droplets. *Environmental Progress & Sustainable Energy, 3*1, pp. 277–287.

Calvert, S. (1977). *Scrubbing.* In: Stern, A. C. (1977). Air Pollution, Volume IV, Engineering Control of Air Pollution. Academic Press, USA, 3rd edition, pp. 267–292.

Calvert, S. & Jhaveri, N. C. (1974). Flux force/condensation scrubbing. *Journal of the Air Pollution Control Association, 24*(10), pp. 946–951.

Cengel, Y. A. (2008). *Heat Transfer: A Practical Approach.* McGraw-Hill Education, USA, 2nd edition.

Chen, W. (2016). *What are filter aids?.* Article on American Filtration and Separation Society website. Source: https://www.afssociety.org/what-are-filter-aids/. Visited 18.3.2019.

Cheremisinoff, N. P. (1998). *Liquid Filtration.* Butterworth-Heinemann, 2nd edition.

Cooper, D. W. (1984) *Wet Scrubber Particulate Collection.* In: Fayed, M. E. & Otten, L., Handbook of Powder Science and Technology. Van Nordstrand Reinhold Company Inc., New york, pp. 793–834.

Cui, H., Li, N., Wang, X., Peng, J. & Wu, Z. (2017). Optimization of reversibly used cooling tower with downward spraying. *Energy, 127*, pp. 30–43.

Cussler, E. L. (2009). *Diffusion: Mass Transfer in Fluid Systems.* Cambridge University Press, UK, 3rd edition.

Drosos, E. I. P., Paras, S. V. & Karabelas A. J. (2006). Counter-current gas-liquid flow in a vertical marrow channel–Liquid film characteristics and flooding phenomena. *International Journal of Multiphase Flow, 32*, pp. 51–81.

EMCEL Filters Ltd. (2019). *Dust & Particle Filter Selection Chart.* Visited 10th of January 2019: http://www.buildingdesign.co.uk/bd-data-sheet/emcel.htm

Finnish Secretary of State (2001). *Valtioneuvoston asetus ilmanlaadusta.* 711/2001, Helsinki, Ympäristöministeriö.

Flagan, R. C. & Seinfeld, J. H (1988). *Fundamentals of air pollution engineering.* Prentice-Hall Inc., USA.

Garcia, J. A. & Fair, J. R. (2002). Distillation sieve trays without downcomers: Prediction of performance characteristics. *Industrial & Engineering Chemistry Research, 41,* pp. 1632–1640.

Gonda, I. & El Khalik, A. F.(1985). On the calculation of aerodynamic diameters of fibers. *Aerosol Science and Technology, 4* (2), pp. 233–238.

Grigorova, I. & Nishkov, I. (2015). Granulometric separation in laminar flow. *Proceedings of XXIV International Mining Congress and Exhibition of Turkey*, April 14-17, 2015 Antalya, Turkey.

Henstock, W. H. & Hanratty, T. J. (1976). The interfacial drag and the height of the wall layer in annular flows. *The AIChe Journal, 22*, pp. 990–1000.

Hinds, W. C. (1999). *Aerosol technology: properties, behavior, and measurement of airborne particles.* Wiley, USA, 2nd edition.

Hobler, T. & Danckwerts, P. V. (1966). *Mass Transfer and Absorbers.* Pergamon, Poland.

Incropera, F. P., Dewitt D. P., Bergman T. L. & Lavine A. S. (2011). *Fundamentals of Heat and Mass transfer,* 7th edition.

Kamppinen, A. (1997). *Optimisation of coating colour properties.* M.Sc. thesis. Lappeenranta University of Technology.

Karapantsios, T. D., Paras, S. V. & Karabelas, A. J. (1989). Statistical characteristics of free falling films at high Reynolds numbers. *International Journal of Multiphase Flow, 15*, pp. 1–21.

Karlsson, H. & Svensson H. (2017). Rate of absorption for CO_2absorption systems using wetted wall column. *Energy Procedia, 114*, pp. 2009–2023.

Kriebel, M. (2008). Absorption, 2. Design of Systems and Equipment. *Ullmann's Encyclopedia of Industrial Chemistry,* Wiley-VCH Verlag GmbH & Co. KGaA, Weinheim.

Kulov, N. N., Maksimov, V. V., Maljusov V. A. & Zhavoronkov, N. M. (1979). Pressure Drop, Mean Film Thickness and Entrainment in Downwards Two-Phase Flow. *The Chemical Engineering Journal, 18*, pp. 183–188.

Lampinen, M. J. & Seppälä A. (2017). *Aineensiirto-oppi.* Espoo, Yliopistokustannus.

Lampinen, M. J. (2015). *Thermodynamics of Humid Air.* Department of Energy Technology, Ene-39.4027 - Mass transfer P, *23.*

Lancaster, B. W. & Strauss W. (1971). A study of steam injection into wet scrubbers. *Industrial & Engineering Chemistry Fundamentals, 10*(3), pp. 362–369.

Lehtinen, P. E. (2017). *Funktionsprincipen hos en reversibelt använd skrubber.* B.Sc. thesis. Åbo Akademi University.

Lockhart, R. W. & Martinelli, R. C. (1949) Proposed correlation of data for isothermal two-phase, two-component flow in pipes. *Chemical Engineering Progress, 45*(1), pp. 39–48.

Lokanathan, M. & Hibiki, T. (2016). Flow regime, void fraction and interfacial area transport and characteristics of co-current downward two-phase flow. *Nuclear Engineering and Design, 307*, pp. 39–63.

Loosmore, G. A. & Cederwall, R. T. (2004). Precipitation scavenging of atmospheric aerosols for emergency response applications: testing an updated model with new real-time data. *Atmospheric Environment, 38,* pp. 993–1003.

Lugg, G. A. (1968). Diffusion coefficients of some organic and other vapors in air. *Analytical Chemistry, 40*(7), pp. 1072–1077.

McQuillan, K. W. & Whalley, P. B. (1985). Flow patterns in vertical two-phase flow. *International Journal of Multiphase Flow, 11,* pp. 161–175.

Meyer, M., Hendou, M., Prevost, M. (1995). Simultaneous heat and mass transfer model for spray tower design : Application on VOCs removal. *Computers & Chemical Engineering, 19,* Supplement 1, pp. 277–282.

Ministry of the Environment (2003). *Rakennusten sisäilmasto ja ilmanvaihto. Määräykset ja ohjeet.* Helsinki, Ympäristöministeriö.

Moreno-Beltrán, D. L. & Grau-Rios, M. (2001). *Occupational Exposure Limit Values.* In: Goodfellow, H. & Tähti, E. Industrial Ventilation Design Guidebook. Academic Press, USA, pp. 362–373.

Noll, K. E., Nichols, G. B., Crowder, J. W. & Senkan, S. M. (1986). *Control Devices: Electrostatic Precipitation, Scrubbing, Mist Elimination, Adsorption and Combustion of Toxic and Hazardous Wastes.* In: Stern, A. C. (1986). Air Pollution, Volume VII, Supplement to Measurements, Monitoring, Surveillance and Engineering Control. Academic Press, USA, 3rd edition, pp. 267–338.

Paiman, N. A., Leman, A. M., Abdull, N. & Ismail, M. (2013). Respiratory effects of exposure to respirable dust at paper based mill in Malaysia, *International Proceedings of Chemical, Biological and Environmental Engineering, 51,* pp. 143–148.

Perry, R. H. & Green, D. W. (1998). *Perry's Chemical Engineers' Handbook.* McGraw-Hill, USA, 7th edition.

Purchas, D. B. (1984). *Filtration of solids from liquid streams.* In: Fayed, M. E. & Otten, L., Handbook of Powder Science and Technology. Van Nordstrand Reinhold Company Inc., New york, pp. 687–729.

Richter, H. L. (1981). Flooding in tubes and annuli. *International Journal of Multiphase Flow, 7,* pp. 647–658.

Sander, R. (2015). Compilation of Henry's law constants (version 4.0) for water as solvent. *Atmospheric Chemistry and Physics, 15,* pp. 4399–4981.

Seinfeld, J. H. & Pandis, S. N. (2016). *Atmospheric Chemistry and Physics: From Air Pollution to Climate Change.* Wiley, USA, 3rd edition.

Sinnott, R. K. et al. (2005). *Chemical Engineering Design: Chemical Engineering Volume 6.* Elsevier Butterworth-Heinemann, 4th edition.

Slinn, W. G. N. (1983). *Precipitation Scavenging*, Atmospheric Sciences and Power Production - 1979. Division of Biomedical Environmental Research, US Department of Energy, Washington DC, Chapter 11.

Sommerfeld, M. (1992). Modelling of particle-wall collisions in confined gas-particle flows. *International Journal of Multiphase Flow, 18*(6), pp. 905–926.

Sparks, L. E. & Pilat, M. J. (1970). Effect of diffusiophoresis on particle collection by wet scrubbers. *Atmospheric Environment, 4,* pp. 651–660.

Sparks, T. (2012). Solid-liquid filtration: Understading filter presses and belt filters. *Filtration + Separation, 49*(4), pp. 20–24.

Spedding, P. L. (2010). *Falling film flow.* Article on Thermopedia. Source: http://www.thermopedia.com/content/19/. Visited 30.11.2018.

Sudo, Y. (1996). Mechanism and effects of predominant parameters regarding limitation of falling water in vertical counter-current two-phase flow. *Journal Heat Transfer, 118,* pp. 715–724.

Tarleton, E. S. & Wakeman, R. J. (2007). *Solid/Liquid Separation: Equipment Selection and Process Design.* Elsevier Butterworth-Heinemann, 4th edition.

Terrie, K & Boguski, P. E. (2006). *Understanding Units of Measurements.* Environmental Science and Technology Briefs for Citizens, Center for Hazardous Substance Research, Kansas State University, USA, Issue 2.

The International Water Association, 2019. *Sedimantation Process.* Article on The International Water Association website. Source: https://www.iwapublishing.com/news/sedimentation-processes. Visited 18.3.2019.

TM Systems Finland Oy, 2019. Personal correspondence with the experts in the company.

Tähti, E., Selin, M., Railio, J., Sainio, S., Hagström, K., Niemelä, R., . . . Pöntinen, K. (2000). *Teollisuusilmastoinnin opas.* Finnish Development Center for Building Services Ltd, 1st edition.

Törnqvist, P. (2011). *Beräkningsverktyg för dimensionering av värmeväxlare med fuktig luft som värmeavgivande medium.* M. Sc. thesis. Laboratory for Heat and Flow Engineering, Institution for Chemical Engineering, Åbo Akademi University.

Usui, K. (1989). Vertically Downward Two-Phase Flow, (II). *Journal of Nuclear Science and Technology, 26*(11), pp. 1013–1022.

Usui, K. & Sato, K. (1989). Vertically Downward Two-Phase Flow, (I). *Journal of Nuclear Science and Technology, 26*(7), pp. 670–680.

Vreman, A. W. (2015). Turbulence attenuation in particle-laden flow in smooth and rough channnels. *Journal of Fluid Mechanics, 773,* pp. 103–136.

Westberg, H., Elihn, K., Andersson, E., Persson, B., Andersson, L., Bryngelsson, I-L., . . . Sjögren, B. (2016). Inflammatory markers and exposure to airborne particles among workers in a Swedish pulp and paper mill. *International Archives Occupational and Environmental Health, 89*(5), pp. 813–822.

Wolverine Tube Inc. (2007). *Engineering Data Book III,* Chapter 7, Condensation on External Surfaces.

Zapke, A. & Kröger, D. G. (2000a). Countercurrent gas-liquid flow in inclined and vertical ducts – I: Flow patterns, pressure drop characteristics and flooding. *International Journal of Multiphase Flow, 26*, pp. 1439–1455.

Zapke, A. & Kröger, D. G. (2000b). Countercurrent gas-liquid flow in inclined and vertical ducts – II: The validity of the Froude-Ohnesorge number correlation for flooding. *International Journal of Multiphase Flow, 26*, pp. 1457–1468.

Zevenhoven, R. (2015). *Massöverföring och separationsteknik,* Unpublished lecture compendium for the course Massöverföring och separationsteknik at Åbo Akademi University.

Zhang, J., Wang, Y., Yu, G., Mao, X. & Wang, F. (2015). Experimental study of two phase flow characteristics on the dual-flow tray. *Chemical Engineering Research and Design, 102*, pp. 90–99.

Appendix

Cartridge filter materials for some different process conditions

	Electroplating Solutions	Filter Tube (Material/Core)
Acid		
Fluoborates	Cu, Fe, Pb, Sn	Polypropylene (PP) or Dynel/PP
Nonfluoborates	Cu, Sn, Zn: <6 oz/gal H_2SO_4	PP or cotton/PP
	Cu, Sn, Zn: >6 oz/gal H_2SO_4	PP or Dynel/PP
	Cr	PP or Dynel/PP
	Au, In, Rh, Pd	PP or Dynel/PP
	$FeCl_2$ (190°F)	PP/rigid PP (RPP) or porous stone
	Ni (Woods)	PP or Dynel/PP
	Ni (Watts type & bright)	PP or cotton/PP
	Ni (high-chloride)	PP or cotton/PP
	Ni (sulfamate)	PP or cotton/PP
	Electrotype Cu and Ni	PP or cotton/PP
Alkaline	Sn (stannate)	Cotton/stainless steel (SS)
Cyanide	Brass, Cd, Cu, Zn[a]	Cotton/SS, PP or Dynel/PP
	Au, In, Pt, Ag	Cotton/SS, PP/PP
Pyrophosphate	Cu, Fe, Sn, etc.	Cotton/SS or PP
Eletroless	Ni plating: <140°F	Cotton/SS or PP
	Ni plating: > 140°F	PP/RPP, cotton/SS
	Cu: <140°F	PP/PP
	Cu: >140°F	PP/RPP
	Chemicals	**Filter Tube (Material/Core)**
Acids	Acetic: dilute	Cotton/SS, PP/PP
	Acetic: concentrated	PP or Dynel/PP
	Boric	Cotton/SS, PP/PP
	Chromic, hydrochloric, nitric, phosphoric, sulfuric	PP or Dynel/PP, porous stone[b]
	Hydrofluoric, fluoboric	PP or Dynel/PP
Alkalies	NaOH or KOH	PP/PP
	NH_4OH: dilute.	Cotton/SS, PP/PP
	NH_4OH: concentrated	PP or Dynel/PP
Misc. Chemicals	Biological solutions	Cotton/SS, PP/PP, porous stone[b] Porous stone, PP/PP
	Electropolishing solutions	Pharmaceutical solutions
	Photographic solutions	Cotton/SS, PP/PP
	Radioactive solutions	Cotton/SS, porous stone[b]
	Ultrasonic cleaning solutions	Cotton special B compound/SS
	Nickel acetate (190°F)	Cotton/SS
	Food products	Cotton/SS, PP/PP
Organic Liquids	CCl_4	Cotton/steel or SS
	Dichloroethylene	Cotton/steel or SS
	Hydraulic fluids	Cotton/steel or SS
	Lacquers	Cotton/steel or SS
	Per- and trichloroethylene	Cotton/steel or SS
	Solvents	Cotton/steel or SS
Petroleum Products	Fuel oil, diesel, kerosene, gasoline, lube oil	Cotton/steel or SS

[a] When operated as high-speed baths at high temperatures (> 140°F) or with high alkali content, use PP or Dynel/PP.

[b] Porous stone is recommended for all acids except hydrofluoric and fluoboric.